COMPUTATIONAL FLUID DYNAMICS STUDY OF THE WAKE OF A HIGH-CLEARANCE AGRICULTURAL BOOM SPRAYER

A Thesis Submitted to the
College of Graduate and Postdoctoral Studies
In Partial Fulfillment of the Requirements
For the Degree of Master of Science
In the Department of Mechanical Engineering
University of Saskatchewan
Saskatoon

By

BENJAMIN J. GAGNON

PERMISSION TO USE

In presenting this thesis/dissertation in partial fulfillment of the requirements for a Postgraduate degree from the University of Saskatchewan, I agree that the Libraries of this University may make it freely available for inspection. I further agree that permission for copying of this thesis/dissertation in any manner, in whole or in part, for scholarly purposes may be granted by the professor or professors who supervised my thesis/dissertation work or, in their absence, by the Head of the Department or the Dean of the College in which my thesis work was done. It is understood that any copying or publication or use of this thesis/dissertation or parts thereof for financial gain shall not be allowed without my written permission. It is also understood that due recognition shall be given to me and to the University of Saskatchewan in any scholarly use which may be made of any material in my thesis/dissertation.

DISCLAIMER

The model of a John Deere 4830 Agricultural Sprayer was exclusively created to meet the thesis requirements for the degree of Master of Science at the University of Saskatchewan. Reference in this thesis to any specific commercial products, process, or service by trade name, trademark, manufacturer, or otherwise, does not constitute or imply its endorsement, recommendation, or favoring by the University of Saskatchewan. The views and opinions of the author expressed herein do not state or reflect those of the University of Saskatchewan, and shall not be used for advertising or product endorsement purposes.

Requests for permission to copy or to make other uses of materials in this thesis/dissertation in whole or part should be addressed to:

Head of the Department of Mechanical Engineering
57 Campus Drive
University of Saskatchewan
Saskatoon, Saskatchewan S7N 5A9 Canada

OR

Dean
College of Graduate and Postdoctoral Studies
University of Saskatchewan
116 Thorvaldson Building, 110 Science Place
Saskatoon, Saskatchewan S7N 5C9 Canada

Abstract

Self propelled agricultural sprayers are commonly found on farms in Saskatchewan. These vehicles are used to spray pesticides onto crops to increase the productivity of the field. Spray drift occurs when pesticides are carried away from their target. It has been estimated that up to 30% of all pesticides sprayed onto a crop will drift. The literature contains multiple studies on how particles released from a nozzle will travel, but there is a lack of research towards understanding how the airflow patterns around an agricultural sprayer might affect spray drift.

The present thesis research modeled the airflow around a John Deere 4830 agricultural sprayer using computational fluid dynamics (CFD), with a focus on the sprayer wake. Since agricultural sprayers are large vehicles, the numerical grid must include enough elements to realistically model the wake of the sprayer, while keeping the number of elements low enough to make the simulations possible in a reasonable amount of time. Several grids with different element size and type were investigated to meet this requirement. Benchmarking studies were performed on a circular cylinder to determine the performance of different grids. The best performing grids were then tested on a small section of the sprayer boom. In the sample boom tests the smaller elements provided more detail, but there were stability issues, the coarse elements were ultimately chosen as they performed realistically.

The full-scale simulations were performed using the STAR-CCM+ commercial CFD code. Using the grid developed earlier, three simulations were performed on the agricultural sprayer. The three simulations represented different boom heights and sprayer travel speeds to determine how different operating conditions may affect the airflow around the sprayer. The simulations showed that the wake of a sprayer has four different zones, corresponding to different parts of the vehicle and boom geometry.

The wake of the sprayer was shown to be largest directly behind the vehicle. The downstream extent of the wake decreases along the boom up to the folding knuckle where the size increases again due to the increased blockage of the flow. The simulations showed that increasing the sprayer travel speed and increasing the boom height both caused significant increases to the turbulence intensity in the wake of the sprayer and in the region near the nozzles. This in turn could increase the potential for spray drift occurring.

Acknowledgements

The work in this thesis has been supported by many individuals and organizations who deserve to be recognized for their efforts.

I would like to thank my supervisors Dr. Donald Bergstrom and Dr. David Sumner for the dedicated advice and feedback that they have provided. Additional thanks is extended to the members of my advisory committee Dr. Jim Bugg and Dr. Travis Wiens.

This research would not be possible without the funding provided by Alberta Pulse Growers, Manitoba Crop Alliance, Manitoba Pulse and Soybean Growers, Sask Pulse Growers, and the Western Grains Research Foundation, with support from Agriculture and Agri-Food Canada and the Canadian Agricultural Partnership.

The team at the Prairie Agricultural Machine Institute (PAMI) has been a research partner since day one, and they provided the license and computing time necessary to carry out this research. I would like to personally thank Ian Paulson for his work managing this project and additionally Justin Gerspacher for his work in data collection.

Project collaborators Hubert Landry, Tom Wolf, and Brian Caldwell have provided insights into the working of agricultural sprayers and have provided useful feedback and critiques of this research.

Cervus Saskatoon provided an agricultural sprayer and a field for this project which allowed for the needed field research to be completed.

I would also like to thank my partner Kaitlyn Kennedy for her support, feedback, and help getting though this research.

Dedication

I would like to dedicate this work to my grandparents, Paul, Maureen, Mike, and June. The best supporters, role models, and teachers I have had.

Table of Contents

Abstract ii

Acknowledgements iii

Dedication iv

List of Tables viii

List of Figures ix

Chapter 1: Introduction 1

1.1 Motivation 2

1.2 Objectives 2

1.3 Research Contribution 3

1.4 Outline of the Thesis 3

Chapter 2: Literature Review 4

Chapter 3: Computational Fluid Dynamics and Benchmark Simulations of the Flow Over a Circular Cylinder 7

3.1 Turbulence Modeling 8

3.2 Using CFD for Complex Flow Simulations 8

3.3 Benchmark Flow Simulations 9

3.4 Domain, Geometry, and Boundary Conditions 9

3.5 Description of the Meshing Methods and Meshes Used 11

3.6 Results 14

3.6.1 Wake Velocity Profiles 14

3.6.2 Wake Velocity Profiles at x = 6D 15

3.6.3 Wake Velocity Profiles at x = 2D 18

3.6.4 Wake Velocity Profiles at x = 0.5D 18

3.6.5 Centerline Velocity Profiles 19

3.6.6 Pressure Coefficient on the Cylinder Surface 22

3.7 Discussion 23
3.8 Conclusion 24
Chapter 4: Simulating Flow Over a Section of the Boom of an Agricultural Sprayer 27
4.1 Domain, Geometry, and Meshing 27
4.2 Results 29
4.3 Conclusions 36
Chapter 5: Full Scale Simulation 37
5.1 Geometry and Domain 37
5.2 Meshing 41
5.3 Boundary Conditions 46
5.4 Cases 48
5.5 Convergence 49
5.6 Base Case: The Wake of an Agricultural Sprayer 53
5.6.1 Turbulence and Large-Scale Structures 53
5.6.2 Contour Plots 57
5.6.3 Velocity Vector Plots 60
5.7 Wake Comparison for Different Operating Conditions 62
5.7.1 Case 2: Low Boom Height and Slow Travel Speed 63
5.7.2 Case 3: High Boom Height and Fast Travel Speed 71
5.8 Discussion of Results for all Three Cases 82
5.8.1 Turbulence Kinetic Energy 82
5.8.2 Assessing the Wake Near the Nozzles 87
5.8.3 Comparison to 2019 Field Data 89
5.8.4 A Generalized Description for the Wake of an Agricultural Sprayer 91
Chapter 6: Conclusions 93

References 96

Appendix A - 2019 Field Data 1

List of Tables

Table 3.1: Element sizing for mesh generation 11
Table 3.2: Details of tested meshes and associated quality. 13
Table 3.3: Differences in the Poly I and Poly IV meshes to be carried forward for further study 26
Table 4.1: Mesh characteristics for boom section model. 29
Table 5.1: Mesh element size for the surfaces in the sprayer simulation. 41
Table 5.2: Details on the Sizing of the mesh for the full-scale simulations. 45
Table 5.3: Boundary conditions for all the faces of the simulation domain. 48
Table 5.4: Details of sprayer speed and boom height for the three cases simulated. 48

List of Figures

Figure 1.1: Image of a high-clearance boom sprayer with a rear-mounted boom parked in a soybean field near Dundurn SK. 2
Figure 3.1: The domain used to simulate the flow over a cylinder. 10
Figure 3.2: Poly I mesh showing elements on a plane through the middle of the domain, on the inlet, outlet, and the cylinder surface. 14
Figure 3.3: Comparison of velocity profiles for Polyhedral meshes at x = 6D downstream of the cylinder compared with data from Maryami (2020). 16
Figure 3.4: Comparison of velocity profiles for Cutcell meshes at x = 6D downstream of the cylinder compared with data from Maryami (2020). 17
Figure 3.5: Comparison of velocity profiles for Poly II meshes with different numbers of inflation layers at x = 6D downstream of the cylinder compared with data from Maryami (2020). 17
Figure 3.6: Comparison of velocity profiles for Polyhedral meshes at x = 2D downstream of the cylinder compared with data from Norberg (1998) 18
Figure 3.7: Comparison of velocity profiles for Polyhedral meshes at x = 0.5D behind a cylinder and comparing to two sets of data from the literature 19
Figure 3.8: Comparison of streamwise velocity along the centerline of the wake of a cylinder using different polyhedral meshes. 20
Figure 3.9: Comparison of streamwise velocity along the centerline of the wake of a cylinder using different cutcell meshes. 21
Figure 3.10: Comparison of streamwise velocity along the centerline of the wake of a cylinder using the Poly II mesh with different numbers of inflation layers. 22
Figure 3.11: Pressure coefficient around a cylinder with polyhedral meshes 23
Figure 4.1: Domain used to model the flow around a section of the sprayer boom 27
Figure 4.2: Coarse poly mesh through the centre of the domain showing the mesh 28
Figure 4.3: Close up view of the coarse mesh on the boom structure and in the near boom region of the flow 28
Figure 4.4: Streamwise velocity 0.1 m behind the boom section. 30
Figure 4.5: Vertical velocity 0.1 m behind the boom section. 31
Figure 4.6: TKE 0.1 m behind the boom section. 32

Figure 4.7: Streamwise velocity 0.5 m behind the boom section. 33
Figure 4.8: Vertical velocity 0.5 m behind the boom section. 33
Figure 4.9: TKE 0.5 m behind the boom section. 34
Figure 4.10: Streamwise velocity 2m behind the boom section. 35
Figure 4.11: Vertical velocity 2m behind the boom section. 35
Figure 4.12: TKE 2 m behind the boom section. 36
Figure 5.1: CAD model of the sprayer used in the simulations. 38
Figure 5.2: Dimensioned drawing of the sprayer showing major dimensions in meters (m) and in vehicle widths (W). 39
Figure 5.3: Model of the domain size for the simulation with the sprayer located within the domain. All dimensions in m and vehicle widths [W] 40
Figure 5.4: Mesh shown on the boundaries of the simulation domain and on the sprayer body.. 41
Figure 5.5: Mesh on a plane running through the tires of the sprayer. 42
Figure 5.6: Mesh on a plane 82" From the sprayer wheels. 42
Figure 5.7: Extent of the Refined Wake Zone – dimensions in meters 43
Figure 5.8: Exterior faces meshed in the refined zone wake. 44
Figure 5.9: Refined wake zone mesh on a plane through the tires. 44
Figure 5.10: Refined zone wake on a plane 2.08 m from the tires. 45
Figure 5.11: Refined wake zone mesh on a plane 3.45 m from the tires. 45
Figure 5.12: Domain with boundary conditions labeled. V_{in} is the assigned inlet velocity, V_{plane} is the assigned velocity of the ground plane, $V_{tractor}$ is the velocity of the sprayer. 47
Figure 5.13: Monitor of the residual in continuity equation for the simulation of the sprayer with the low boom height and low vehicle speed condition (Case 1). 49
Figure 5.14: Continuity residual showing Peak 1 (a), Valley (b), Peak 2 (c), and Floor (d). 50
Figure 5.15: Centerline profiles of streamwise velocity 0.43 m behind the sprayer from 1580-1695 iterations (a) and from 1760-1875 iterations 51
Figure 5.16: Centerline profiles of TKE 0.43 m behind the sprayer from 1580-1695 iterations (a) and from 1760-1875 iterations 51
Figure 5.17: Centerline profiles of streamwise velocity 1.40 m behind the sprayer from 1580-1695 iterations (a) and from 1760-1875 iterations 52

Figure 5.18: Centerline profiles of TKE 1.40 m behind the sprayer from 1580-1695 iterations (a) and from 1760-1875 iterations 52
Figure 5.19: Force coefficient on the sprayer body per iteration. 53
Figure 5.20: 3D visualization of TKE in the wake of the sprayer. 54
Figure 5.21: 3D visualization of the wake as a region with streamwise velocity less than 87.5% of the freestream, where the free stream velocity is 11 m/s 55
Figure 5.22: Streamlines showing airflow patterns around the sprayer. 56
Figure 5.23: 3D visualization of vorticity in the vertical (y) direction, counterclockwise is positive. 57
Figure 5.24: Lateral development of the wake visualized by streamwise velocity contour plots at the centerline (a), a plane next to the tank edge (b), a plane through the tires (c), down boom locations of 3.45 m (d), and 6.78 m (e), ... 59
Figure 5.25: Velocity vectors showing the secondary flow field through the nozzles of the agricultural sprayer. 60
Figure 5.26: Velocity vectors showing the secondary flow field in a vertical transverse plane 0.9 m behind the boom of the agricultural sprayer. 61
Figure 5.27: Velocity vectors showing the secondary flow field in a vertical transverse plane 5 m behind the boom of the agricultural sprayer. 62
Figure 5.28: Wake region where the fluid velocity is less than 87.5% of the freestream for the low boom height and slow travel speed (Case 2). The freestream velocity in this simulation is 4 m/s. 63
Figure 5.29: Streamlines for the low boom height and slow travel speed (Case 2). 64
Figure 5.30: TKE for the low boom height and slow travel speed (Case 2) 64
Figure 5.31: TKE for the low boom height and slow travel speed (Case 2) plotted for low turbulence values. 65
Figure 5.32: Normalized streamwise velocity for Case 1 and Case 2 at three locations downstream of the boom, 0.43 m, 0.79 m, and 1.40 m. The plots are located at the centerline (a), next to the tank (b), through the wheels (c), and at distances down boom from the tire of 2.08 m (d), 3.45 m (e),5.11 m (f) and 6.78 m (g). 69
Figure 5.33:Comparing normalized turbulent kinetic energy (a) to turbulent kinetic energy (b) for the profile at the centerline 0.43 m behind the sprayer. 70

Figure 5.34: Wake of the sprayer displayed as the region where the velocity is less than 87.5% of the freestream for the high boom height and fast travel speed (Case 3) simulation. 71
Figure 5.35: Streamlines for the high boom height and fast travel speed (Case 3) simulation. ... 72
Figure 5.36: TKE for the high boom height and fast travel speed simulation. 73
Figure 5.37: Wake of the agricultural sprayer visualized with vertical (y) vorticity for the high boom height and fast travel speed simulation (Case 3). 73
Figure 5.38: Progression of the wake visualized as streamwise velocity at the centerline (a), a plane next to the tank edge (b), a plane through the tires (c), down boom locations 3.45 m (d), and 6.78 m (e). 75
Figure 5.39: Plots showing normalized streamwise velocity to compare the low boom height and fast travel speed (Case 1) simulation to the high boom height and fast travel speed (Case 3) at three downstream locations, 0.43 m, 0.79 m, and 1.40 m, to visualize downstream recovery of the wake. The plots are made at the centerline (a), next to the tank (b), through the wheels (c), and at distances down boom from the tire of 2.08 m (d), 3.45 m (e), 5.11 m (f) and 6.78 m (g). Note that the sprayer boom is in the high position. 79
Figure 5.40: Velocity vectors in a cross-sectional plane aligned with the nozzles of the sprayer for the high boom height and fast travel speed (Case 3) simulation. 81
Figure 5.41: Velocity vectors in a cross-sectional plane 0.9 m behind the sprayer boom for the high boom height and fast travel speed (Case 3) simulation. 81
Figure 5.42: Velocity vectors in a cross-sectional plane 5 m behind the sprayer boom for the high boom height and fast travel speed (Case 3) simulation. 82
Figure 5.43: Progression of the wake visualized using profiles of turbulent kinetic energy at the centerline (a), a plane next to the tank edge (b), a plane through the tires (c), down boom locations of 2.08 m (d), 3.45 m (e), 5.11 m (f), and 6.78 m (g). 87
Figure 5.44: Streamwise velocity along a line close to the nozzles where spray initially interacts with the flow. 88
Figure 5.45: Turbulent kinetic energy along a line close to the nozzles. 89
Figure 5.46: Comparison between 2019 field data for sprayer with a low boom height and the low boom height and fast travel speed (Case 1) simulation. 90
Figure 5.47: Top view showing the four wake zones behind the agricultural sprayer. 91
Figure A.1: Image of the agricultural sprayer with the anemometer frame attached to the boom. 2

Figure A.2: Locations of anemometers mounted to the agricultural sprayer during field tests. Dimensions are in inches. 3
Figure A.3: Field data captured at a boom height of 28 in above the ground. The local mean velocity (u) is normalized with the effective external velocity (U_∞) accounting for wind effects. 3

Chapter 1: Introduction

In Saskatchewan, and in most of North America, the most common method of applying field crop pesticides is with a high-clearance boom sprayer. Pesticides are used to increase the productivity of crops by removing unwanted plants or insects from the field which would otherwise limit the growth of the desired crop. However, thirty to fifty percent of pesticides applied to fields drift away from the target location (Van Den Berg et al. 1999). While pesticides improve productivity of farmland, they can cause damage to neighbouring fields, native plants, and waterways when drift occurs. Efforts have been made to limit spray drift: the United Kingdom has adopted minimum buffer zones needed between sprayed crops and waterways (Butler Ellis et al. 2017), spray shields and other devices to change the airflow around sprayers have been developed (Tsay et al. 2002), and there is a knowledge base for operator controlled variables that cause spray drift (Nuyttens et al. 2007). Although significant progress has been made in modeling and recommending methods for reducing spray drift, there is limited knowledge of how the airflow around a high-clearance boom sprayer affects spray drift.

The design of a high-clearance agricultural sprayer varies between different manufacturers, but generally the vehicle has significant ground clearance of roughly 1.5 m with a large boom that is between 20 and 30 m long. For most sprayers, the boom is mounted on the rear of the vehicle, but in some cases the boom is front-mounted. These sprayers can travel up to 48 km/h (13.3 m/s), but much slower speeds are used for spraying operations, generally 14-40 km/h (4-11 m/s). The nozzles which spray the pesticides are spaced along the boom at about 0.5 m intervals. The spray solution is held in a large tank mounted on the chassis of the vehicle and a pump is used to deliver the pesticide to the nozzles. Figure 1.1 shows a high clearance boom sprayer with a rear-mounted 24 m boom.

Figure 1.1: Image of a high-clearance boom sprayer with a rear-mounted boom parked in a soybean field near Dundurn SK.

1.1 Motivation

Research into the air flow field around agricultural sprayers is quite limited. Wind tunnel studies (Teske et al. 2015; Teske, Thistle, et al. 2016a; Teske, Thistle, et al. 2016b) have been made which study the vehicle wake, but these studies were limited because the vehicle model does not have spinning tires, and changes in the height of the boom and different vehicle speeds were not tested. Comparison of field data and computer simulations (H. Landry and Wolf 2019) have also been made, but this single study was limited by modeling the wake using only the turbulent kinetic energy instead of looking at the individual velocity components to better understand the air flow field of the vehicle. A comprehensive study of the wake of an agricultural sprayer using computational fluid dynamics (CFD) is needed to better understand features of the air flow field surrounding the vehicle that could potentially contribute to spray drift.

1.2 Objectives

The objective of the research described in this thesis is to accurately model the air flow field and wake of a generic agricultural boom sprayer to determine the properties of the wake and any features of the vehicle that could cause spray drift to occur. The air flow is modeled using CFD and the results are compared with available literature and field tests that occurred in October 2019 (Appendix A). The field tests only serve as a tool for comparison to the CFD results and are not used to formally validate the simulation.

The scope of the research is limited to a steady Reynolds Averaged Navier-Stokes (RANS) simulation. Using a steady RANS approach allowed a realistic simulation of the sprayer to be performed with a finite sized grid and within the limited simulation time. The mesh used was unstructured and spray droplets were not considered, hence spray drift was not simulated. The sprayer was simulated in a no-wind condition to only show the sprayer wake.

1.3 Research Contribution

This thesis will provide new insights to better model spray drift. Current drift models do not account for any air flow effects caused by the sprayer body or boom; instead, the only parameters used are the ambient wind, vehicle speed, and nozzle type. With further increases to the accuracy of drift modeling there will be increases to the efficiency of agricultural spraying. A reduction in spray drift will lead to lower amounts of pesticides needed, financial savings to farmers, increased productivity of cropland, and less contamination of waterways and neighbouring fields.

1.4 Outline of the Thesis

This thesis contains six chapters. The first chapter introduces the research problem, motivation, and contribution. The second chapter is a literature review of spray drift and investigations into the wake of an agricultural sprayer. The third chapter investigates the grid required to simulate the flow around a circular cylinder. The fourth chapter utilizes the grid from the third chapter and applies it to a section of an agricultural sprayer boom. The fifth chapter presents the simulation of one-half of the entire agricultural sprayer at three different operating conditions. The sixth chapter presents the conclusions of this research and offers suggestions to farmers and manufacturers of agricultural sprayers on how to control the sprayer wake to reduce the potential for spray drift.

Chapter 2: Literature Review

The study of agricultural sprayers and spray drift is a very broad topic. The work of this thesis is limited to the application of pesticides on ground crops. Several studies exist which use CFD to model spray drift in fruit orchards (Delele et al. 2005; Endalew et al. 2009), but these are only of minor importance to this thesis. Pesticides can be applied to ground crops through different methods including by person with a spray bottle or backpack (Thistle et al. 2017), with an aircraft, or with a ground vehicle. There is a larger body of literature for aerial spraying due to the belief that aerial spraying is more likely to drift, and it becomes a dual area of study since aerial firefighting is performed in a method like aerial spraying. For ground spraying at a scale large enough to cover the average farm in Saskatchewan there are two options, the first being a tow-behind unit which can be attached to a tractor and pulled through the field, and the second is a self-propelled sprayer, which is also known as a high-clearance sprayer.

Spray drift is a major concern for environmental protection, since it is known that up to 30%-50% of pesticides applied to crops are emitted into the atmosphere (Van Den Berg et al. 1999). Spray drift is increased by atmospheric effects such as high wind speeds (Gil et al. 2015), by droplet size (Gil and Sinfort 2005), or operator controlled variables of the sprayer (Nuyttens et al. 2007). Of the operator controlled variables it is known that increasing vehicle velocity and increasing boom height both increase the potential for spray drift (Murphy, Miller, and Parkin 2000).

European studies on spray drift tend to consider the tow-behind units (Baetens et al. 2007; Nuyttens et al. 2007), but only consider vehicle speed and boom height and not the aerodynamic effects of the vehicle on spray drift. Research from Canada and the United States tends to consider high-clearance sprayers and looks to characterize the wake of the vehicles (Teske, Thistle, et al. 2016a; 2016b; Landry et al. 2019). The research for the wake of a self-propelled sprayer is being used to develop a drift model based on the current AGDISP (AGricultural DISPersal) computer code model for aerial spraying (Teske et al. 2009).

The research conducted by Teske et al. (2009; 2015; 2016a; 2016b) was focused on wind tunnel measurements of a $1/25^{th}$ scale model of a generic agricultural sprayer. The work of Landry and Wolf (2019) was focused on field measurements of two different models of sprayer and early

CFD work to compare the simulated and measured wakes of a large agricultural sprayer. Both research studies have concluded that the wake of the high-clearance sprayer is complex, and the structure of the wake is influenced by several different parts of the sprayer. Landry and Wolf (2019) described the wake using turbulence kinetic energy, showing the wake as a region of highly turbulent airflow. Teske et al. (2015; 2016a; 2016b) considered the mean velocity and dynamic pressure of wake of the sprayer in all three directions.

The study by Landry and Wolf (2019) showed a region of high turbulence generated by the rotating tires that is not represented by Teske et al. (2015; 2016a; 2016b) since in their wind tunnel experiments the sprayer wheels were not allowed to rotate. Landry and Wolf (2019) were also able to show that at a low speed of 7.2 km/h (2 m/s) highly turbulent regions are limited to just air flow around the vehicle body and rotation of the tires with no meaningful turbulence generated by the boom. When the speed of the sprayer is increased to 28.8 km/h (8 m/s) the entire vehicle generates appreciable turbulence, but there is a region of higher turbulence behind the sprayer because of the vehicle body and the rotating tires. Additionally, it was shown that simple modifications to the sprayer such as including mudguards will reduce the turbulence from the tires.

Measures have been undertaken to reduce spray drift. Spray shields are added to sprayers to protect the nozzles from wind to reduce drift (Tsay et al. 2002). The effectiveness of spray shields varies based on the type used and whether the experiments were performed in laboratory settings or in the field. Spray shields have been shown to reduce drift by 33% to 84% depending on the design of the shield (perforated vs. solid) and wind conditions (Wolf et al. 1993). CFD simulations of various types of spray shields show that the best conditions for reducing spray drift are shields that create a lower velocity in the area of spraying, and drift is reduced further with aerofoil-type shields that direct air downwards behind the nozzle to force droplets towards the ground (Tsay et al. 2002).

CFD has been used to model different types of agricultural spraying. Drift models have been made which track particles flowing from nozzles into a cross wind (Baetens et al. 2007), modeling spray from a mistblower (Weiner and Parkin 1993), and flow from a forestry airblast sprayer (Sidahmed and Brown 2002). These studies were conducted using ANSYS Fluent, a commercially available CFD code. The work of Weiner and Parkin (1993) and that of Sidahmed

and Brown (2002) are similar in that both are two-dimensional (2D) CFD studies and use the k-ε turbulence model. The work previously discussed by Tsay et al. (2002) is also a 2D simulation of the airflow around the spray nozzle, but includes some of the geometry of the sprayer boom to model a spray shield. Many of the existing models for spray drift do not consider the geometry of the vehicle that is applying the pesticides.

Simplification of the domain to understand spray drift has been necessary in many of the drift models to complete the simulations in a reasonable time. For example, the three-dimensional (3D) drift model by Baetens et al. (2007) required 65,000 CPU seconds (18 h) to complete the calculation necessary for one speed and boom height. These models were performed on a single core CPU with 1 GB of RAM. The growth in computational power of modern computers has made it possible for simulations of an entire high-clearance sprayer to be performed, like the work of Landry and Wolf (2019).

Holterman et al. (1997) have developed a well used and cited model for spray drift from a single nozzle in 2D that can be extended to 3D by simulating each nozzle individually. This model does not consider the wake of the spraying vehicle, instead only considering the height above the ground of the nozzle and the speed of the sprayer.

Chapter 3: Computational Fluid Dynamics and Benchmark Simulations of the Flow Over a Circular Cylinder

CFD is a numerical method for calculating complex fluid flows that would otherwise be impossible to solve analytically from the Navier-Stokes equations. The process works by dividing a fluid domain into control volumes, and within each control volume conservation equations are used to solve for the flow field. CFD simulations can be performed for a flow field that changes with time (transient), or a steady flow field. When the Reynolds Averaged Navier-Stokes equations (RANS) technique is used a so-called turbulence model is required to represent the Reynolds stress terms. The RANS equation for conservation of momentum, in Einstein notation for a Cartesian coordinate system is given as Equation 3.1 (Siemens PLM Software 2019).

$$\rho\bar{u}_j\frac{\partial\bar{u}_i}{\partial x_j} = \rho\bar{f}_i + \frac{\partial}{\partial x_j}\left[-\bar{p}\delta_{ij} + \mu\left(\frac{\partial\bar{u}_i}{\partial x_j} + \frac{\partial\bar{u}_j}{\partial x_i}\right) - \rho\overline{u'_\iota u'_\jmath}\right], \tag{3.1}$$

where,

$\rho\bar{u}_j\frac{\partial\bar{u}_i}{\partial x_j}$ = mean momentum of a fluid element from unsteadiness and convection in the flow,

ρ = fluid density,

$\bar{f}_i$ = body forces acting on the fluid element,

$\bar{p}\delta_{ij}$ = mean pressure stresses,

δ_{ij} = Kronecker delta,

$\mu\left(\frac{\partial\bar{u}_i}{\partial x_j} + \frac{\partial\bar{u}_j}{\partial x_i}\right)$ = viscous stresses,

μ = dynamic viscosity,

$-\rho\overline{u'_\iota u'_\jmath}$ = Reynold Stress term, from the fluctuating velocity field,

$\bar{u}$ = mean velocity, and

u' = fluctuating velocity.

3.1 Turbulence Modeling

To numerically solve the RANS equations for turbulent flows, a turbulence model must be introduced to solve for the Reynolds stress terms. For this thesis, the shear-stress transport (SST) model as described by Menter (1994) is chosen as the turbulence model. The SST model uses two existing eddy viscosity models, the k-ε model and the k-ω model. The SST models plays to the strengths of each of the two models: the k-ω can predict near wall effects, and the k-ε works well for free shear flow. A blending function is used to control which model is being used. Menter (1994) describes the SST model as the choice model for aerodynamic applications including flows with adverse pressure gradients.

3.2 Using CFD for Complex Flow Simulations

CFD has been used to study many different flows. The work of Landry and Wolf (2019) shows the application of the method to flows around agricultural sprayers. Other very large vehicles that have been studied with CFD include: tractor-trailers (Hsu and Davis 2010), naval ships (Forrest and Owen 2010; Watson et al. 2019), single seat research aircraft (Elmiligui, Abdol-Hamid, and Parlette 2015), multi-engine aircraft (Casadei, Könözsy, and Lawson 2019), and high speed trains (Yao et al. 2013). There is significant diversity in the types of flows studied with CFD; which shows the versatility of the software when used cautiously. While the operating conditions, boundary conditions, and physics of all these examples are different, lessons may be learned from these simulations on best practices for predicting flows over large vehicles, such as agricultural sprayers.

Learning from these simulations and adapting them to the agricultural sprayer was done by considering the similarities between these simulations and the problem at hand. Starting with ships, in several studies (Forrest and Owen 2010; Watson et al. 2019) the inlet conditions considered an atmospheric boundary layer. In the literature an atmospheric inlet boundary layer condition was used for studies that compare to field data, whereas inlet conditions from wind tunnel tests were used for CFD studies that compare to wind tunnel data (Viola et al. 2014). The idea of comparing naval testing to agricultural testing is logical because in both settings there are minimal features to block the flow before it reaches the test object. This is truer for the ocean

than a farm field where barns, grain bins, small towns, tree belts, and other features may obstruct and influence the approach flow. As well, roughness of the ground and height of the crops when spraying occurs could affect the flow near the ground.

Considering the art of grid creation, the literature shows both similarities and differences between many studies. Generally, with complex studies, the mesh is unstructured, but a variety of element types are used: tetrahedral elements, hexahedral elements (Viola et al. 2014), or a highly orthogonal method of hexahedral elements in a trimmed or cutcell mesh (Yao et al. 2013), or polyhedral elements (Nasir et al. 2012). In the available literature, the meshes are most refined on the surface of the body being considered. Understanding the flow being studied will aid in the design of mesh refinement, such as on the leading edge of an aircraft wing, as done by Casadei, Könözsy, and Lawson (2019).

3.3 Benchmark Flow Simulations

Significant fundamental studies have been devoted to understanding the flow around basic non-streamlined shapes immersed in a fluid flow. Basic shapes include cylinders and square prisms. Knowledge of the flow around these isolated bodies is important, but many industrial flows occur around bodies that are made up of an arrangement of many of these shapes or are of completely different geometries. To model the flow around an entire agricultural sprayer the computational effort needed requires sacrificing some of the geometric complexity and refinement in the mesh being used to model the flow. In the present thesis research, to create a mesh for the entire agricultural sprayer and be confident in the results, it was necessary to benchmark the method using a known and well-studied body. The chosen body was a two-dimensional cylinder because the sprayer boom is often made up of a collection of many circular long slender tubes welded together into a truss arrangement.

3.4 Domain, Geometry, and Boundary Conditions

The benchmark flow simulation used a cylinder of diameter D = 40 mm, similar in size to the 1.5” (38.1 mm) truss members on the sprayer, oriented such that the inlet to the domain would create a flow across the cylinder. The domain and cylinder had a length of 4D in the spanwise direction, the inlet was 10D upstream of the center of the cylinder, as were the top and bottom walls. The outlet was located 30D from the center of the cylinder to give sufficient length for the

wake to develop and dissipate. The size of the domain was similar to the work of Alves Portela, Papadakis, and Vassilicos (2017), who studied the turbulence cascade behind a square prism. Figure 3.1 shows the domain that was used for these simulations. The coordinate system is located at the center of the cylinder with positive *x* oriented downstream, and positive *y* oriented upwards. The streamwise velocity is denoted by the letter *u*, with *U* representing the inlet flow in the streamwise direction.

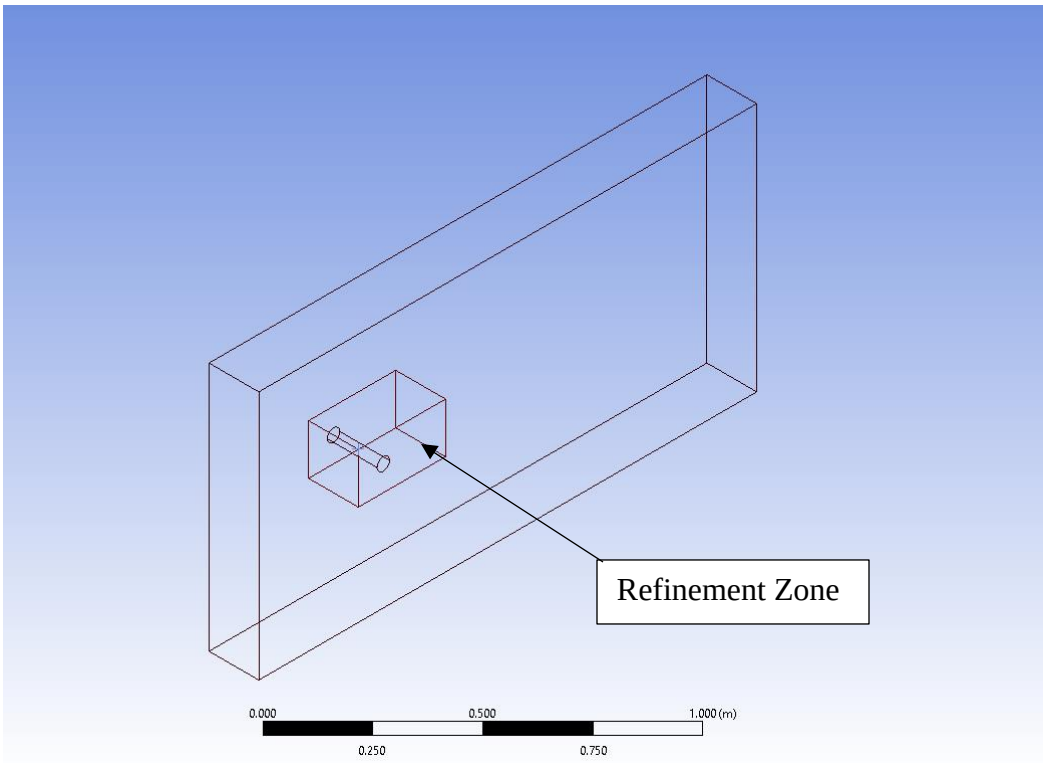

Figure 3.1: The domain used to simulate the flow over a cylinder.

A proper choice of boundary conditions is necessary to ensure the physics of the problem are properly modelled. The inlet was modeled as a uniform velocity inlet, with a 6 m/s inlet velocity and a turbulence intensity of 5%. The inlet conditions were chosen to represent the median velocity of the sprayer travel speed, and turbulence was chosen to represent the turbulence observed in field conditions. The outlet was a pressure outlet. The top and bottom walls were modeled as slip walls, and the sides of the domain which run perpendicular to the cylinder were symmetry planes. The inlet velocity and diameter of the cylinder leads to a Reynolds number of Re = 16,000, calculated using the properties of air at 15°C. The Reynolds number is calculated using Equation 3.2.

$$Re = \frac{\rho U_\infty D}{\mu}, \tag{3.2}$$

where,

Re = Reynolds Number,

ρ = fluid density,

U_∞ = free stream velocity in the streamwise direction,

D = diameter of the cylinder in the flow, and

μ = dynamic fluid viscosity.

3.5 Description of the Meshing Methods and Meshes Used

Using ANSYS Fluent, different meshes were designed to determine how mesh refinement near the cylinder and in the near wake affects the far field. The element size is defined in three different zones of the simulation: on the surface of the cylinder, in the region very close to the cylinder known as the refinement zone, shown in Figure 3.1, and in the far field. The far field mesh had the same default element size and growth rate for all simulations. Meshes were generated with ANSYS Meshing using assembly meshing techniques. Two types of elements were tested: cutcell and polyhedral. Mesh elements are characterized in four groups: far field, coarse, medium, and fine. The element sizing is based on the cylinder diameter, as shown in Table 3.1.

Table 3.1: Element sizing for mesh generation

Element Name	Size Relative to Cylinder Diameter	Size [mm]
Far Field	4D	160
Coarse	D/10	4
Medium	D/20	2
Fine	D/40	1

A total of ten meshes were made, plus an additional three meshes that had inflation layers on the cylinder surface. An inflation layer is a very small element on the surface of a geometric body created with the intention of giving better resolution in the boundary layer. Different meshes were generated by changing the element sizing in either the refinement zone or on the surface of the cylinder. Furthermore, inflation layers were added to one mesh to determine the effect that inflation has on the far wake. To create the meshes it was determined that the cylinder surface should be the most refined, followed by the refinement zone, with the far field being the coarsest region. No meshes were made which had surface elements larger than refinement zone elements. The meshes were evaluated using minimum orthogonal quality, maximum orthogonal skewness, and maximum aspect ratio. Orthogonal quality assesses the mesh shape quality, orthogonal skew represents how symmetric an element is, and aspect ratio represents the size transition from one element to another. It was desired to keep orthogonal quality above 0.25, skewness below 0.8, and aspect ratio less than 10. Table 3.2 shows the statistics for the meshes that were tested, and Figure 3.2 shows an example mesh.

Table 3.2: Details of tested meshes and associated quality.

Mesh Name	Number of Elements	Surface Size	Refined Zone Size	Orthogonal Quality Min	Orthogonal Skew Max	Aspect Ratio Max
Poly I	294,298	Coarse	Coarse	0.362	0.638	8.91
Poly II	328,193	Medium	Coarse	0.366	0.634	9.29
Poly III	480,340	Fine	Coarse	0.372	0.628	9.73
Poly IV	1,555,886	Medium	Medium	0.397	0.603	9.94
Poly V	1,671950	Fine	Medium	0.388	0.612	10.1
Cutcell I	278,294	Coarse	Coarse	0.632	0.205	4.65
Cutcell II	336,298	Medium	Coarse	0.431	0.412	7.39
Cutcell III	582,399	Fine	Coarse	0.402	0.375	6.45
Cutcell IV	1,423,482	Medium	Medium	0.431	0.412	7.39
Cutcell V	1,629,354	Fine	Medium	0.402	0.375	6.45
Meshes with Inflation Layers						
Poly II Inf. 1	335,404	Medium	Coarse	0.272	0.728	10.5
Poly II Inf. 2	337,626	Medium	Coarse	0.349	0.651	10.0
Poly II Inf. 5	345,697	Medium	Coarse	0.347	0.652	11.7

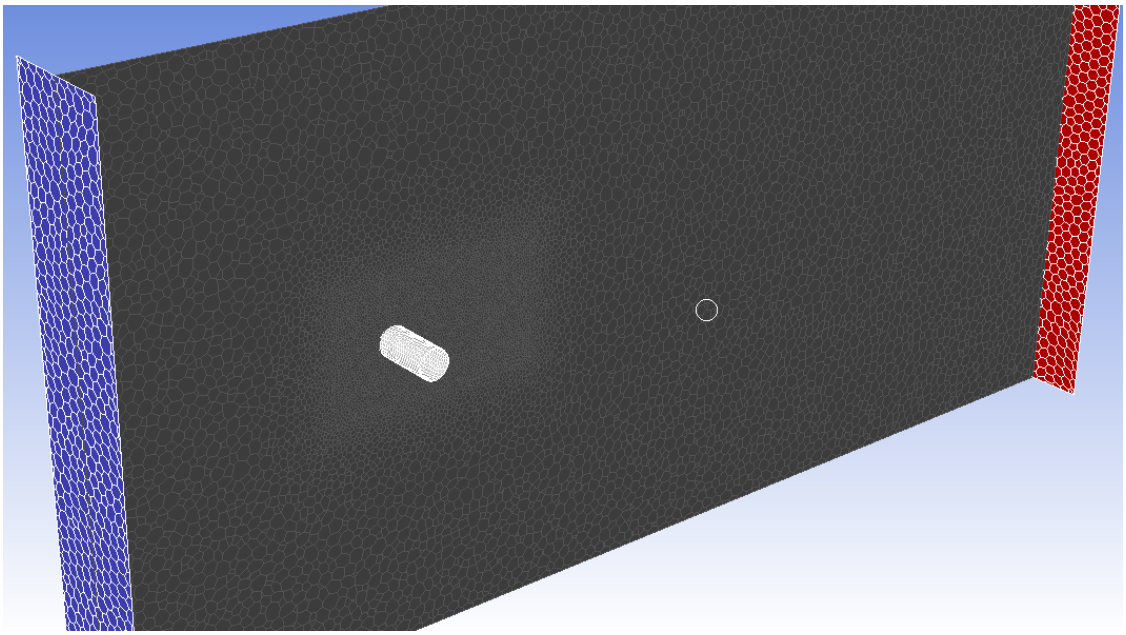

Figure 3.2: Poly I mesh showing elements on a plane through the middle of the domain, on the inlet, outlet, and the cylinder surface.

3.6 Results

Results are described in three zones for the cylinder: wake data, centerline data, and wall data. To describe the wake, velocity profiles are examined at various points downstream of the cylinder to show the shape of the wake and compare the data with the literature. The centerline is a line starting at the inlet, ending at the outlet, and running through the middle of the cylinder. The velocity along the centerline will give good information on the recirculation zone of the cylinder and the rate of recovery of the wake to the free stream velocity. Data was recorded on the wall of the cylinder, which can be used to show the pressure distribution and predict boundary layer separation points. Additionally, force coefficients and the base pressure coefficient are computed to give more values to compare to the literature.

3.6.1 Wake Velocity Profiles

The wake of a cylinder has been well studied by many researchers in wind tunnels and using CFD software in both RANS models and more complex models such as large eddy simulation (LES). Here, streamwise velocity profiles are considered at the rear edge of the cylinder x = 0.5D, and at two locations downstream, x = 2D and x = 6D. Two sources from the literature are used to compare the profiles. First, Norberg (1998) studied the flow over a cylinder using laser

Doppler velocimetry (LDV) in a wind tunnel, and second, Maryami (2020) focused on turbulent flow interaction with a cylinder, using hot wire anemometry. The Reynolds number for this study is Re = 16,000. From the data from Norberg (1998) the closest available Reynolds number is Re = 8,000, whereas Maryami (2020) had a Reynolds number of Re = 14,700.

Given the expectation of extending this work for use on extremely large CFD studies, it is expected to sacrifice mesh refinement near the body being considered. This sacrifice will lead to stronger deviation from experimental studies very close to the immersed body. It is expected however, even with a relatively coarse mesh, that the wake of the body far downstream should approximate the experimental results. Wake profiles will be presented starting at 6D downstream, and then moving closer to 2D and to 0.5D downstream of the cylinder.

3.6.2 Wake Velocity Profiles at x = 6D

Considering the far downstream location of x = 6D shows several significant results in the effort to create a meshing technique that will deliver realistic results with a relatively coarse mesh. Figure 3.3, Figure 3.4, and Figure 3.5 show results for polyhedral meshes, cutcell meshes, and meshes with inflation, respectively. From all the figures an interesting observation was made, as the mesh on the surface of the cylinder was further refined, the results became more asymmetric and less realistic. This is attributed to the introduction of vortex shedding on the surface of the cylinder, which is a true physical occurrence, but should not exist in a steady RANS calculation. The introduction of vortex shedding makes most of the highly refined meshes unsuitable for application on an agricultural sprayer, leaving only Poly I, Poly II, and Poly IV as acceptable. Additionally, the cutcell meshes (Figure 3.4) did not perform well for the far downstream profiles and were deemed unsuitable.

Figure 3.5 considered a mesh with inflation layers. It was found that the introduction of the inflation layers intensified the vortex shedding instability that was found in the simulations with very fine resolution on the cylinder surface. Two methods were tested to remove this instability. The first was by using a pseudo time step. This method uses the steady-RANS equations but introduces a “false time-step” term into the equations. Using this pseudo time step did remove the vortex shedding, but substantially increased the deficit shown behind the cylinder. The second method was by performing an unsteady simulation. This method simulated the flow over the cylinder for ten vortex shedding cycles and then averaged the results to give an averaged

unsteady flow field. In this simulation the vortex shedding did occur, but it was averaged out with time to give results that approximated the experimental results.

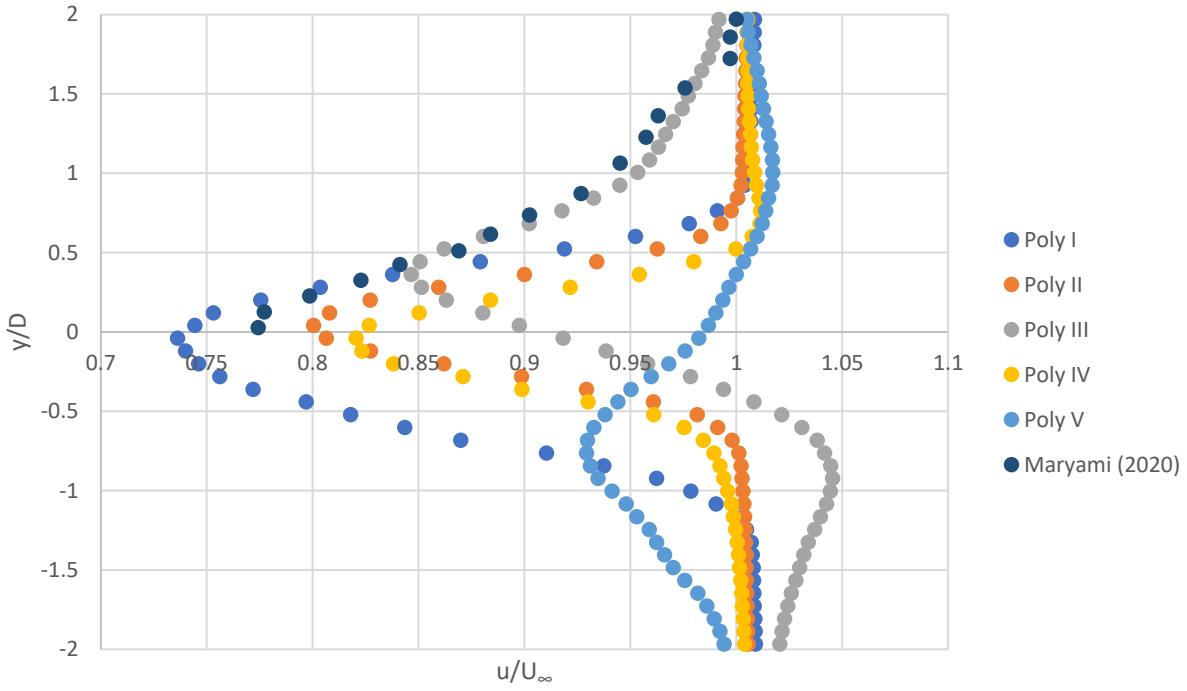

Figure 3.3: Comparison of velocity profiles for Polyhedral meshes at x = 6D downstream of the cylinder compared with data from Maryami (2020).

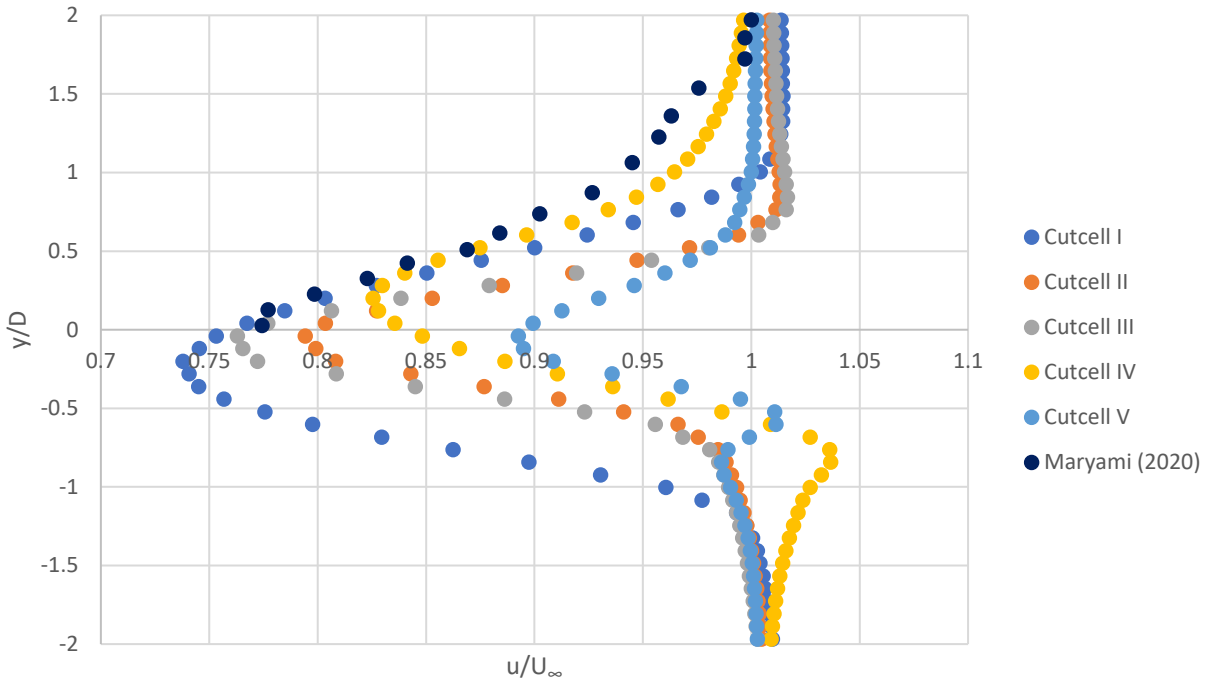

Figure 3.4: Comparison of velocity profiles for Cutcell meshes at x = 6D downstream of the cylinder compared with data from Maryami (2020).

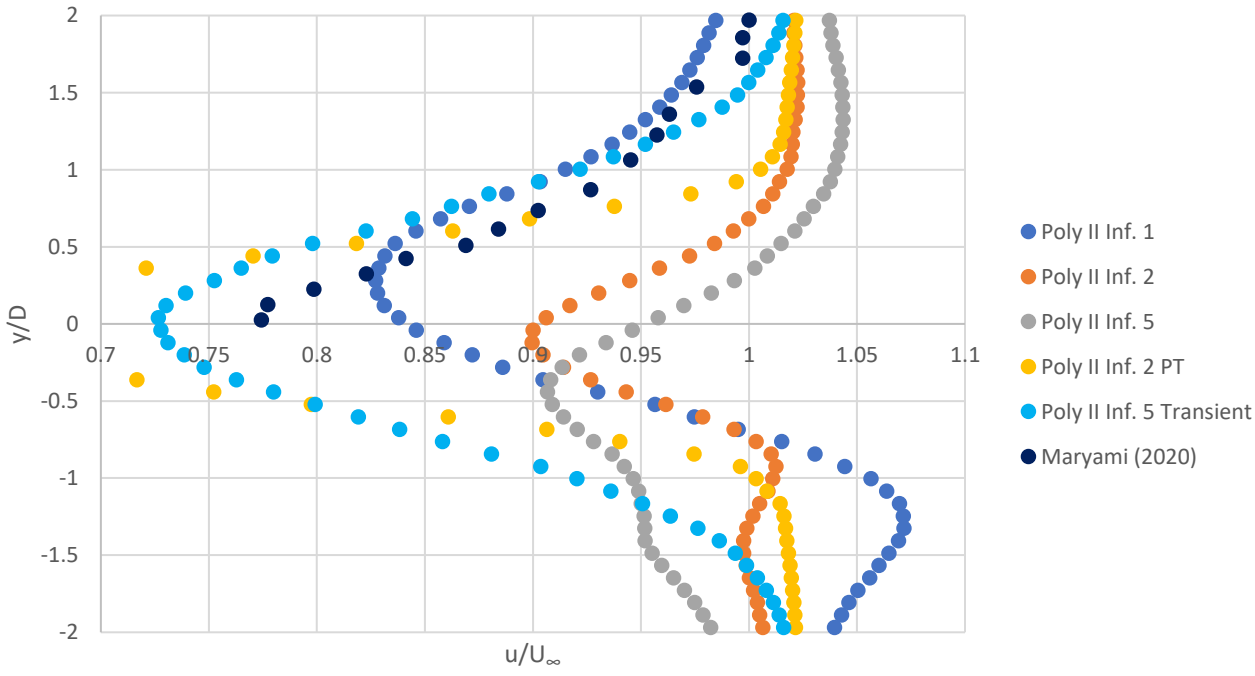

Figure 3.5: Comparison of velocity profiles for Poly II meshes with different numbers of inflation layers at x = 6D downstream of the cylinder compared with data from Maryami (2020).

3.6.3 Wake Velocity Profiles at x = 2D

At x = 2D downstream, shown in Figure 3.6, plots are shown for the three meshes that gave acceptable results at 6D downstream. This data is compared to the experimental work of Norberg (1998). All three simulations show good similarity to the experimental data (Norberg 1998), with the coarsest mesh, Poly I, giving the best approximation of the profile. Poly I showed both the highest acceleration above and below the cylinder, and the greatest deficit behind the cylinder. It can also be seen in Figure 3.6 that in the two more refined meshes, Poly II and Poly IV, there is a slight asymmetric feature; further emphasizing the result that a more refined mesh does not necessarily lead to a better result.

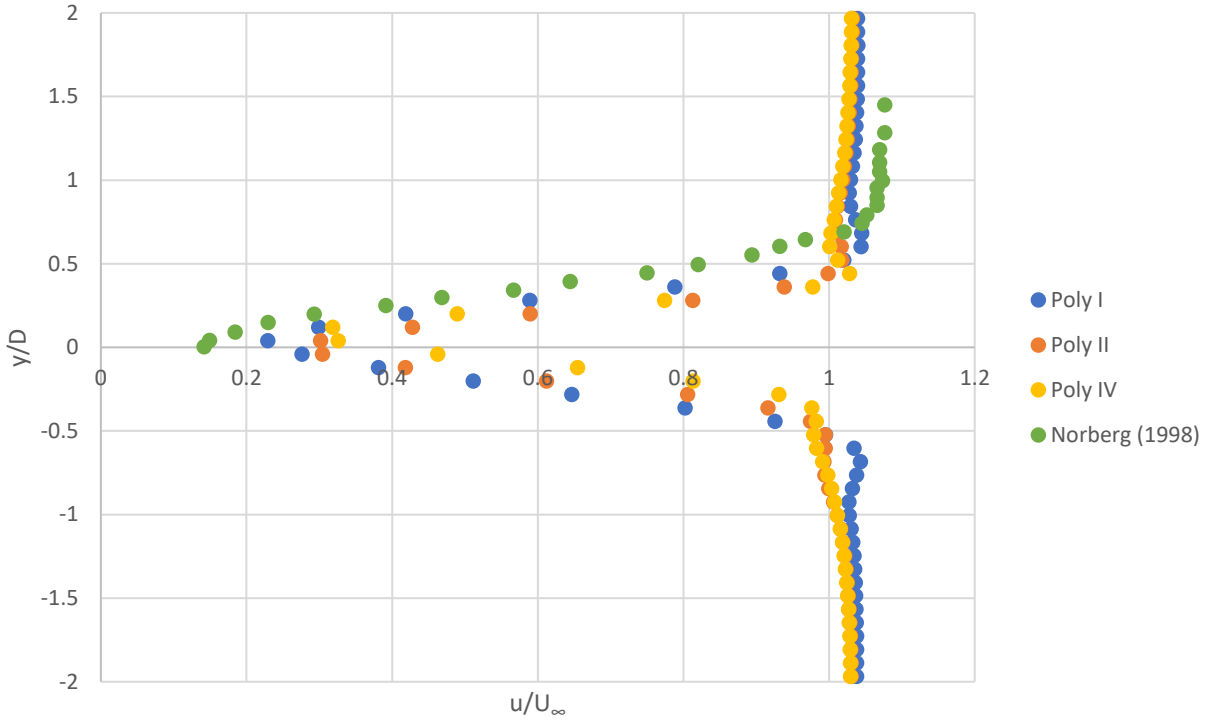

Figure 3.6: Comparison of velocity profiles for Polyhedral meshes at x = 2D downstream of the cylinder compared with data from Norberg (1998)

3.6.4 Wake Velocity Profiles at x = 0.5D

The downstream location of x = 0.5D is a line that is tangential to the rear surface of the cylinder, intersecting the rearmost point on the cylinder. Figure 3.7 compares the profiles of the three acceptable simulations to the experimental data from Maryami (2020). All three

simulations showed good results for most of the profile. Poly I showed the best fit to the accelerated flow above and below the cylinder, but for this profile the difference between Poly I and Poly II was quite small even though the size of the elements in Poly II is half that of Poly I. Poly IV showed a good approximation of the curve, giving very similar results to Poly II, but at a substantially higher computational cost.

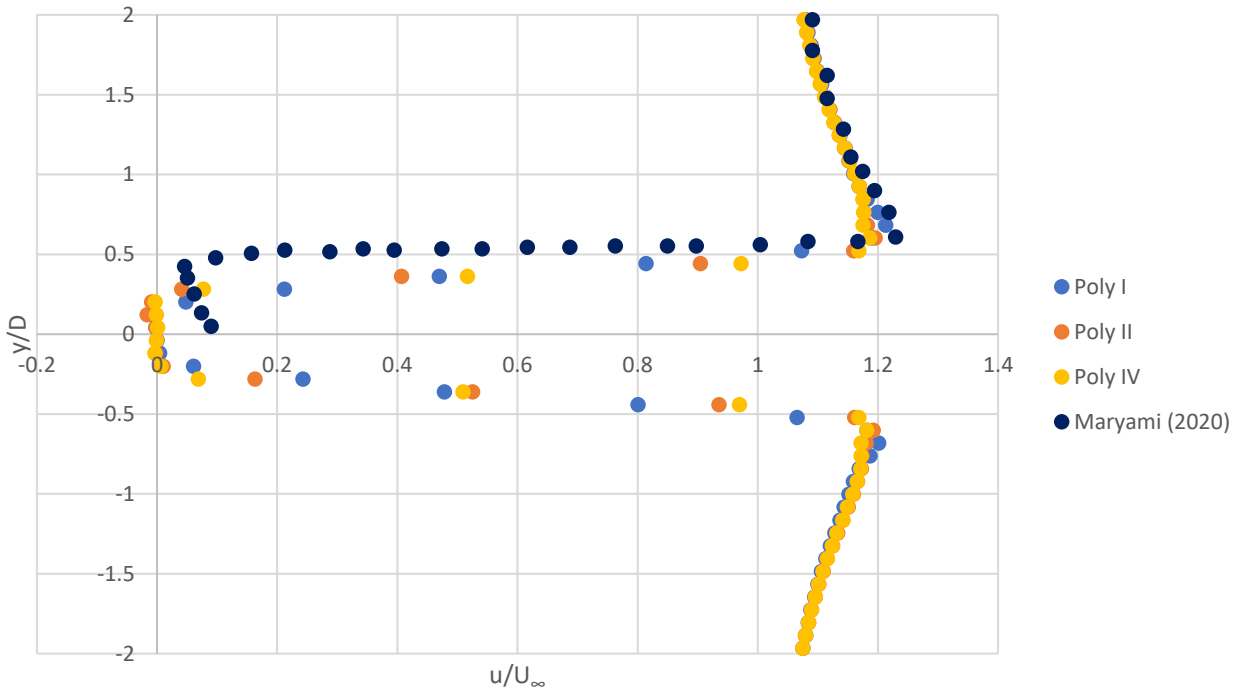

Figure 3.7: Comparison of velocity profiles for Polyhedral meshes at x = 0.5D behind a cylinder and comparing to two sets of data from the literature

3.6.5 Centerline Velocity Profiles

The centerline velocity profiles are used to describe what occurs along the x-axis from inlet to outlet of the domain while passing through the center of the cylinder. The line runs through the middle of the wake and is used by many researchers in wind tunnel and CFD studies to characterize the velocity deficit and recovery in the near wake. Norberg (1998) used the centerline profiles to characterize the flow around a cylinder in a wind tunnel at several different Reynolds numbers, with the experimental plots at Re = 10,000 being the closest to the Reynolds number of the current simulation (Re = 16,000).

Considering the Polyhedral mesh velocity profiles, including profiles that were deemed non-realistic earlier, some results are shown in Figure 3.8. Two observations were drawn from these studies. The coarser the mesh the less the overall profile will match the shape of the experimental work (Norberg 1998), with Poly I showing a very small deficit immediately behind the cylinder, and showing a much slower recovery to the free stream than the meshes which were more refined. However, increasing the refinement in the mesh showed the vortex shedding instability that was discussed earlier. Poly III and Poly V, where the finest element size was used on the surface of the cylinder, produced large instabilities in the centerline profile, further showing that this meshing style would not lead to a realistic result. Of the three meshes remaining, Poly I and Poly II show little variation between them, suggesting that the less computationally intensive mesh, Poly I, is a better choice. Poly IV gave a better downstream recovery of the velocity profile from 1.5D downstream onwards, but also did not fully capture the extent of the velocity deficit immediately behind the rear surface of the cylinder.

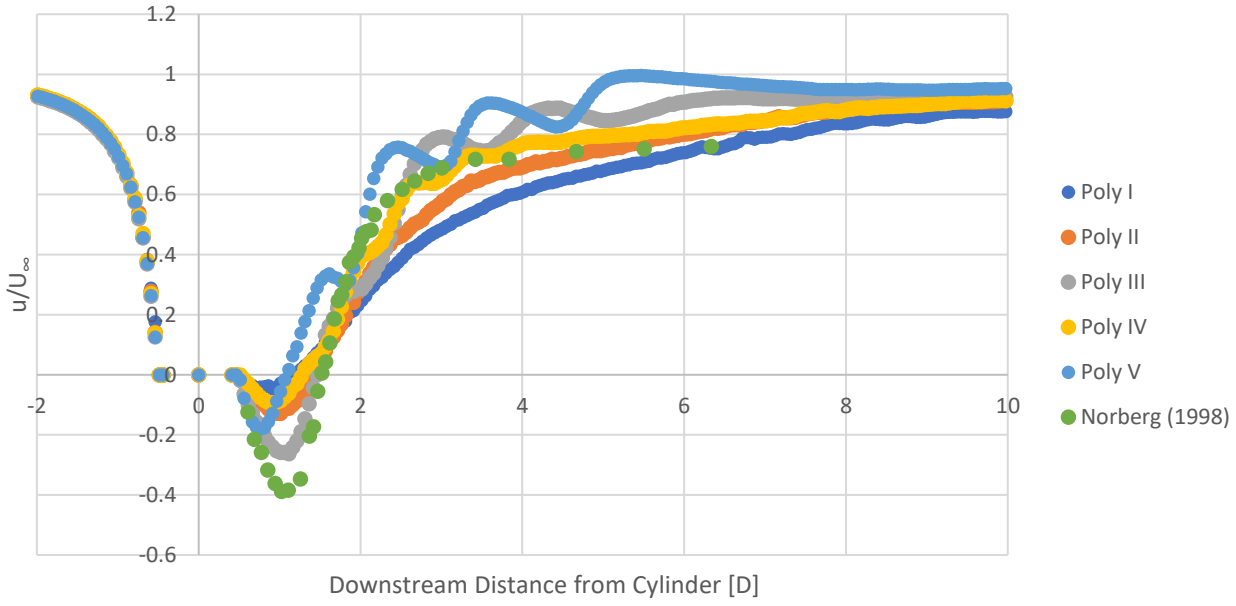

Figure 3.8: Comparison of streamwise velocity along the centerline of the wake of a cylinder using different polyhedral meshes.

Figure 3.9 shows the cutcell meshes which were eliminated earlier due to dramatic asymmetry shown in the wake plots. All the cutcell plots are showing the vortex shedding instability, due to the smaller size of a cutcell element versus a polyhedral element. Figure 3.10 shows the simulations that were conducted using inflation layers. The three steady-RANS studies that used inflation layers all show the vortex shedding instability. The pseudo-transient simulation did not show any vortex shedding, a favourable outcome, but the downstream recovery is a poor prediction of the experimental data (Norberg 1998). The transient simulation shows a realistic prediction of the flow: although the reversed flow zone behind the cylinder is predicted to be smaller than what was observed in the experimental results (Norberg 1998), the recovery to free stream is very accurate from 2D downstream onwards. Even though the transient simulation gave good results, it is not an acceptable method for larger simulations due to the dramatically higher computational costs to perform an unsteady simulation.

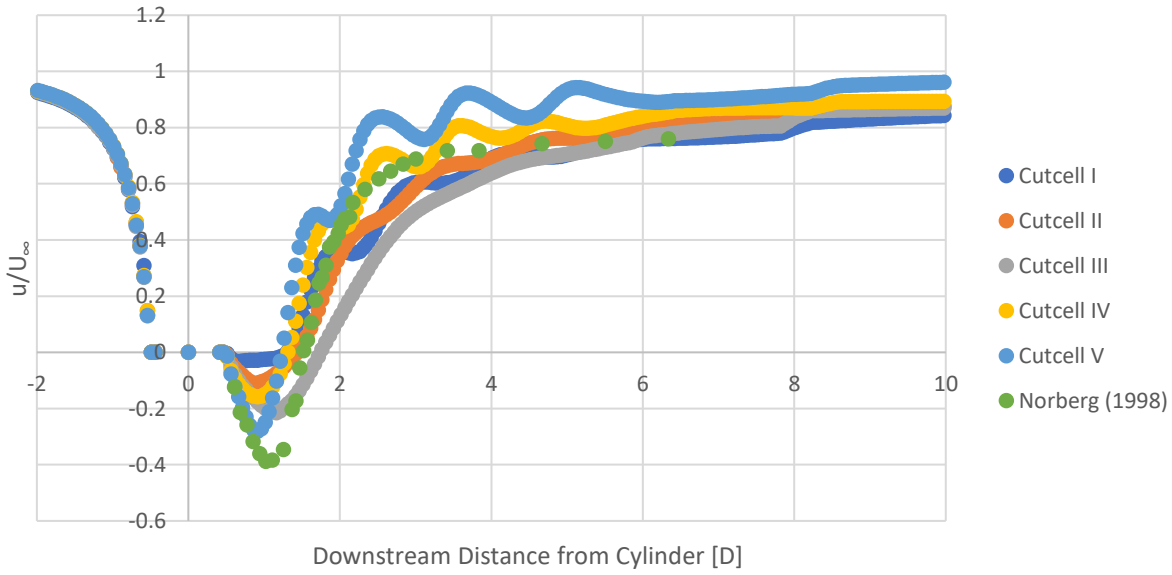

Figure 3.9: Comparison of streamwise velocity along the centerline of the wake of a cylinder using different cutcell meshes.

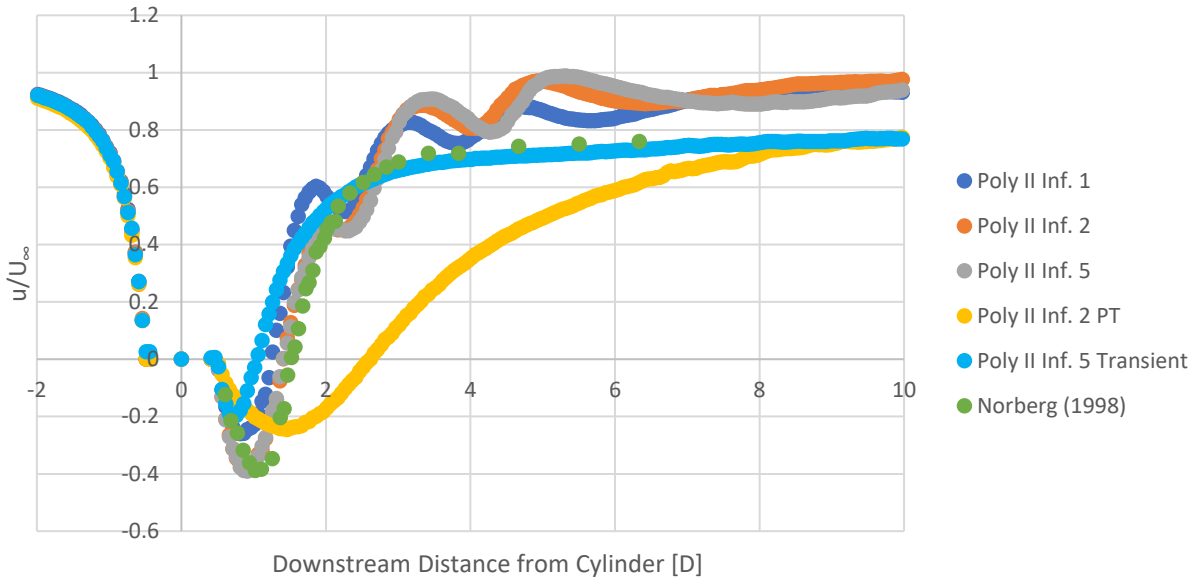

Figure 3.10: Comparison of streamwise velocity along the centerline of the wake of a cylinder using the Poly II mesh with different numbers of inflation layers.

3.6.6 Pressure Coefficient on the Cylinder Surface

One way to analyze the flow around the cylinder is to examine the pressure coefficient (c_p) on the surface of the cylinder in terms of the angular location θ (where $\theta = 0°$ is the forward stagnation point). Ong et al. (2009) and Catalano et al. (2003) show pressure coefficient data in their simulations of the flow over a cylinder using LES and RANS, respectively. The polyhedral meshes, Figure 3.11, show acceptable conformity to the simulations performed in the literature to 120°, and after the simulations give a higher pressure coefficient than the literature.

Comparisons to the data from Ong et al. (2009) ($Re = 3.4 \times 10^6$) and Catalano et al. (2003) ($Re = 1.0 \times 10^6$) are made very generally since their works have a far higher Reynolds number where the boundary layer is turbulent, whereas it is expected in this simulation, and for the actual sprayer, that the boundary layer is laminar. The expectation is that for a turbulent boundary layer, separation will occur at a greater angle than in a laminar boundary layer. The results of these current simulations tend to better follow the RANS results from Catalano et al. (2003), with a maximum coefficient of pressure occurring before $\theta = 90°$. Past the $\theta = 120°$ point on the cylinder the tested meshes do not follow the literature data; instead, they show a significantly higher base pressure coefficient than what either of the literature sources showed. The observation from the wall data is that the selected meshes will sacrifice the prediction of the

pressure on the wall to simplify the necessary mesh and provide realistic predictions of the wake far downstream of the cylinder.

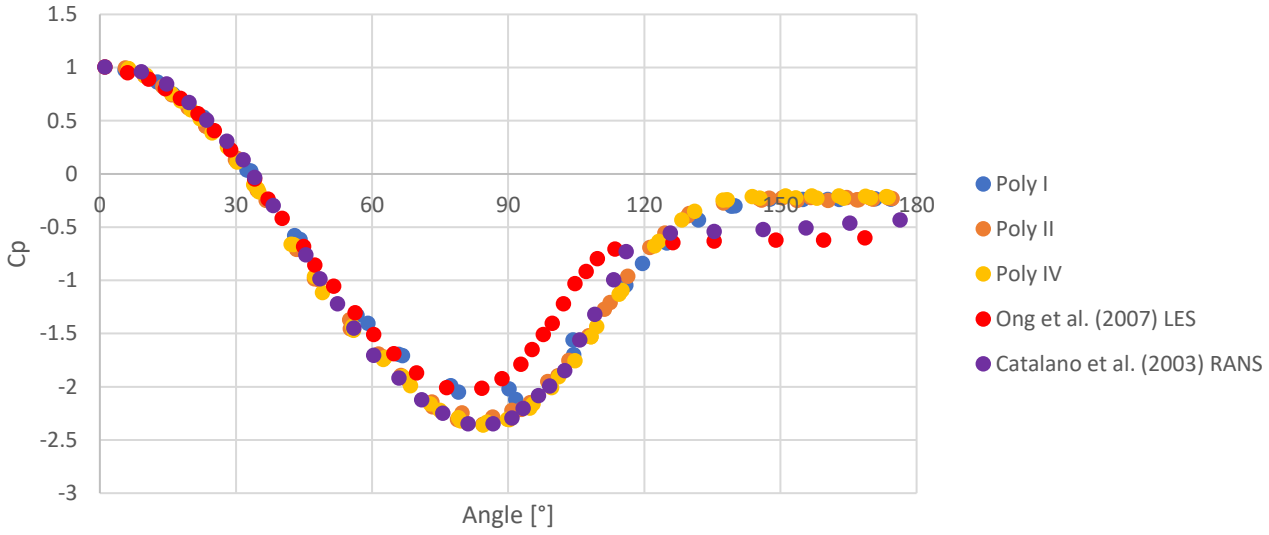

Figure 3.11: Pressure coefficient around a cylinder with polyhedral meshes

3.7 Discussion

The end goal of this series of simulations was to determine which meshes would result in a reasonably accurate simulation of the cylinder wake. Certain sacrifices were expected to be made to give reasonable predictions of the turbulent wake of the cylinder. The results suggest that decreasing the size of elements on the surface of the cylinder is counterproductive to producing a stable result in the simulation. But it is also shown that having smaller elements near the cylinder, and especially in the near wake region, helps to resolve the recirculating zone behind the cylinder where the velocity is reversing.

When creating a coarse mesh, it is important to identify the values which are important for the simulation and to choose the mesh sizing to optimize the accuracy of the desired values. It has been shown from the results that coarse meshes tend to give better results for the velocity downstream of the body, while a finer mesh gives better velocity information close to the body. Unfortunately, finer meshes introduced vortex shedding, an instability in a steady solution field, which made the finest meshes unsuitable for use in larger simulations. It is observed from this set of studies that it is not possible to accurately predict every part of a flow using a very coarse

mesh. But it is possible to generate a set of reasonably good results for selected variables and accept the imperfections that arise from performing such a coarse simulation.

3.8 Conclusion

The importance of understanding how coarse meshes behave should be known when performing large scale simulations on bodies that are too large for an extremely fine mesh (such as the agricultural sprayer). The cylinder studied in this problem had a surface area of 0.02 m^2. Using the coarse elements defined in this simulation resulted in approximately 1300 elements used on the surface of the cylinder, the medium elements required about 5000 surface elements, and the fine mesh used about 20,000 surface elements. Many published studies of the flow around a cylinder have used far more elements on the cylinder surface than this work and are often studied in 2D instead of 3D to allow for more refinement on the cylinder surface to better model all the effects in the flow. The numbers of elements used in these studies become unrealistic to be used on larger scale problems, such as the flow around an agricultural sprayer. To estimate the complexity of the number of necessary elements for the agricultural sprayer boom it will only be considered as three 40 mm cylinders running the full 24 m length of the boom. This results in 9 m^2 of surface area to cover, or 600,000 coarse elements, 2.26M medium elements, or 9M fine elements. If there were to be 500 elements to run the circumference of the cylinder, and each element was to have equal width and height, it would be necessary to have 142M elements on the surface of the three cylindrical tubes that make up some of the support structure of the boom. This quick “back of the envelope” calculation is meant to explain how unfeasible it becomes to use this type of mesh sizing to model flow around very large vehicles.

Considering all the meshes tested, the following recommendations are made for further studies:

1. The polyhedral meshing method seems to perform equal to or better than the cutcell method in most applications. The centerline velocity predictions from the cylinder flow simulation show that the polyhedral method is stable up to the medium element size, whereas cutcell meshes show instabilities at this level of refinement.

2. Instabilities in the solution arise from meshes that are too refined on the surface. With either fine meshes or inflation layers the model attempts to solve for vortex shedding, which is a true aspect of the flow over a cylinder but should not arise in a model solved

using the RANS equations. The suggestion here is to prevent the surface size from increasing to a small enough value to allow for vortex shedding to be observed and rely on the blending function in the SST turbulence model to predict what will happen in the near wall region.

3. Increasing refinement of the mesh near the cylinder wall leads to better prediction of the velocity field in the recirculation zone, but coarse meshes still provide good velocity predictions in the wake at the locations x = 2D and x = 6D downstream of the cylinder. In further tests of the performance of the mesh over a small section of the boom, the meshing methods used in the Poly I, and Poly IV meshes should be used as cases of the simplest and most complex meshes, respectively, that gave reasonable results.

The two meshing styles to be adopted for further studies on a small section of the boom are the Poly I and Poly IV meshes. Cutcell meshes at the same levels will be investigated, but with less detail to inflation layers and solution method. Table 3.3 provides information on the differences observed in the two meshing styles. The two methods show generally similar results if the prediction is acceptable or unacceptable, but the main difference is the Poly I mesh showed the recirculation zone behind the cylinder as an area of dead air with no velocity, where the Poly IV mesh showed this zone with having negative velocity about 75% smaller than the data from Norberg (1998). The results in Figure 3.8 from the Poly IV mesh do show that the location of the minimum velocity is the same as experimental results, and the shape of the curve is similar. Past the recirculation zone the velocity recovery from experimental data is like that of the Poly IV mesh. The Poly I mesh shows a slower than expected recovery explaining why it is underpredicting the minimum velocity in the far wake profiles. Both meshes show a tighter spread of the wake compared to Norberg (1998).

Table 3.3: Differences in the Poly I and Poly IV meshes to be carried forward for further study

Value	Poly I	Poly IV
Recovery Length	Good	Good
Minimum Velocity	Not Acceptable	Not Acceptable
Near Wake Profile x = 0.5 D	Acceptable	Acceptable
Mid Wake Profiles x = 2 D	Good (under prediction)	Good (under prediction)
Far Wake Profile x = 6 D	Good (lower V_{min} and less spread that experiment)	Good (higher V_{min} and less spread that experiment)
Centerline Velocity Recovery	Acceptable past recirculation zone (slower recovery past recirculation zone)	Acceptable past recirculation zone (reasonable recovery past recirculation zone)
Cp on Walls of Cylinder	Good to 120°	Good to 120°

Chapter 4: Simulating Flow Over a Section of the Boom of an Agricultural Sprayer

The next step in the CFD study of the wake of an agricultural sprayer was to model a short section of the boom in ANSYS Fluent. The simulation uses the grids recommended from the Chapter 3 to understand how grid selection affects a more complex flow simulation. A short boom section was chosen as the boom is the largest feature of the sprayer. The wake of the boom was expected to be smaller than behind the sprayer body and increased refinement was needed to capture the smaller scale effects. A wind tunnel study on the flow over a section of a sprayer boom was performed by Teske et al. (2016a); some comparisons may be drawn from this study, but their geometry is quite different from that used in the present study.

4.1 Domain, Geometry, and Meshing

The boom geometry was based on the John Deere 4830 sprayer with a 120 ft (36.6 m) boom attached. The design of the boom in the first section is a truss. Although the design of the actual boom section decreases in height as the boom gets further away from the sprayer, the boom section was modeled based on the average height. The domain used in the two simulations is shown in Figure 4.1.

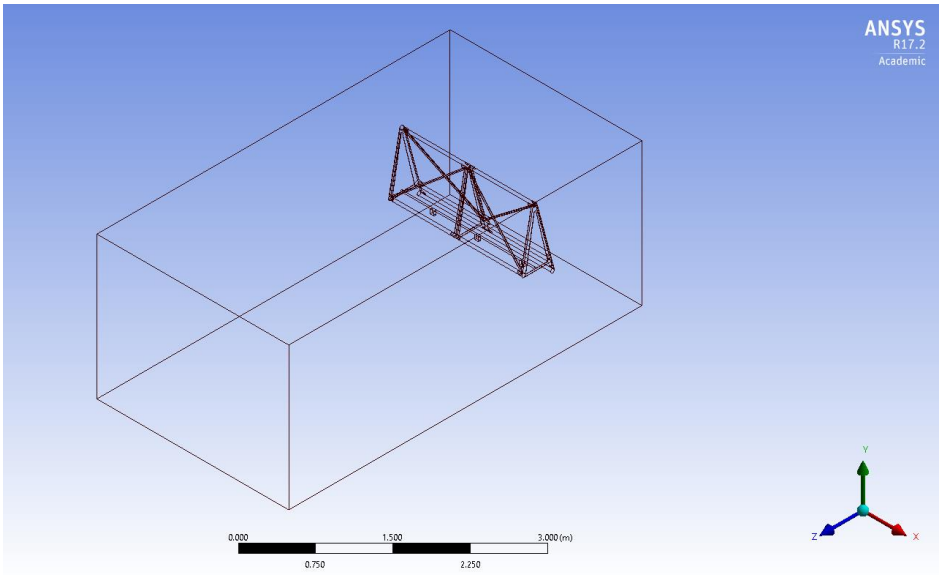

Figure 4.1: Domain used to model the flow around a section of the sprayer boom

Two meshes were used, the first with surface elements 4 mm long, and a second mesh with surface elements half that size. These meshes were made with polyhedral elements to match the meshes Poly I and Poly IV in the cylinder simulations. The maximum element size was 0.512 m to reduce the total number of elements. The coarse mesh is shown in Figure 4.2 and Figure 4.3, and mesh statistics are given in Table 4.1.

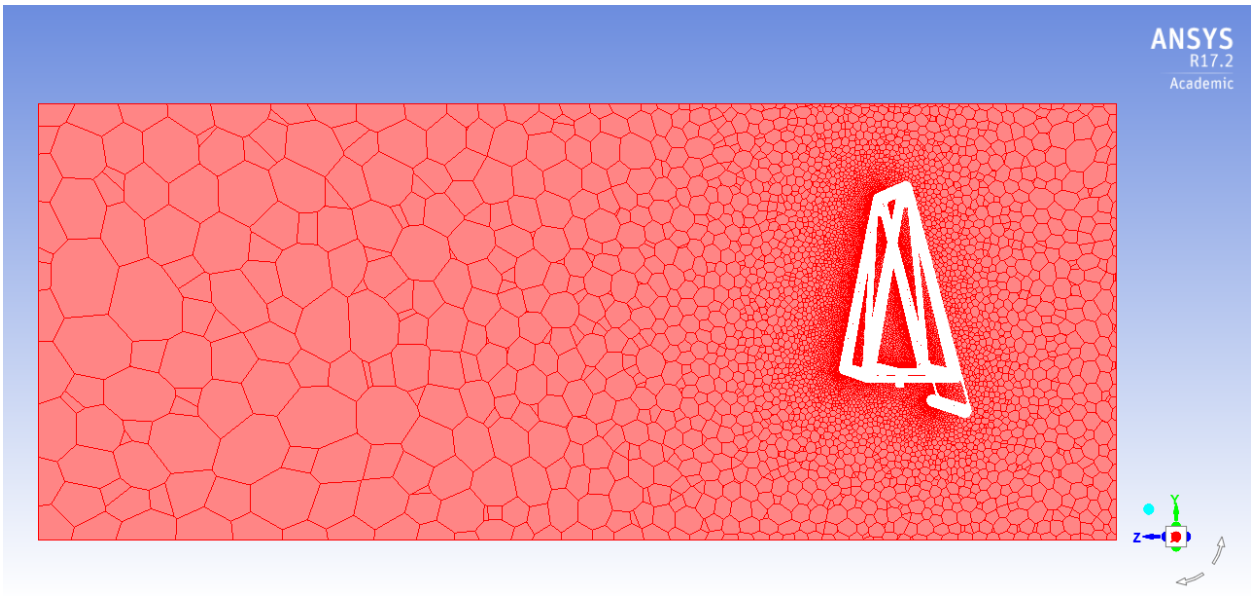

Figure 4.2: Coarse poly mesh through the centre of the domain showing the mesh

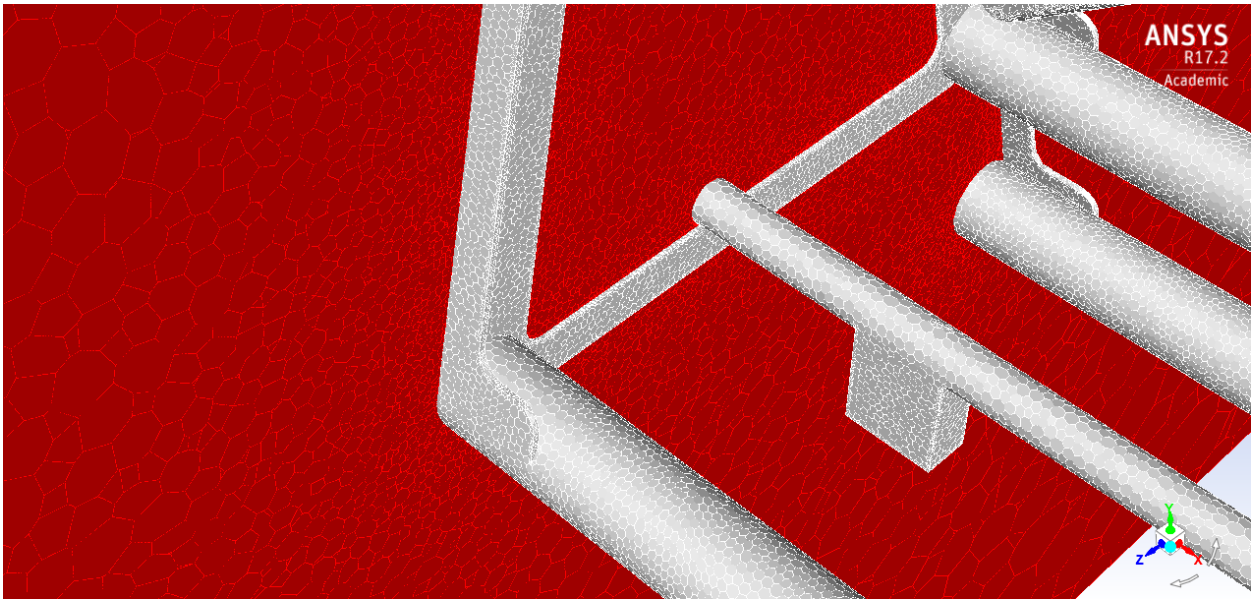

Figure 4.3: Close up view of the coarse mesh on the boom structure and in the near boom region of the flow

Table 4.1: Mesh characteristics for boom section model.

Name	Boom Surface Element Size [mm]	Number of Elements	Min Ortho Quality	Max Ortho Skew	Max Aspect Ratio
Coarse	4	2,600,619	0.141	0.859	44.4
Medium	2	8,161,442	0.143	0.857	31.3

4.2 Results

The primary objective for this study was to determine if it is necessary to refine the mesh around the boom frame to a size smaller than the coarse mesh. The wake of the boom was studied by considering the velocity in the streamwise direction, velocity in the vertical direction, and turbulent kinetic energy. The velocity in the direction along the boom is not considered in this case as it is much smaller compared to the other components. The wake near the trailing edge of the boom is important as this is the region where spray drift is likely to occur. Farther downstream is also worth considering because the spray may enter this region, with the potential for spray drift.

Figure 4.4, Figure 4.5, and Figure 4.6 show the streamwise velocity (u), vertical velocity (v), and turbulent kinetic energy (k) respectively, 0.1 m behind the boom section. Two locations are considered: open, representing the section with minimum blockage of the flow by the boom section, and closed, the location of maximum blockage. The medium mesh gave a larger velocity deficit (Figure 4.4) and stronger Turbulent kinetic energy (TKE) (Figure 4.6). The coarse mesh showed velocity deficits and increases to the TKE in these regions, but not to the same extent. An interesting result was shown in the vertical velocity profiles (Figure 4.5). The velocity is in the upward direction in the closed section profile, and downwards in the open section profile. An upward velocity may lift spray droplets upwards and increase the chance of drift, whereas a downward velocity would move droplets closer to the ground plane and decrease the chance of

drift occurring. While the medium mesh showed a larger wake effect, the coarse mesh was still able to capture all the same features as the medium mesh at a significantly reduced computational cost.

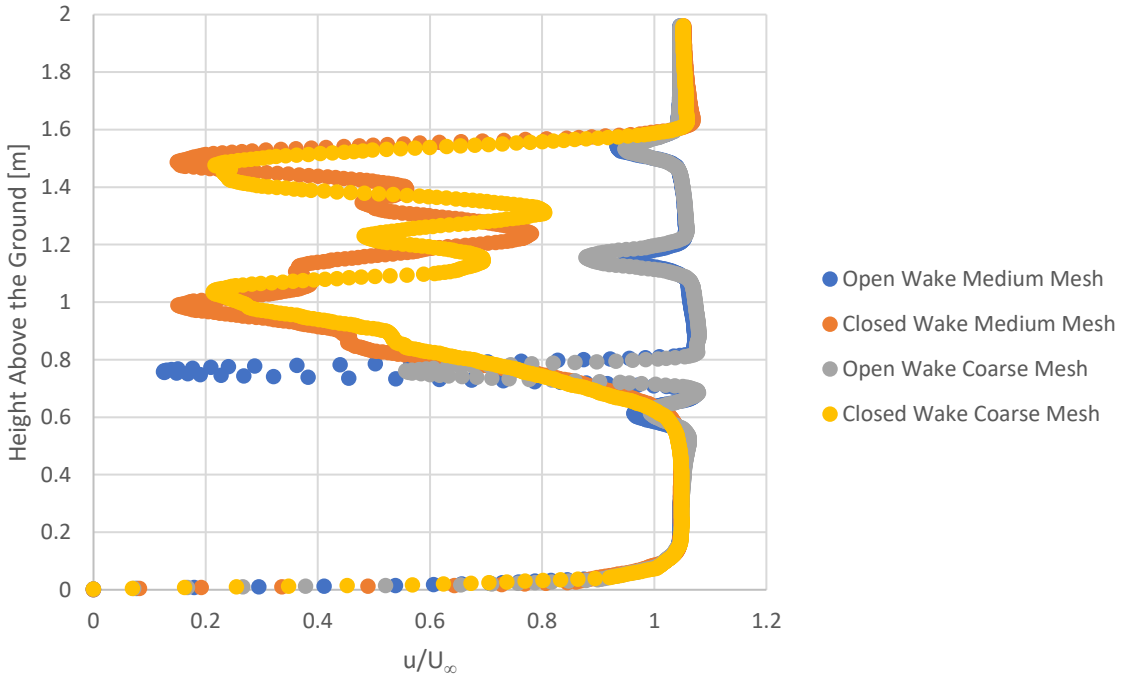

Figure 4.4: Streamwise velocity 0.1 m behind the boom section.

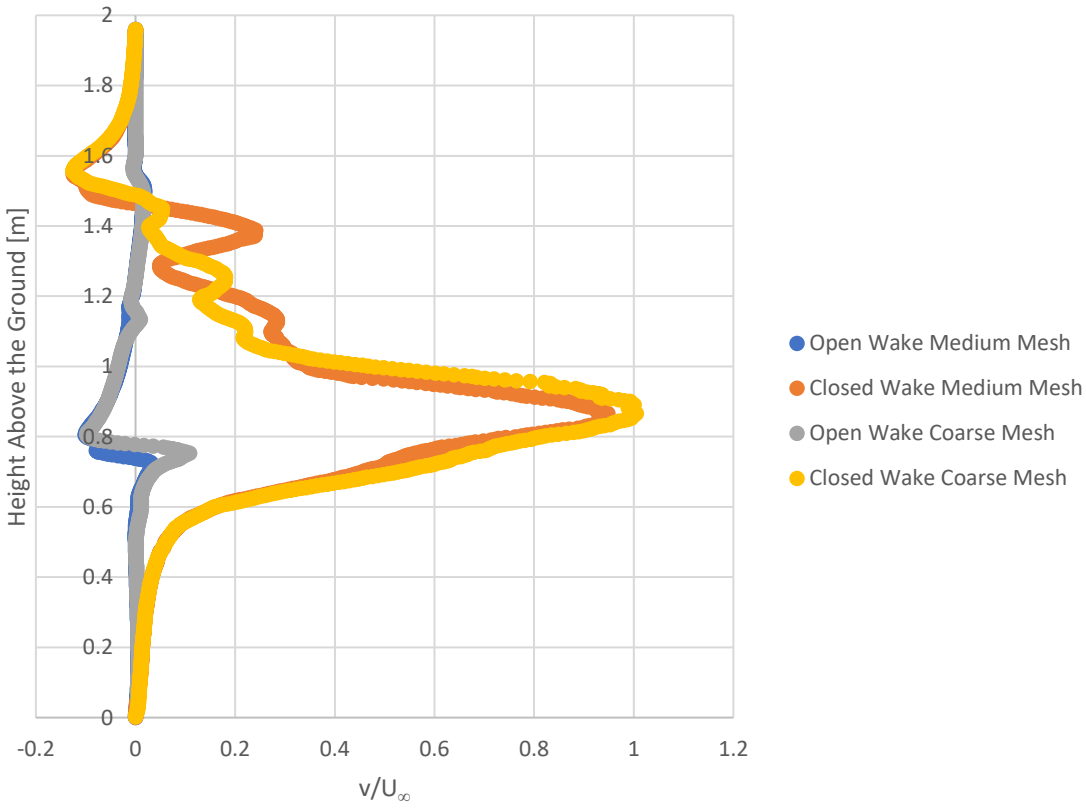

Figure 4.5: Vertical velocity 0.1 m behind the boom section.

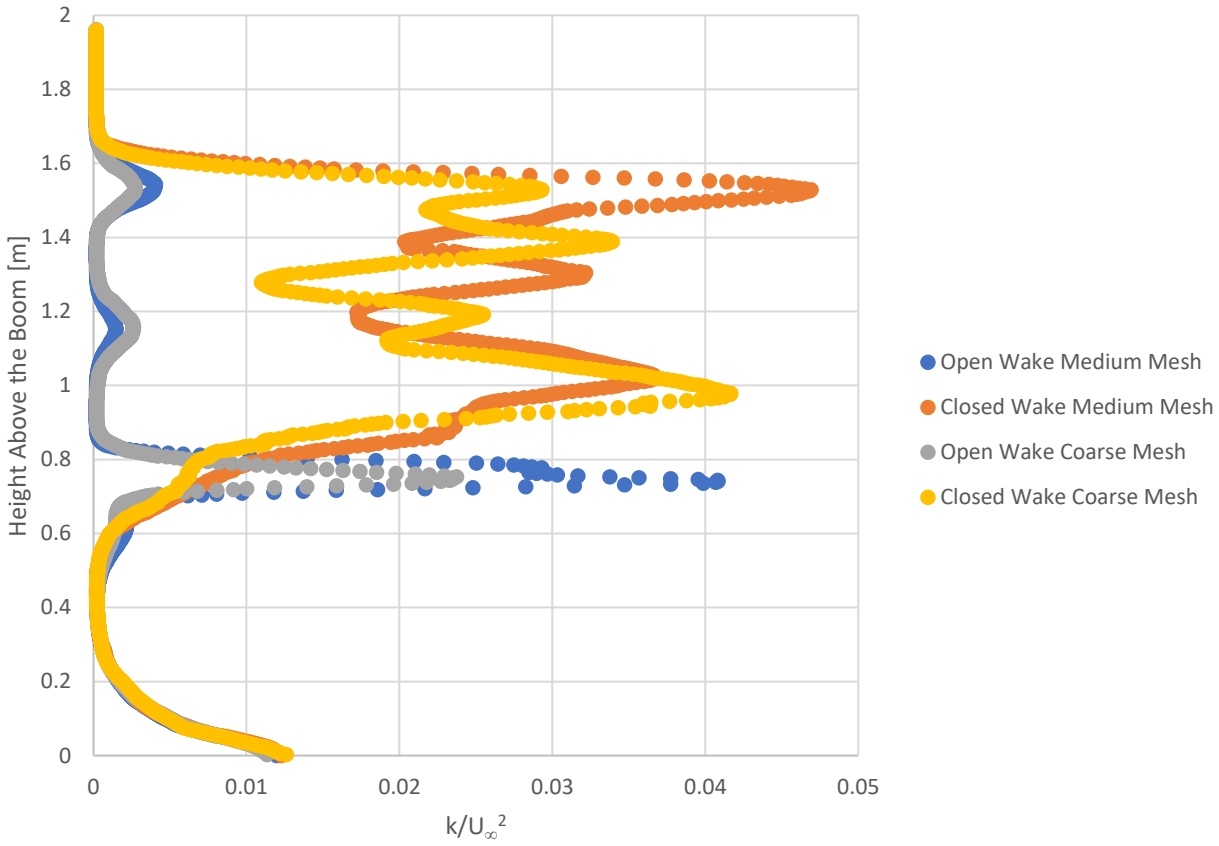

Figure 4.6: TKE 0.1 m behind the boom section.

The wake of the boom at a location 0.5 m behind the sprayer is shown in Figure 4.7, Figure 4.8, and Figure 4.9. At this location, the streamwise velocity (Figure 4.7) defect has decreased, with the minimum velocity recovering from 20% to 60% of the freestream. As well, the wakes of individual members have merged to some degree. The vertical velocity (Figure 4.8) is also significantly reduced at that location behind the boom section, and the turbulent kinetic energy (Figure 4.9) is reduced by about 50%. These profiles again show similar results between the coarse and medium meshes, suggesting that the coarse mesh will provide reasonable results.

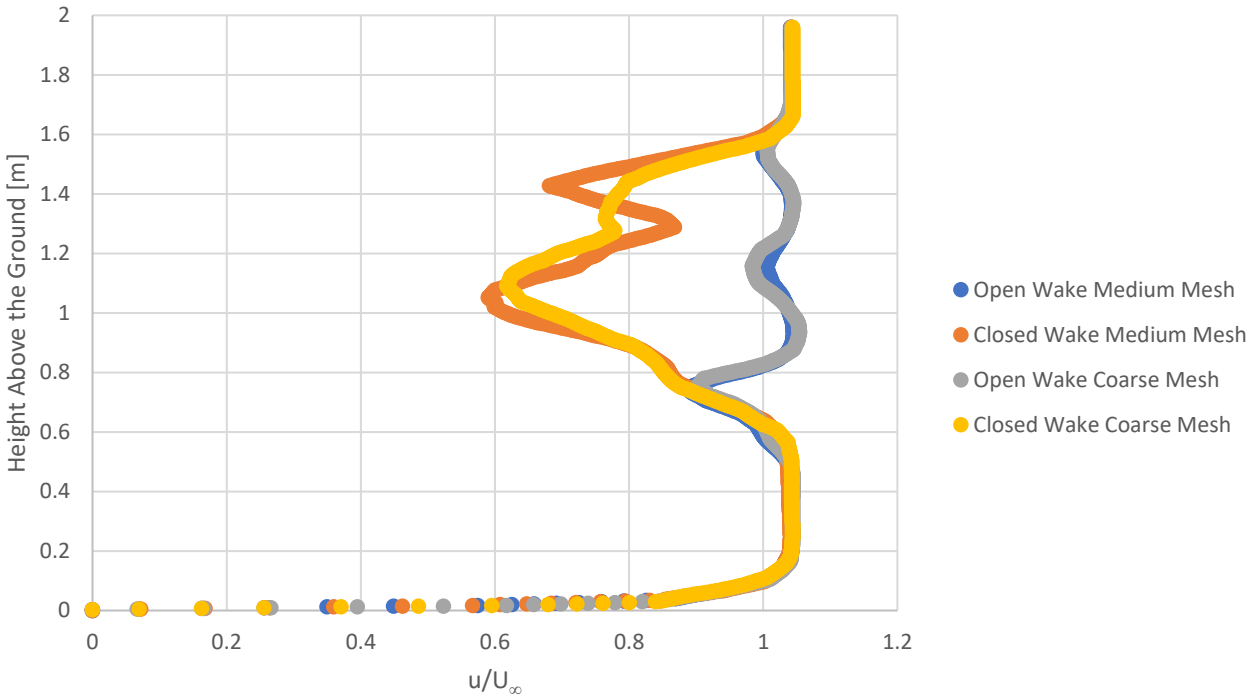

Figure 4.7: Streamwise velocity 0.5 m behind the boom section.

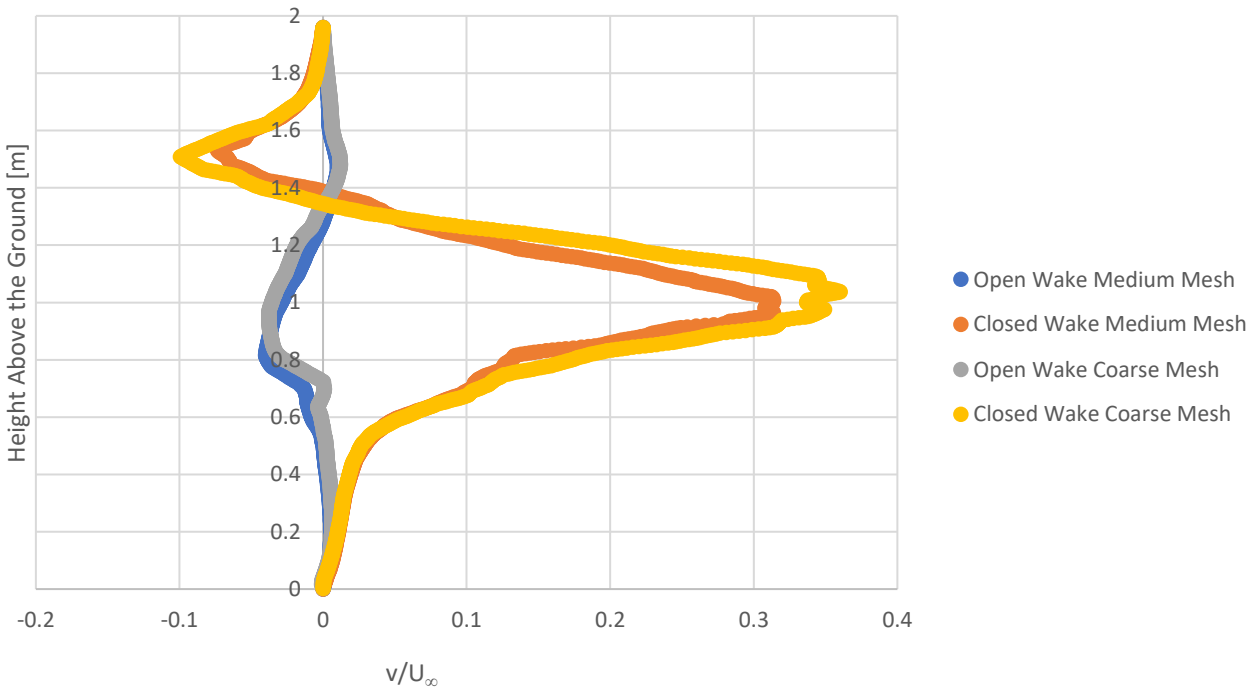

Figure 4.8: Vertical velocity 0.5 m behind the boom section.

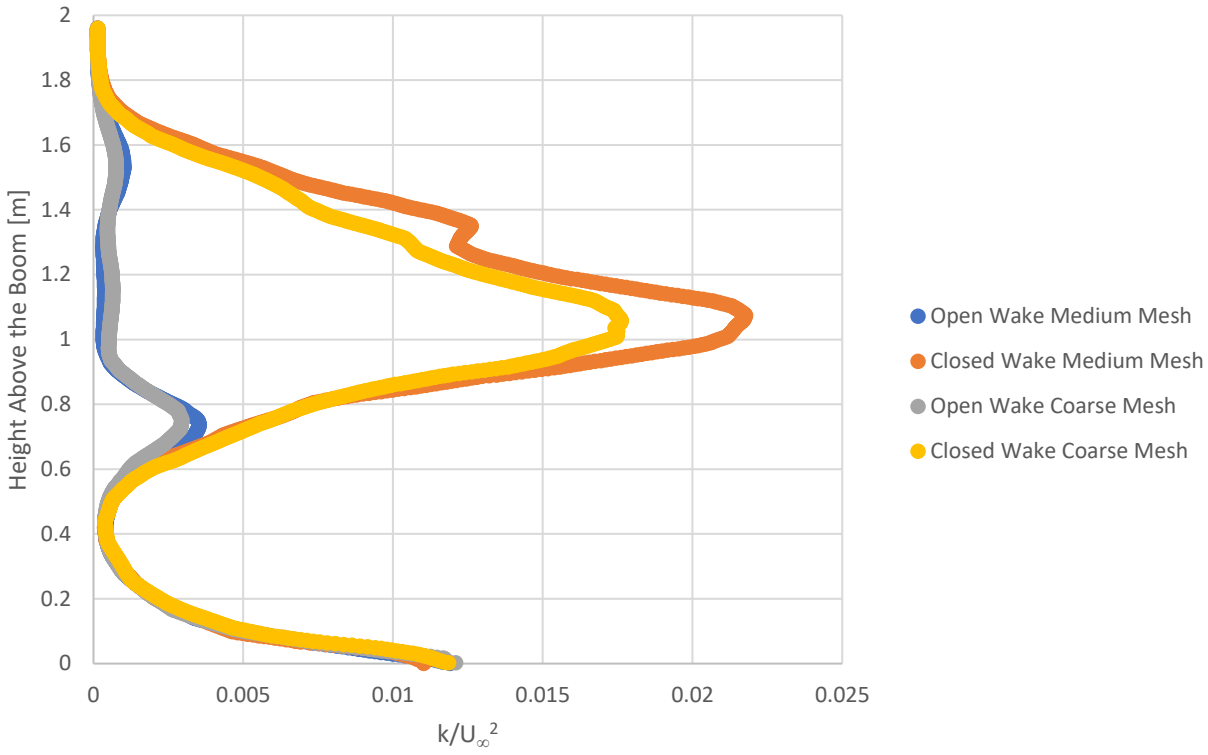

Figure 4.9: TKE 0.5 m behind the boom section.

The last location to monitor is further downstream of the sprayer boom. The present CFD study considers a location 2 m behind the boom section. Figure 4.10, Figure 4.11, and Figure 4.12 show the profiles at these locations. The streamwise velocity (Figure 4.10), for both the open and closed sections and the coarse and medium mesh have converged to give a similar wake profile. Additionally, the individual effects of the boom members are merged to create a single wake behind the boom section. The vertical velocity (Figure 4.11) is also converged between the coarse and medium meshes. In the open sections the vertical velocity is directed towards the ground plane, and in the closed sections the vertical velocity is in the upwards direction. With the turbulent kinetic energy (Figure 4.12), it is observed that there is no significant turbulence from the boom frame at this location, as the ground plane is generating higher levels of turbulence than the boom wake.

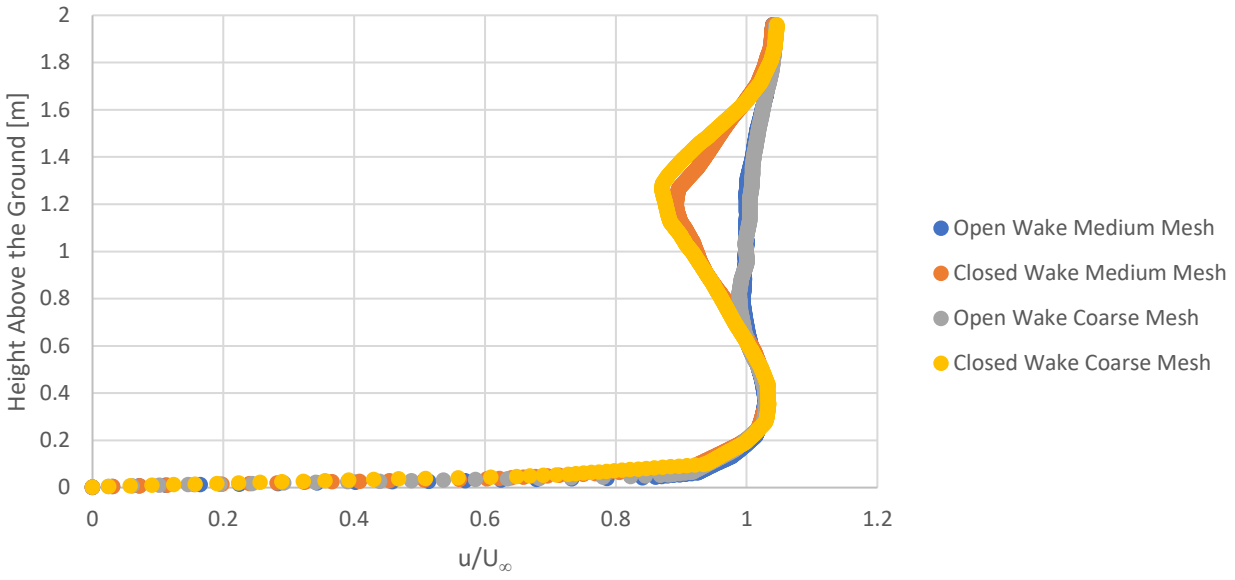

Figure 4.10: Streamwise velocity 2m behind the boom section.

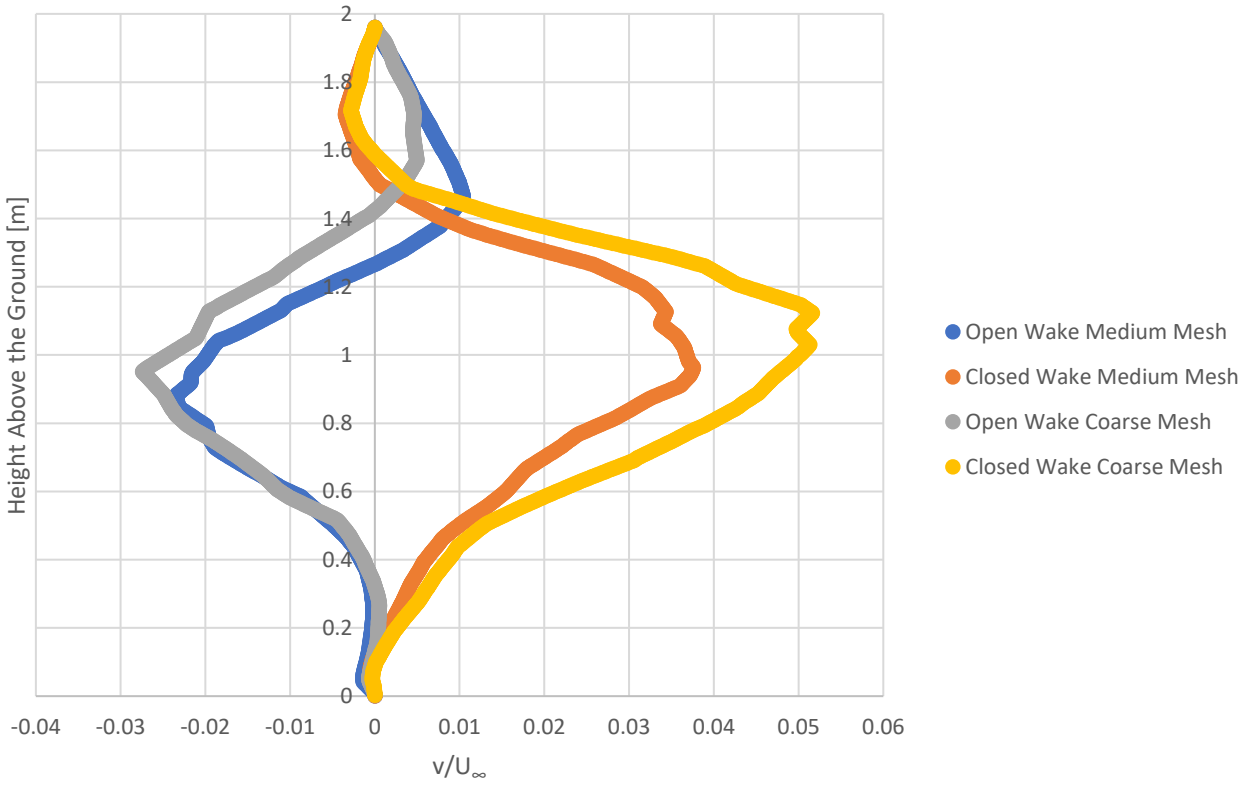

Figure 4.11: Vertical velocity 2m behind the boom section.

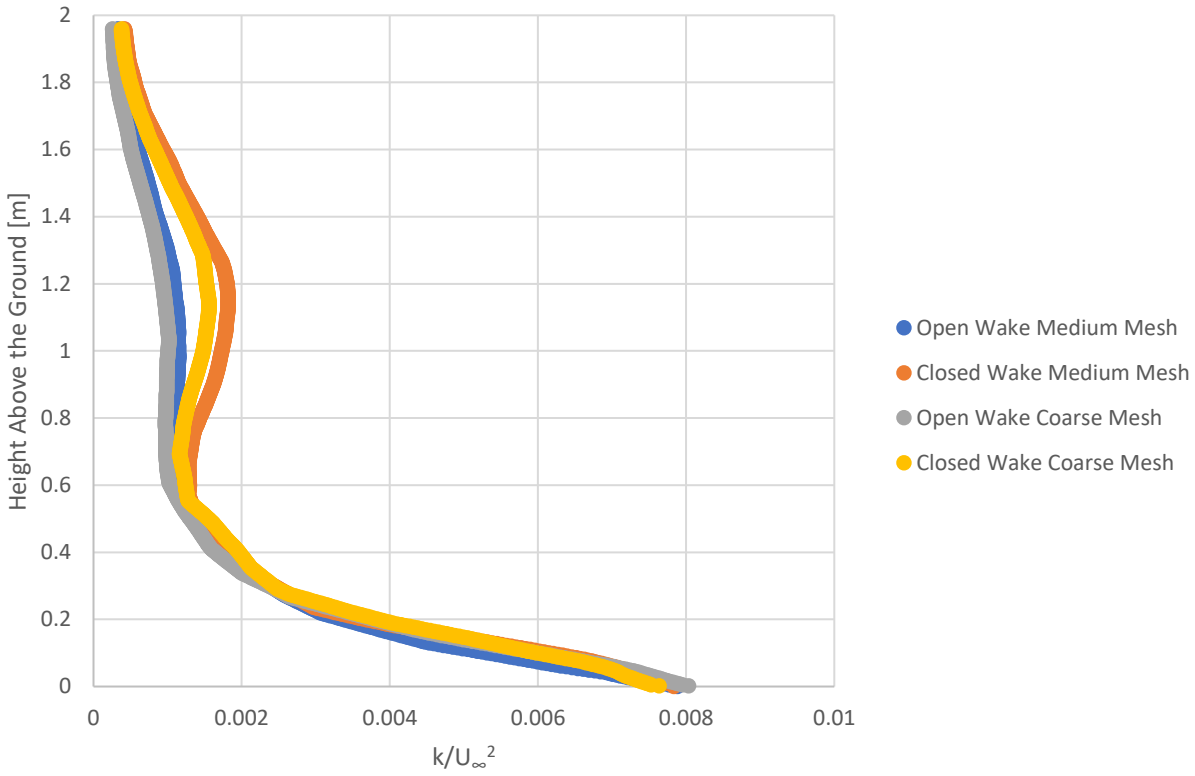

Figure 4.12: TKE 2 m behind the boom section.

4.3 Conclusions

These studies have provided useful information for moving forward with more detailed simulations on the wake of an agricultural sprayer. The coarse and medium meshes provided very similar results, so there is no necessity in refining the mesh further than coarse elements. The boom section wake is mostly recovered by 0.5 m downstream for the open sections, whereas the closed sections are 90% recovered by 2 m downstream. The velocity in the vertical direction is shown the be upwards (positive) behind the vertical section members, and downward (negative) for the rest of the section. This implies a higher likelihood of drift occurring behind vertical members of the boom. The turbulent kinetic energy implies enhanced turbulence behind the closed sections compared to the open sections, and the turbulence is mostly dissipated by 2 m behind the boom.

Chapter 5: Full Scale Simulation

Based on the results of benchmark studies on the cylinder (Chapter 3) and the simulations of a short section of the boom (Chapter 4), full scale simulations of the entire sprayer were performed. Three simulation cases were considered: a base simulation of a fast travel speed and a low boom height, a low speed and low boom height to model a scenario with minimal drift, and a high speed and high boom height to model an enhanced drift scenario. The simulations were conducted using STAR-CCM+, a commercial CFD software.

5.1 Geometry and Domain

A model was made of an agricultural sprayer based on a John Deere 4830 sprayer, the same vehicle that was used in the field trials. The geometry is shown in Figure 5.1, and a dimensioned model is shown in Figure 5.2. The CAD model was simplified, and features that are not symmetric, such as the ladder to the cab, were removed. Only one side of the boom was modeled as only half the sprayer will be used in the simulations. The mudguards were kept on the wheels based on the recommendations of Landry and Wolf (2019), who showed that the turbulence behind the sprayer is affected by the mudguards. This was a more detailed representation of an agricultural sprayer compared to that of Landry and Wolf (2019), who used a more generic model.

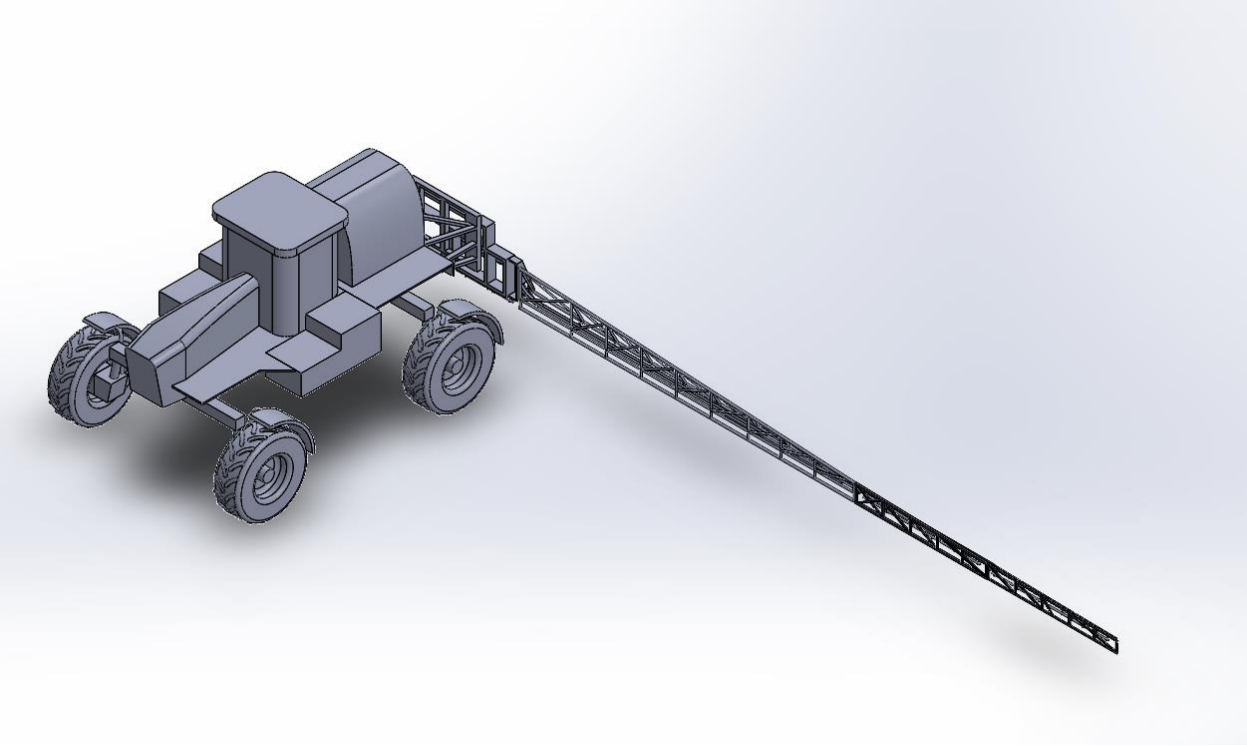

Figure 5.1: CAD model of the sprayer used in the simulations.

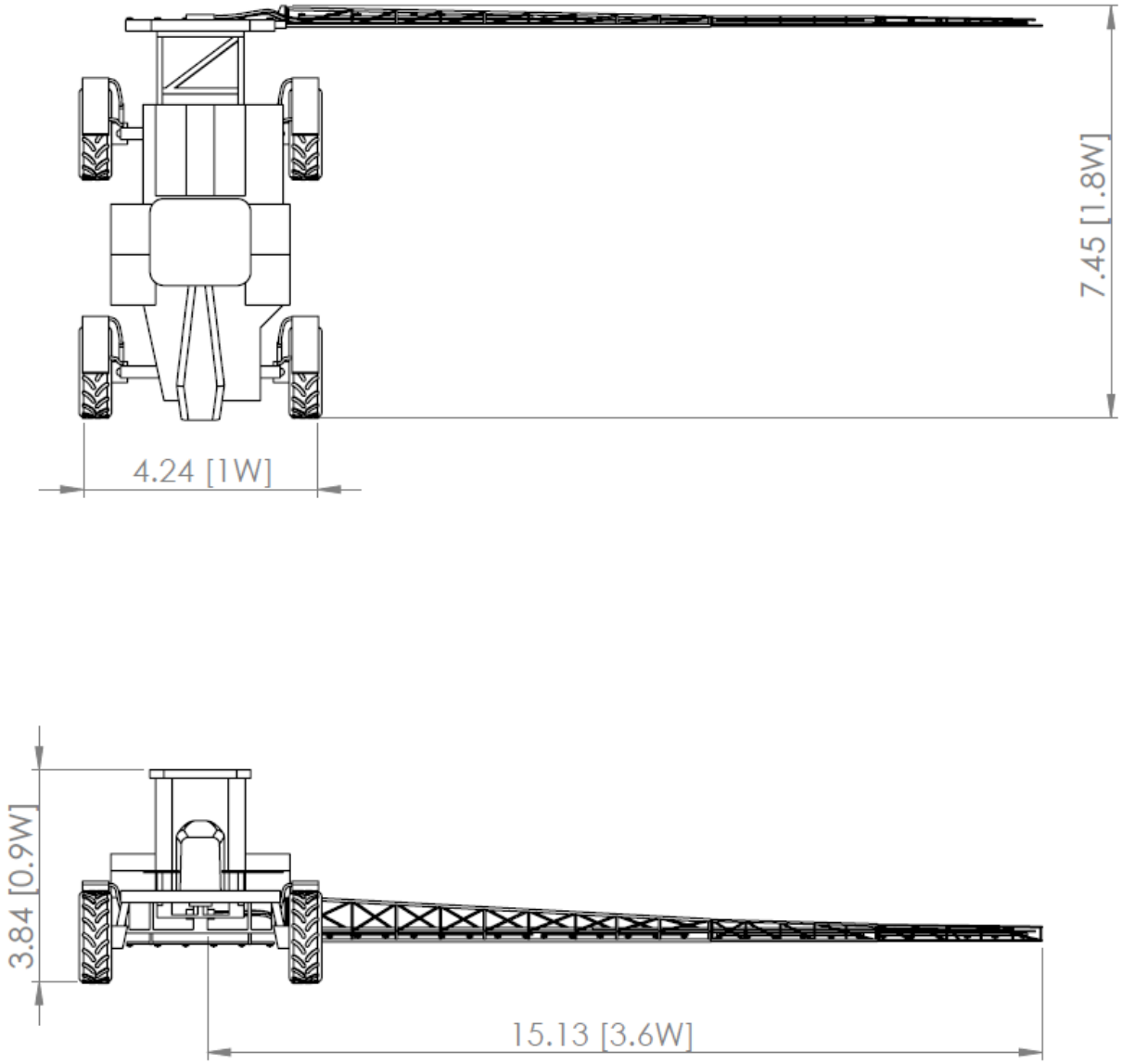

Figure 5.2: Dimensioned drawing of the sprayer showing major dimensions in meters (m) and in vehicle widths (W).

A simulation domain was defined to fully capture the wake of the sprayer, with adequate distance provided in front and behind the sprayer for flow development and recovery. The domain size was 70 m long, 25 m wide, and 16 m high. The sprayer was located 20 m from the inlet, and the distance from the rear surface of the boom to the outlet was 40 m. The dimensions of the simulation domain are shown in Figure 5.3. This domain is smaller than the work of

Baetens et al. (2007), but the goal of that paper was to track particle drift, not the wake of the sprayer. Other related studies include Tsay et al. (2002), who looked at a spray shield in a 2D simulation. Their domain extended 1 m from inlet to the boom, and 2 m behind the shield. The present domain is far larger than this because the sprayer is expected to produce a much larger wake in comparison to the wake of the boom.

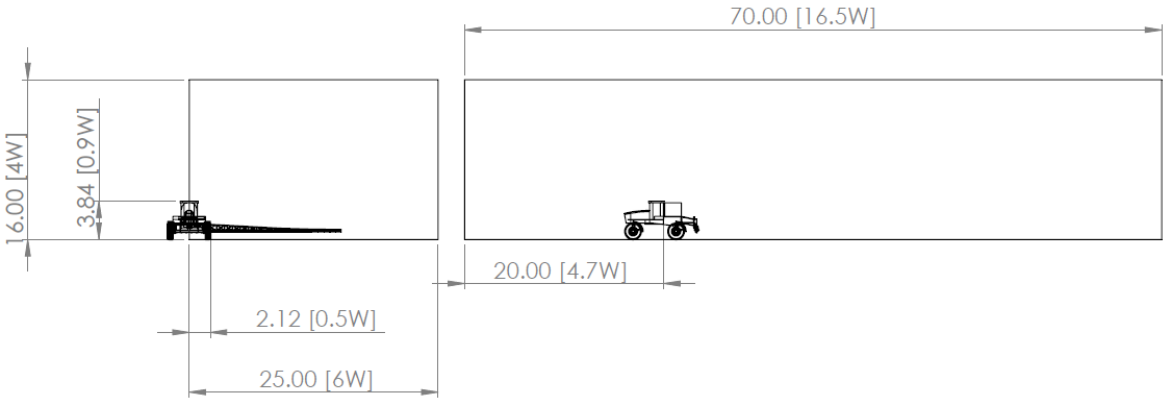

Figure 5.3: Model of the domain size for the simulation with the sprayer located within the domain. All dimensions in m and vehicle widths [W]

The work of Hsu and Davis (2010) is relevant as the tractor-trailer that they studied is a large vehicle similar to a sprayer. In their study they used a domain that had the following dimensions: from inlet to vehicle 1 body length, from vehicle to outlet 5 body lengths, the side walls were 5 body widths away from the vehicle and the height was five body heights above the vehicle. Assuming a vehicle length and width equal to 5 m and a height equal to 4 m, the domain size for the sprayer simulations would be 2 lengths from inlet to vehicle, 8 vehicle lengths from vehicle rear to outlet, a width equal to 5 vehicle lengths, and a height equal to 4 vehicle heights. The length of the domain would be longer than that of Hsu and Davis (2010), with equal width and a smaller height. The lower height might have an impact on the simulation, but the agricultural sprayer has significant airflow below the vehicle body (more ground clearance) which will change how much airflow is directed upwards when compared to a tractor-trailer.

5.2 Meshing

The mesh was generated using an automatic method since the size of the domain would make other methods unfeasible. Once the geometry was loaded into STAR-CCM+ a “surface wrapper” was run over the geometry to reset the surface from the STereoLithography (stl) configuration. Using a Boolean subtract, the sprayer was removed from the domain so only the air space remained. Minimum and target elements were set on all the surfaces; the values are given in Table 5.1. A growth rate of 1.1 was used to ensure a slow transition in the size of cells as they expand from the surface of the sprayer to the domain boundaries. Using these conditions, a mesh was generated; which is shown in Figure 5.4, Figure 5.5, and Figure 5.6.

Table 5.1: Mesh element size for the surfaces in the sprayer simulation.

Region	Target Size [mm]	Minimum Size [mm]
Boundaries	1600	800
Sprayer Body	16	8
Sprayer Boom	4	4

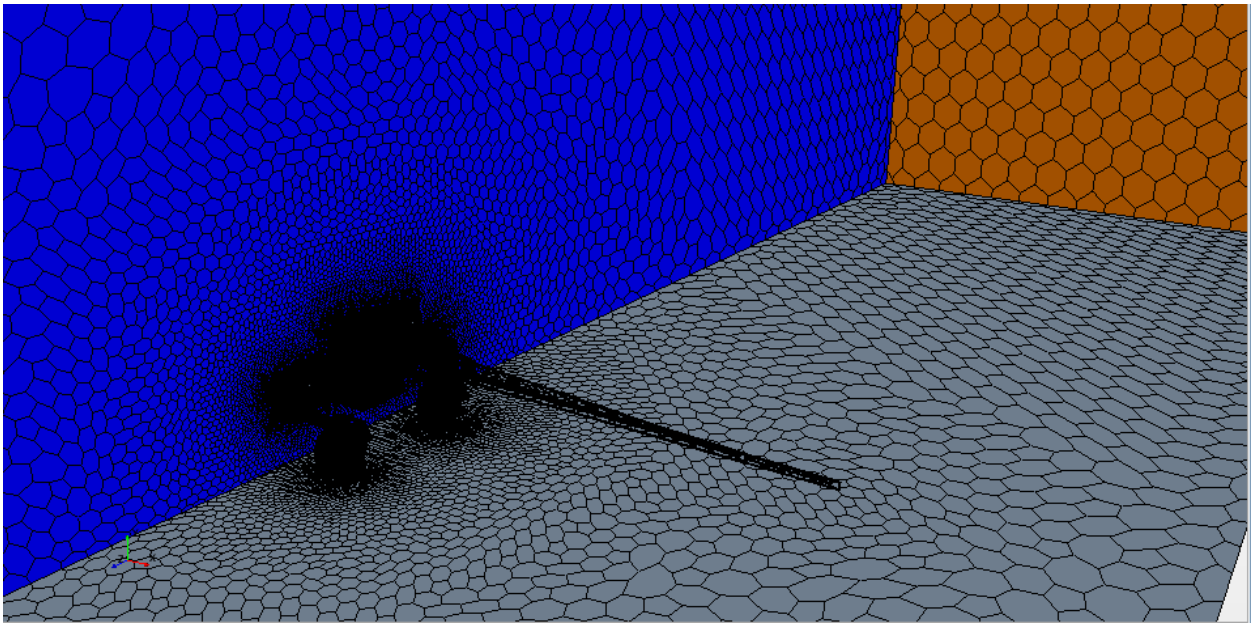

Figure 5.4: Mesh shown on the boundaries of the simulation domain and on the sprayer body.

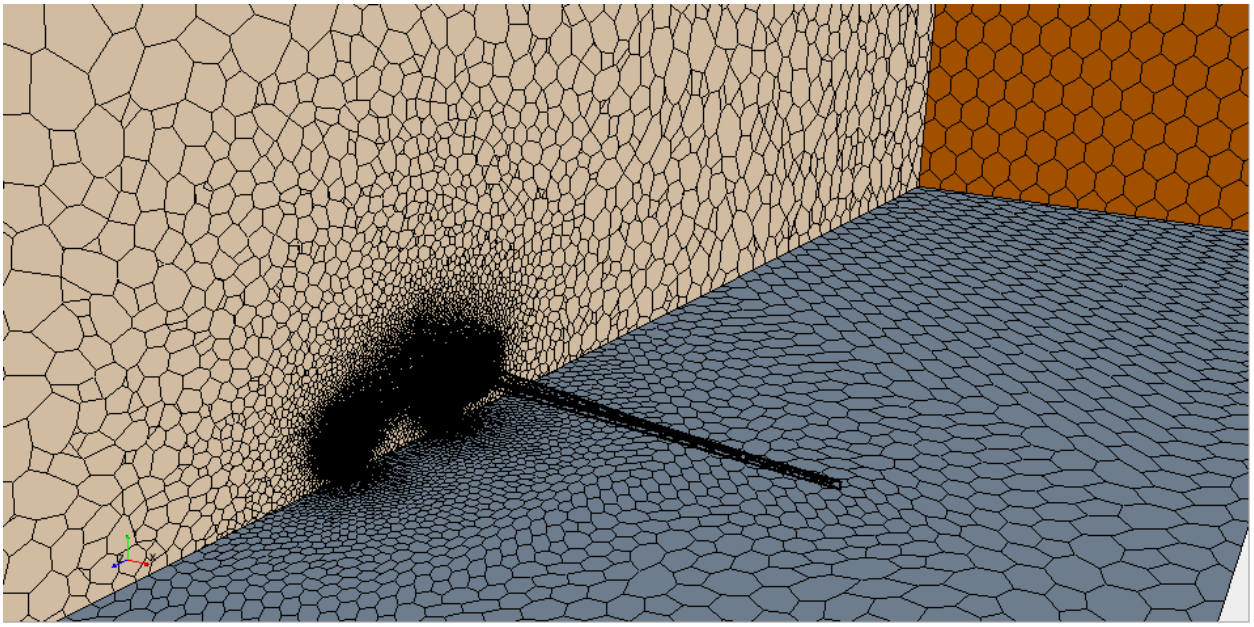

Figure 5.5: Mesh on a plane running through the tires of the sprayer.

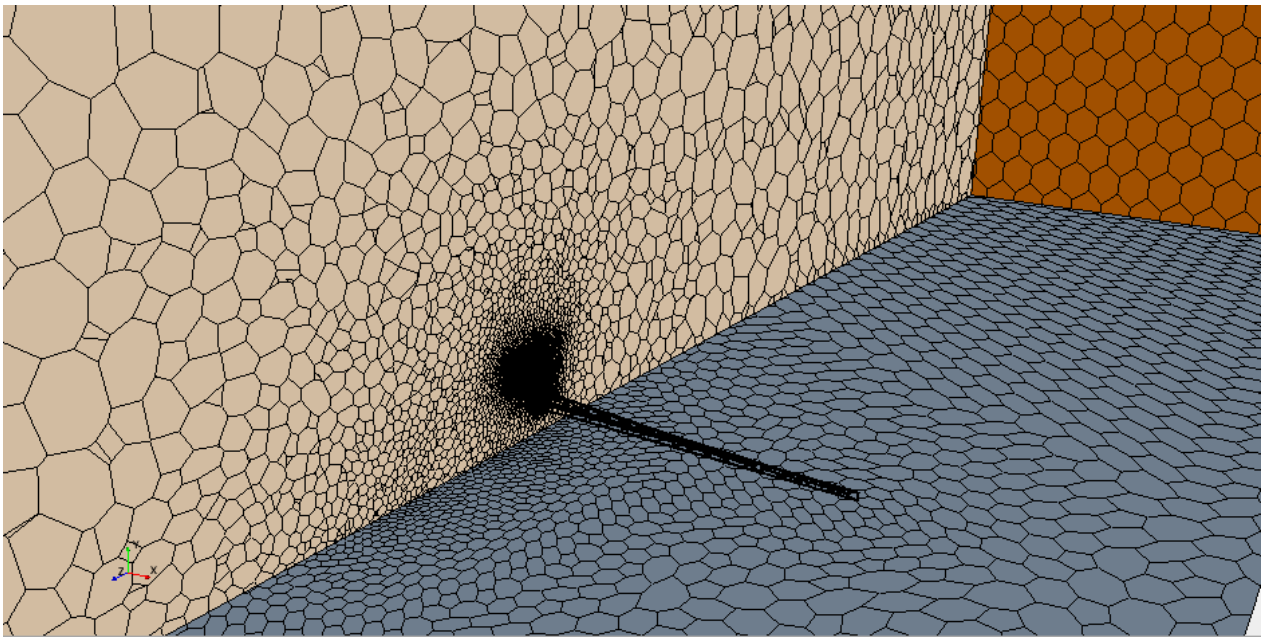

Figure 5.6: Mesh on a plane 82" From the sprayer wheels.

One problem with this meshing condition is that the elements grow to a rather large size in the wake region where significant changes in the flow are expected to occur. To solve this problem a refined wake zone was added, where smaller elements were prescribed to ensure sufficient

refinement. For the wake zone region, element size was set to 80 mm. The refined wake zone extends 5 m behind the sprayer boom and 25 m behind the body of the sprayer, as shown in Figure 5.7. The mesh with the refined zone is shown in Figure 5.8, Figure 5.9, Figure 5.10, and Figure 5.11. A comparison of the two meshes is shown in Table 5.2. Interestingly, the mesh with the refined zone required less elements than the base mesh.

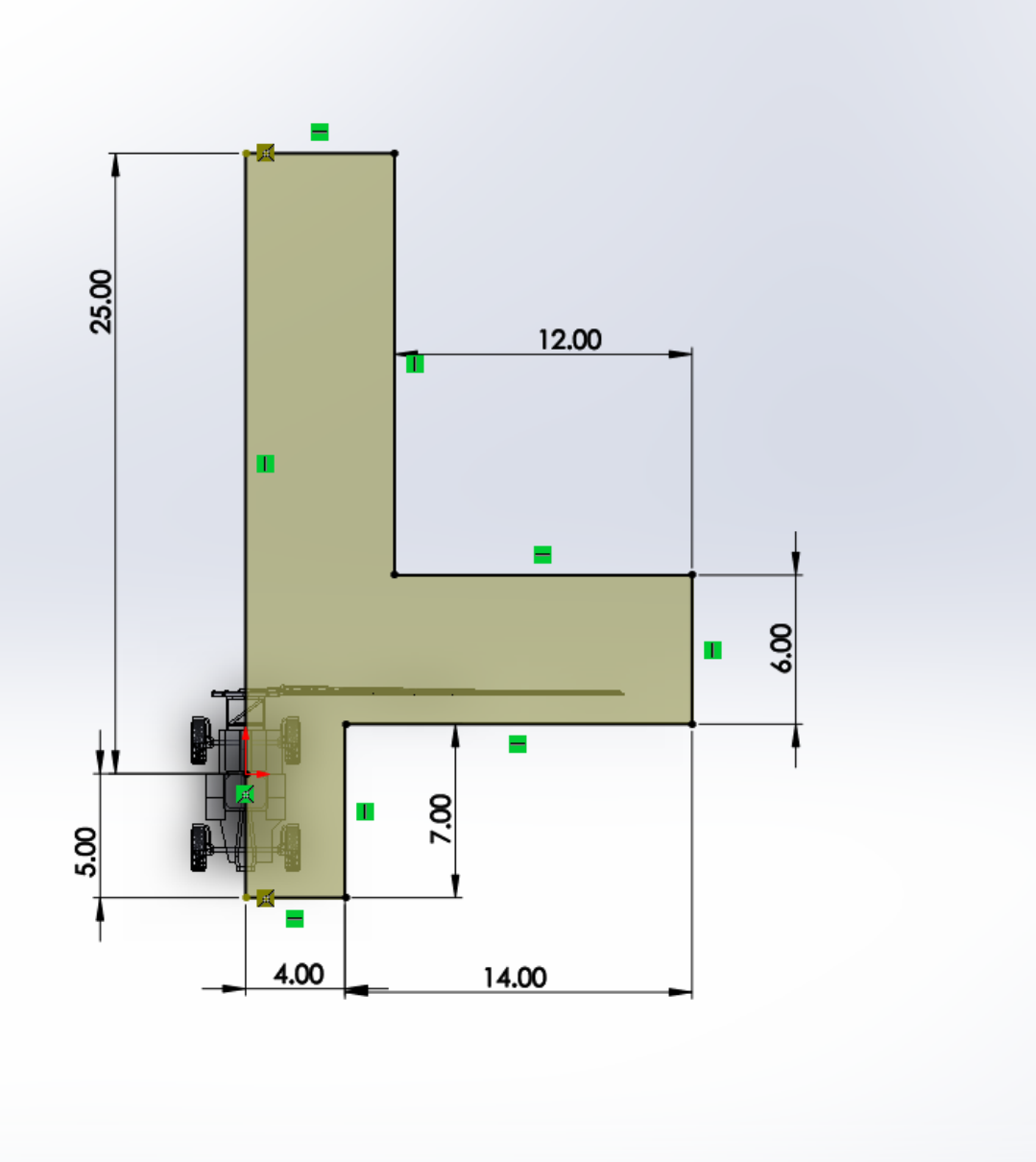

Figure 5.7: Extent of the Refined Wake Zone – dimensions in meters

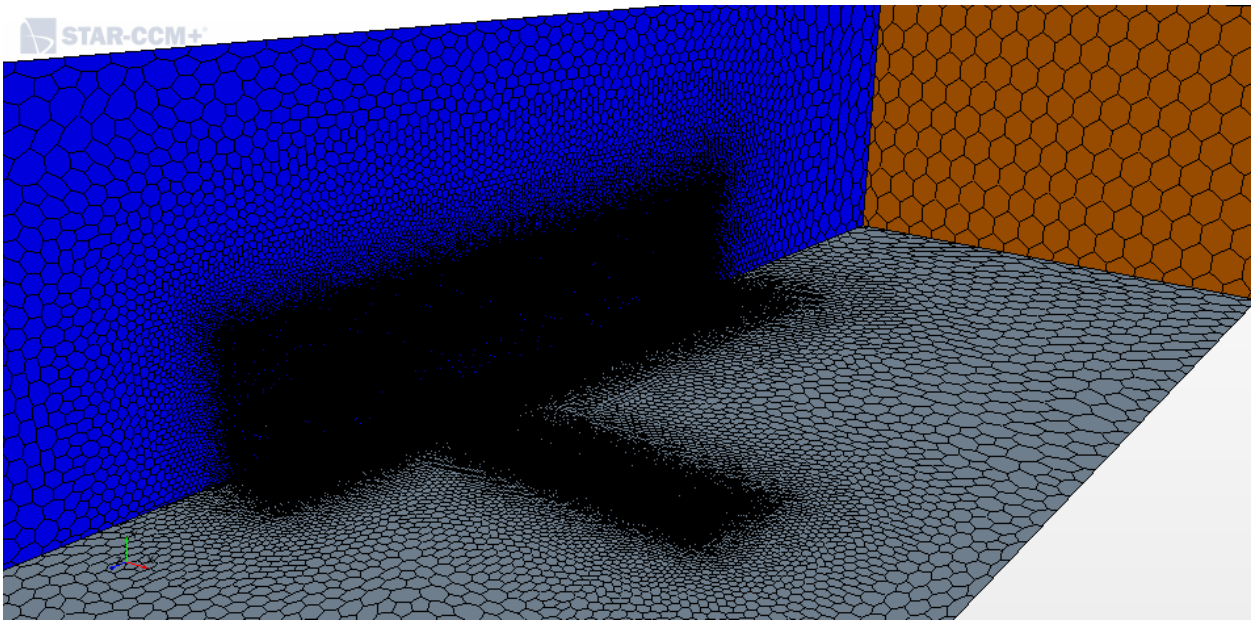

Figure 5.8: Exterior faces meshed in the refined zone wake.

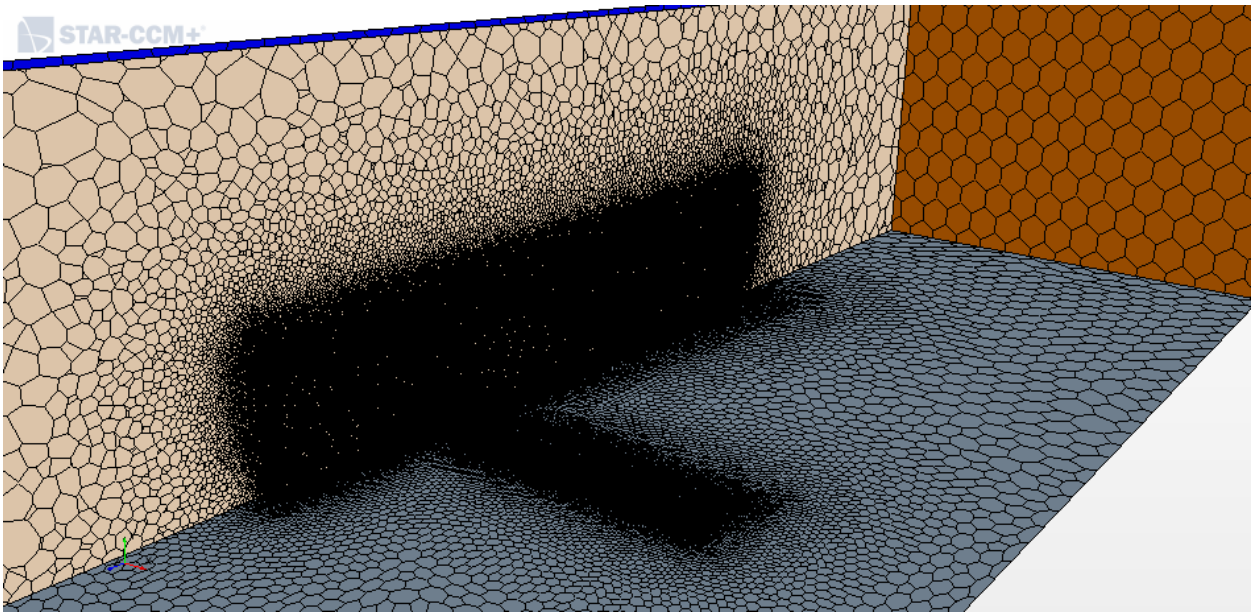

Figure 5.9: Refined wake zone mesh on a plane through the tires.

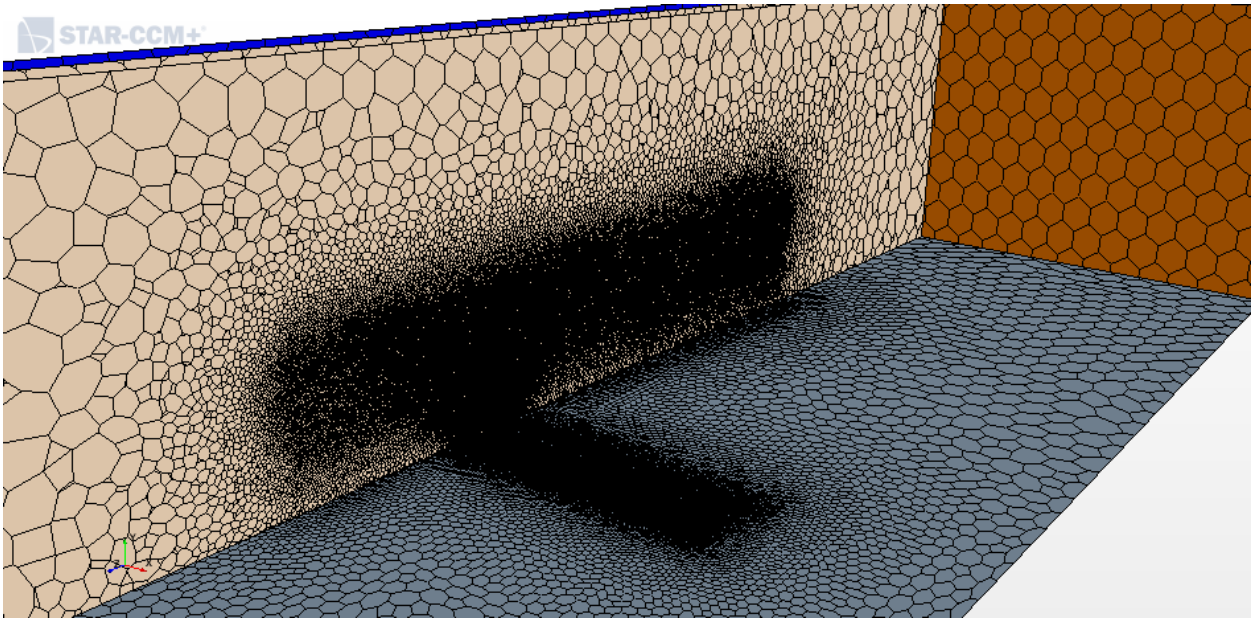

Figure 5.10: Refined zone wake on a plane 2.08 m from the tires.

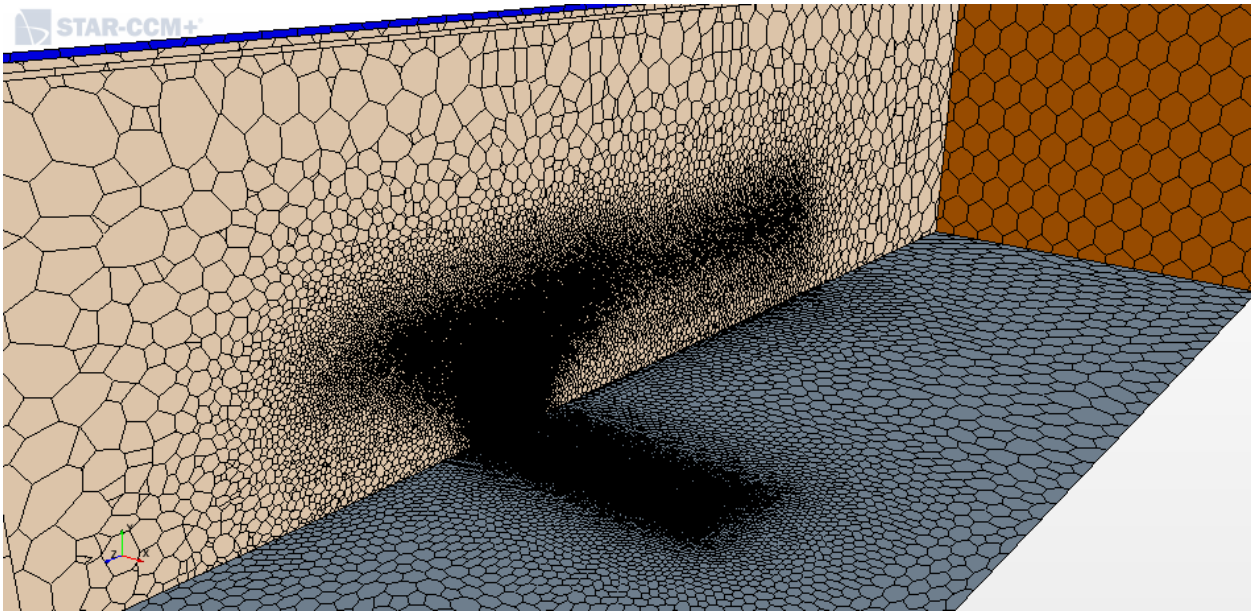

Figure 5.11: Refined wake zone mesh on a plane 3.45 m from the tires.

Table 5.2: Details on the Sizing of the mesh for the full-scale simulations.

Mesh	Cells	Faces	Vertices
Standard	46,080,385	334,824,028	290,462,879
Refined Wake Zone	36,748,807	257,593,488	222,811,453

5.3 Boundary Conditions

For the simulation, boundary conditions were selected to model a no-wind test day over a bare field similar to the field that was used for field testing in 2019 and 2020. There are six faces plus the geometry of the sprayer which require boundary conditions. Each boundary condition is listed in Table 5.3 and a labeled image of the boundaries is shown in Figure 5.12. V_{in} is the assigned inlet velocity, V_{plane} is the assigned velocity of the ground plane, and $V_{tractor}$ is the velocity of the sprayer. The simulation used a coordinate system attached to the rear tire of the sprayer. Downstream is positive z, vertical is positive y, and the driver's left is negative x.

The vehicle was stationary with rotating wheels and the ground plane of the simulation domain moved at the same rate as the inlet velocity. The ground plane is a rough wall with roughness height (z_o) of 0.01 m, to represent a fallow field, (Tieleman 2003) similar to the field used in field testing. That value was also used to represent a pasture or grass field (Baetens et al. 2007). The inlet velocity is set to a velocity equal to the sprayer speed and a turbulence intensity level of 1%. The literature shows that with a roughness height value of 0.01 m the turbulence intensity level is expected to be 10%-15% (Tieleman 2003), so a lower value of 1% might represent a day of very low to no wind. The simulation was run in STAR-CCM+ using a SST turbulence model. A first order upwind scheme is used to gain faster convergence. Furthermore, a segregated solver is selected as opposed to a coupled model which would increase the run time.

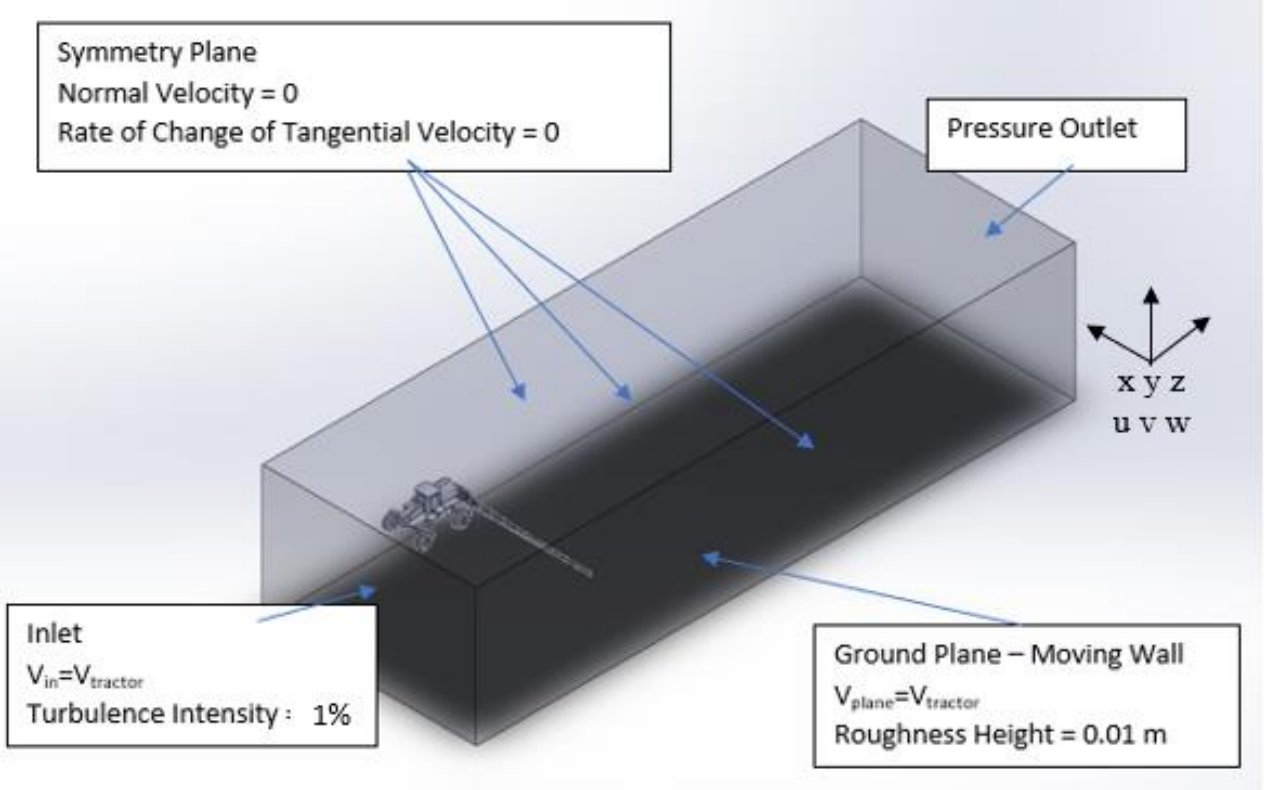

Figure 5.12: Domain with boundary conditions labeled. V_{in} is the assigned inlet velocity, V_{plane} is the assigned velocity of the ground plane, $V_{tractor}$ is the velocity of the sprayer.

Table 5.3: Boundary conditions for all the faces of the simulation domain.

Boundary	Physical Description
Inlet	Inlet velocity equal to sprayer driving speed with a turbulence intensity of 1%
Outlet	Pressure outlet ($P_{outlet} = P_{static}$)
Symmetry Plane (thru sprayer)	Symmetry plane
Top Wall and Far Wall	Symmetry plane which acts as a slip wall Velocity normal to the wall is zero, and the rate of change of the tangential velocity at the wall is zero.
Ground Plane	Rough wall with roughness height (z_o) equal to 0.01 m. Wall is moving at sprayer travel speed.
Sprayer Body and Boom	Smooth wall
Sprayer Wheels	Smooth wall rotating at rotation rate matching sprayer travel speed

5.4 Cases

As discussed in the literature review (Chapter 2), spray drift is affected by boom height and sprayer speed. To minimize the number of simulations, three cases were considered for this study, as shown in Table 5.4. The first case had a low boom height and a fast vehicle speed, this will be defined as the base case. The second case, which should minimize spray drift, has the boom in the low position and the sprayer traveling at a slow speed. The third case had a high boom height and a high tractor speed for which there would be increased spray drift.

Table 5.4: Details of sprayer speed and boom height for the three cases simulated.

Case	Tractor Speed	Boom Height
1 – Low Boom and Fast Vehicle Speed	11 m/s	0.64 m (25 in)
2 – Low Boom and Slow Vehicle Speed	4 m/s	0.64 m (25 in)
3 – High Boom and Fast Vehicle Speed	11 m/s	1.14 m (45 in)

5.5 Convergence

Three methods were employed to assess convergence: residual reduction, force coefficient values, and monitoring velocity profiles at select locations. Convergence results are discussed for Case 2 (low boom height and slow vehicle travel speed) since with lower velocities repetitive patterns were noticed in the convergence of the continuity residual.

It is common in numerical simulations to monitor the residuals of the conservation equations. These residuals represent the absolute error in the solution for a particular variable for each element of the mesh. The Root Mean Square (RMS) error of the continuity equation is plotted in the residual plot (Siemens PLM Software 2019). The continuity equation is of first importance since it reflects the mass imbalance of the system, which is fundamental to solving the other conservation equations. Other conservation equations were considered, but continuity was determined to be the most important. The continuity residual is shown in Figure 5.13.

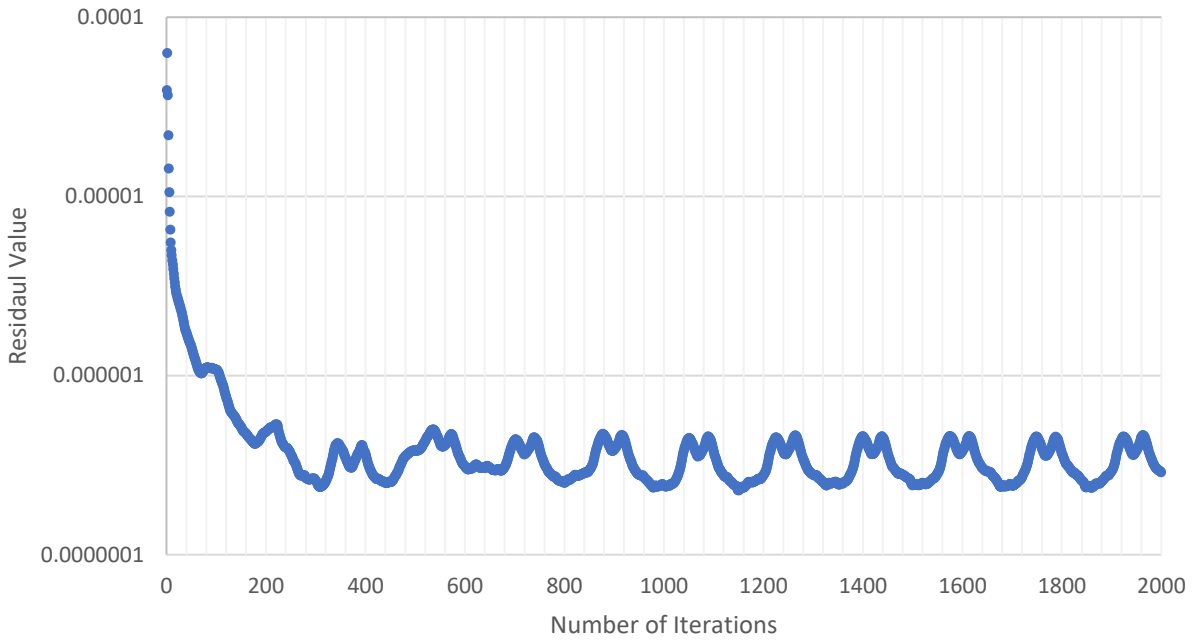

Figure 5.13: Monitor of the residual in continuity equation for the simulation of the sprayer with the low boom height and low vehicle speed condition (Case 1).

The continuity plot shows that after 500 iterations the solution settles into a pattern of peaks and valleys. This pattern could reflect a non-steady flow feature, such as a boundary layer, occurring within the flow field. To investigate this behavior, velocity and turbulent kinetic energy (TKE)

plots were made for the iterations, labeled Peak 1, Valley, Peak 2, and Floor; these iterations are shown in Figure 5.14. The velocity and TKE plots are considered in two locations, behind the nozzles parallel with the ground, and behind the centerline of the vehicle running vertically from the ground plane.

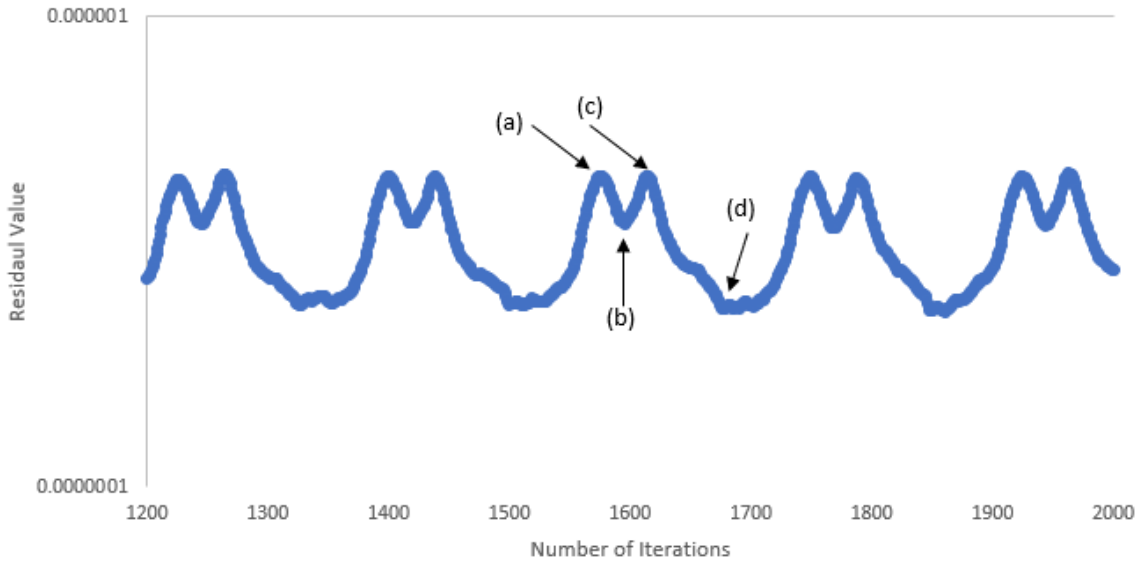

Figure 5.14: Continuity residual showing Peak 1 (a), Valley (b), Peak 2 (c), and Floor (d).

Considering the centerline profile 0.43 m behind the sprayer, the velocity and TKE plots in Figure 5.15 and Figure 5.16, respectively, show similar profiles for each of the streamwise velocity and TKE plots. Similar behavior is shown for 1.40 m behind the sprayer in Figure 5.17 and Figure 5.18. This also holds true for the profiles at 0.79 m behind the sprayer, and for the profiles level to the nozzles at all three downstream locations. The plots show that the streamwise velocity slightly varies in a repeating pattern with iterations, but it is a converged cycle of repetition, and at each similar point in the pattern the velocity and TKE profiles are the same.

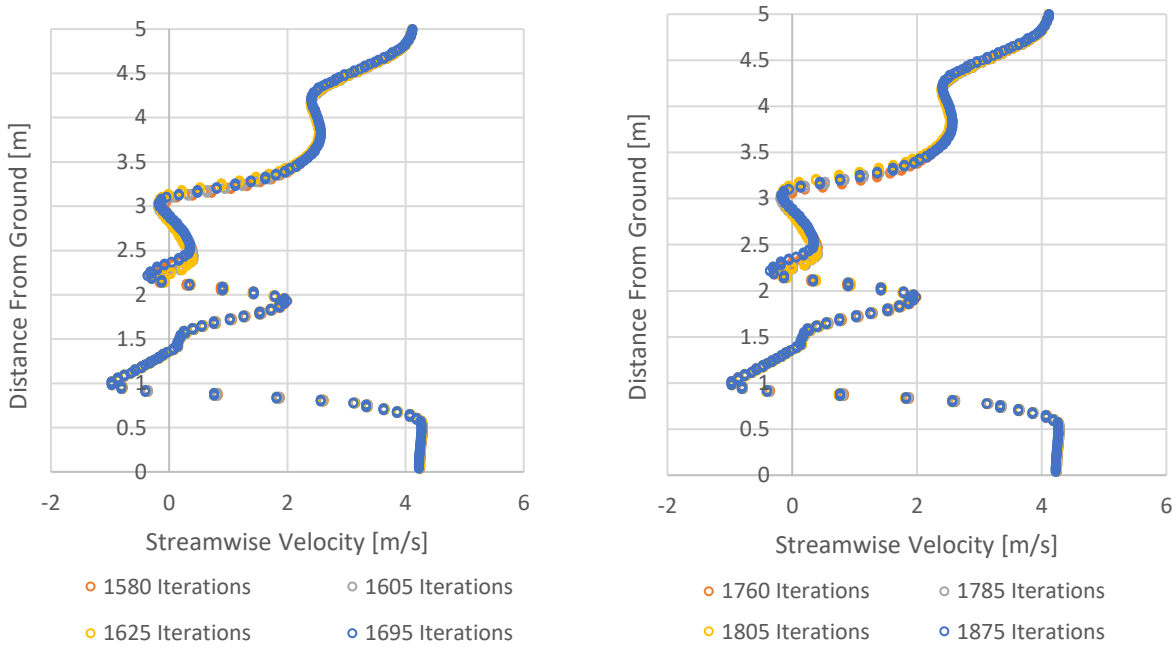

(a) (b)

Figure 5.15: Centerline profiles of streamwise velocity 0.43 m behind the sprayer from 1580-1695 iterations (a) and from 1760-1875 iterations

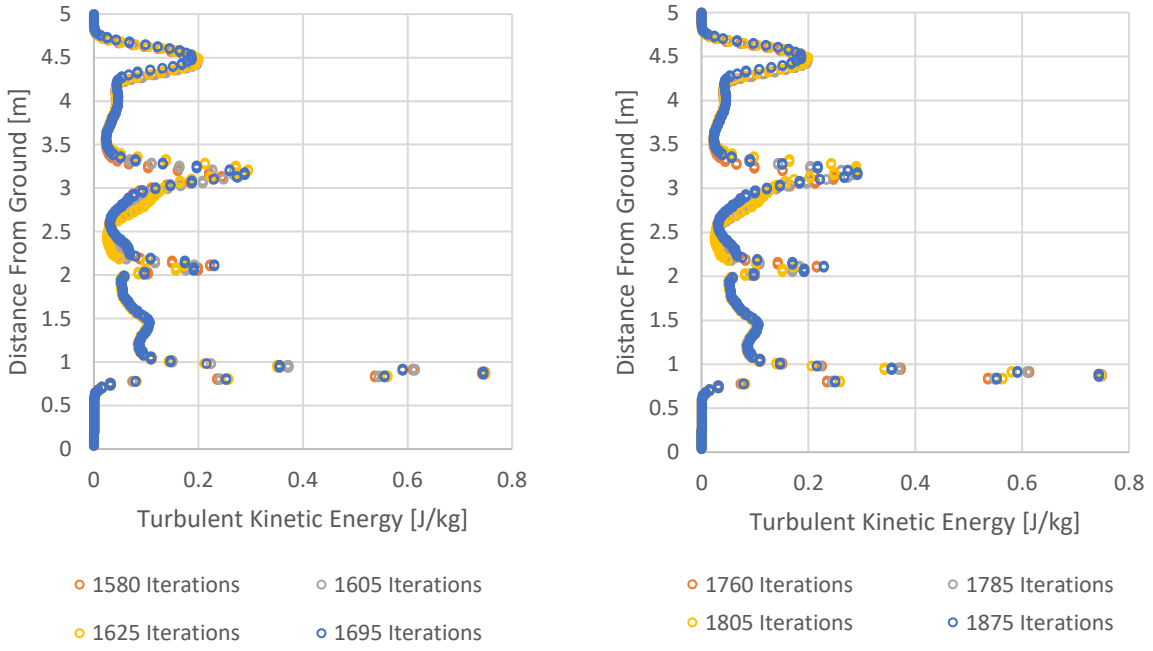

(a) (b)

Figure 5.16: Centerline profiles of TKE 0.43 m behind the sprayer from 1580-1695 iterations (a) and from 1760-1875 iterations

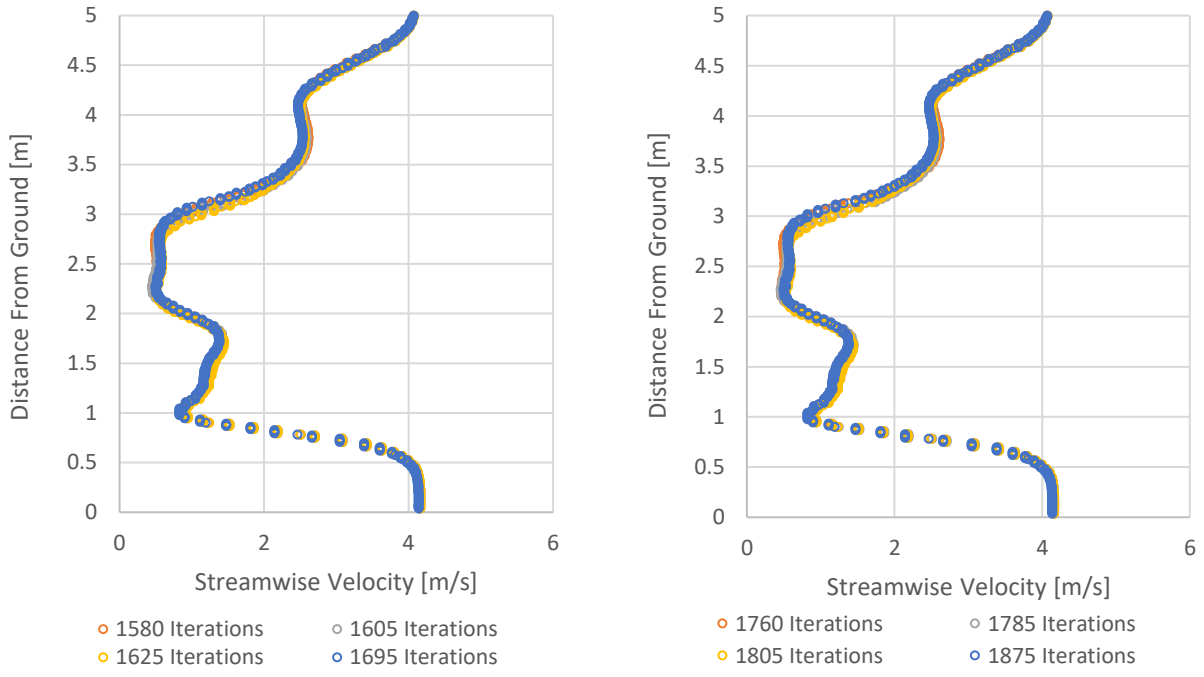

(a) (b)

Figure 5.17: Centerline profiles of streamwise velocity 1.40 m behind the sprayer from 1580-1695 iterations (a) and from 1760-1875 iterations

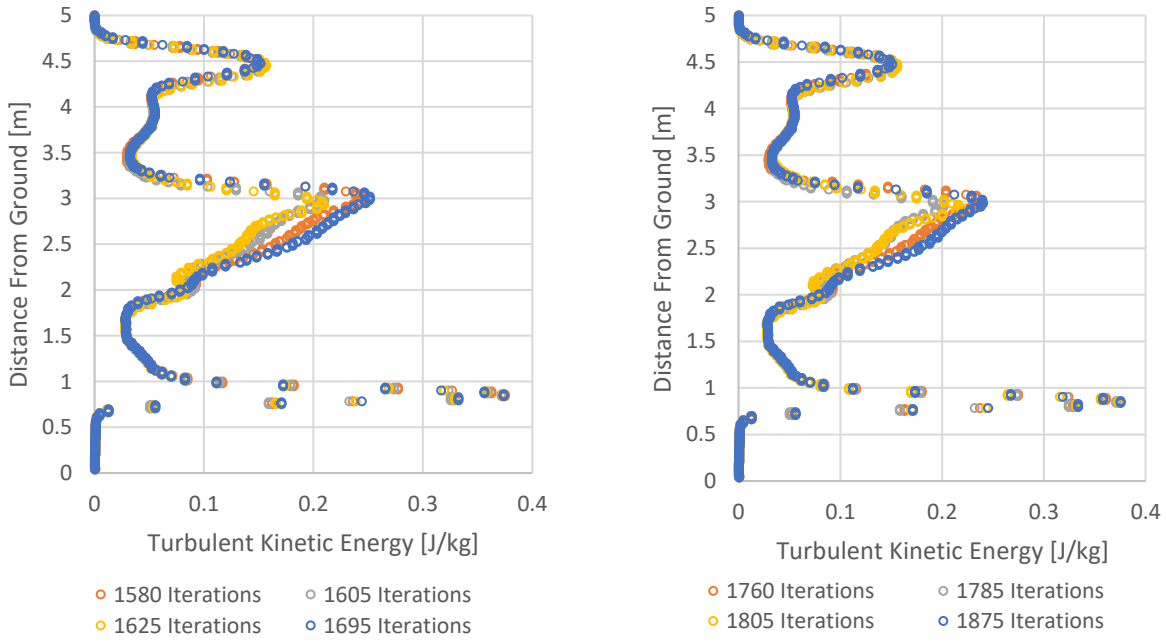

(a) (b)

Figure 5.18: Centerline profiles of TKE 1.40 m behind the sprayer from 1580-1695 iterations (a) and from 1760-1875 iterations

The final method to assess the convergence of the system was to consider the force coefficient on the sprayer. Figure 5.19 shows the variation of the force coefficient with iteration. After quickly dropping from a high value at the start, the force coefficient settles to a value of approximately 143 by 300 iterations.

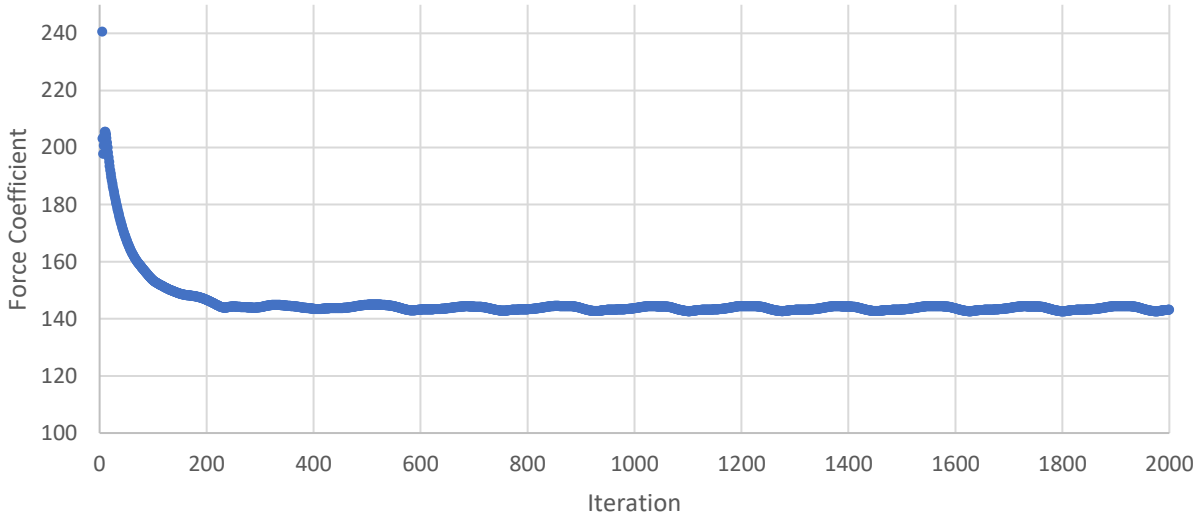

Figure 5.19: Force coefficient on the sprayer body per iteration.

5.6 Base Case: The Wake of an Agricultural Sprayer

The numerical simulations are used to describe the wake of an agricultural sprayer. The sprayer under the operating conditions of a low boom height and high travel speed (Case 1) is defined as the base case against which comparisons will be drawn for the other operating conditions. The results will be presented using several different visualization techniques. The goal is to identify the major flow structures and features, so that comparisons can be made with Cases 2 and 3 to understand how different operating conditions will change the wake structure.

5.6.1 Turbulence and Large-Scale Structures

Wakes are regions of separated flow, with reduced momentum, decreased velocity and pressure, and increased turbulence. It is expected that in regions of increased turbulence there will be an enhanced potential for spray drift, so understanding the locations where turbulence is high is helpful. Landry and Wolf (2019) used turbulent kinetic energy to visualize the wake. In their study they suggested that turbulence levels between 0.5 and 2 J/kg were important for spray drift.

Figure 5.20 shows the TKE results of the current study visualized by the method used by Landry and Wolf (2019). There are several regions of highly turbulent flow in the wake of the agricultural sprayer. Most of these highly turbulent regions exist behind or near the vehicle body.

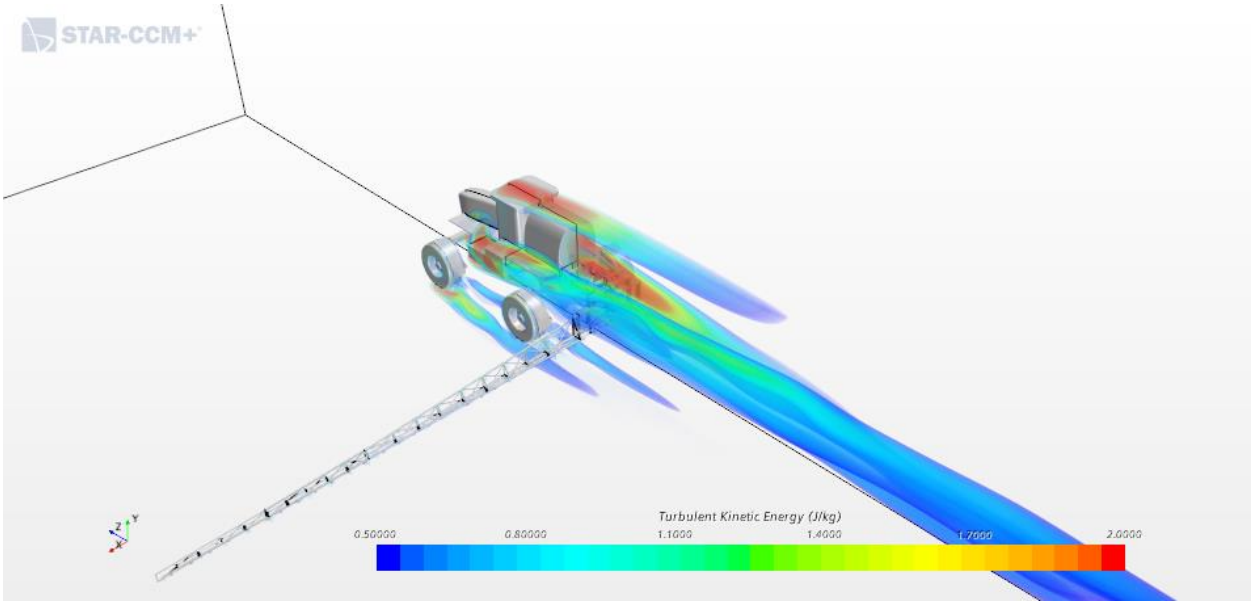

Figure 5.20: 3D visualization of TKE in the wake of the sprayer.

The TKE in the wake of the sprayer is primarily due to the sprayer body, with the boom producing less than 0.5 J/kg of TKE. Five regions of increased turbulent kinetic energy are seen in the wake of the sprayer: above the cab, behind the primary vehicle body, off the side of the tank, and on either side of the rear tire. Further analysis of these highly turbulent regions will be performed to assess the causes of turbulence and how this might affect drift.

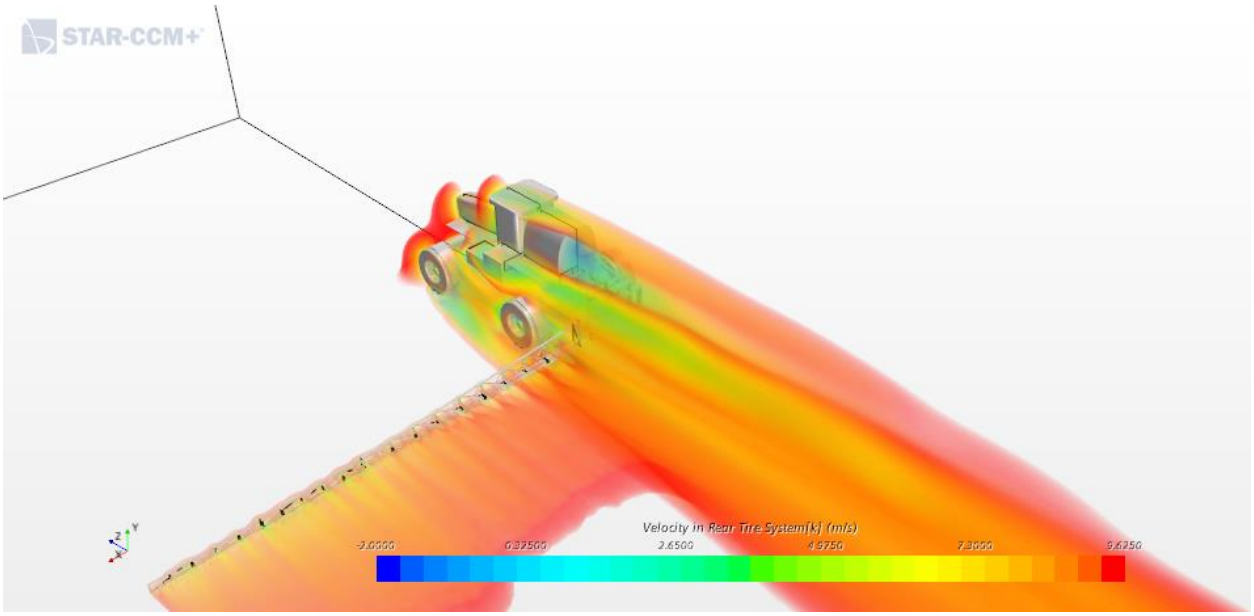

Figure 5.21: 3D visualization of the wake as a region with streamwise velocity less than 87.5% of the freestream, where the free stream velocity is 11 m/s.

Figure 5.21 shows the wake as the region where the streamwise velocity is less than 87.5% of the freestream. The figure indicates that the areas of highest TKE coincide with regions where the streamwise velocity is low or reversed. The wake extends about one vehicle length behind the boom. The lower streamwise velocity in this region will contribute to flow structures which will influence spray drift. The increased size of the wake near the boom tip is an interesting feature of the flow. The larger wake near the tip suggests that there is an increased possibility of drift in the far boom versus in the region near the sprayer.

Streamlines can be used to show the flow direction in regions near the sprayer body. Figure 5.22 shows streamlines around the boom and sprayer body surface coloured by total velocity magnitude. For most of the boom region the streamlines are not affected, suggesting there is little change in direction of the flow. Behind the sprayer however there is significant distortion of the streamlines. Incoming flow is accelerated over or to the side of the cab leaving a large wake behind the sprayer. Behind the tank the flow is directed downwards, and on the side of the tank the airflow curls to respond to the vehicle cab forming what looks like a vortex. Flow is attached to the mudguards and directed downwards, and the downwards flow from the first mudguard moves to the outside of the rear tire due to the flow obstruction.

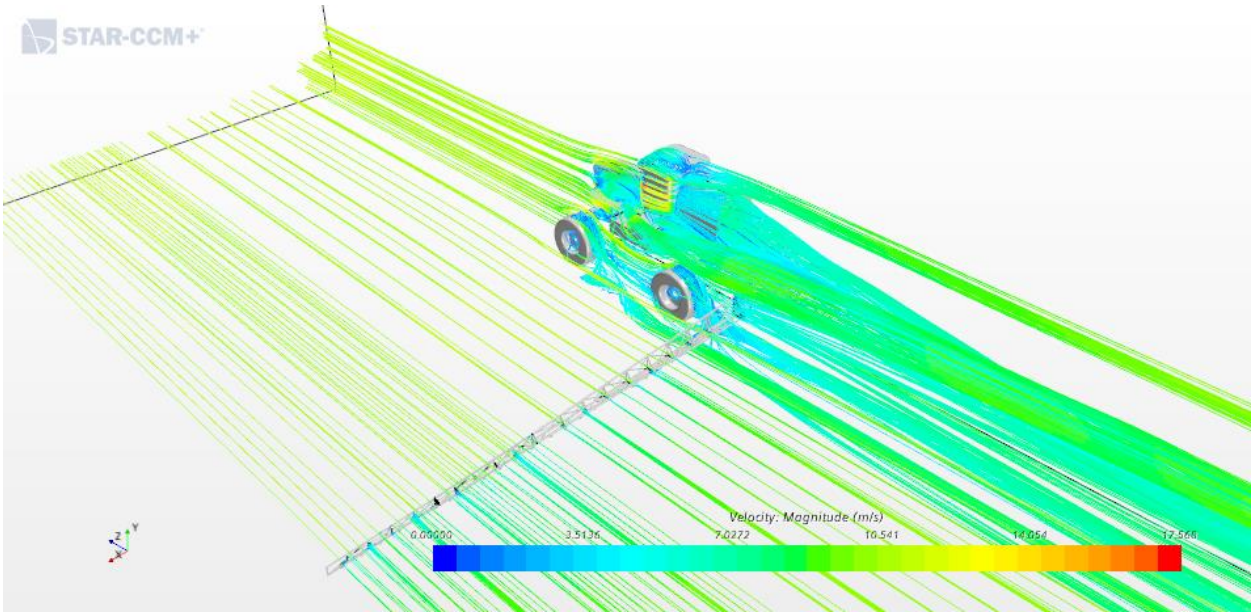

Figure 5.22: Streamlines showing airflow patterns around the sprayer.

Considering the vorticity about the vertical (y) axis shows more evidence of the complex nature of the wake behind the sprayer. In Figure 5.23 the vorticity about the vertical axis is plotted and the highest levels of vorticity align with the highest levels of turbulence, but in addition there is fluid rotation detected just behind the boom of the sprayer, and vorticity is higher near the boom tip. Vorticity is lowest along the boom prior to the first knuckle but increases in the second and third sections where the structure height decreases but overall blockage increases. The vorticity just behind the boom is aligned with the vertical members of the boom structure. This is consistent with the boom simulations performed earlier which showed higher turbulence levels behind the vertical members compared to the open sections of the boom.

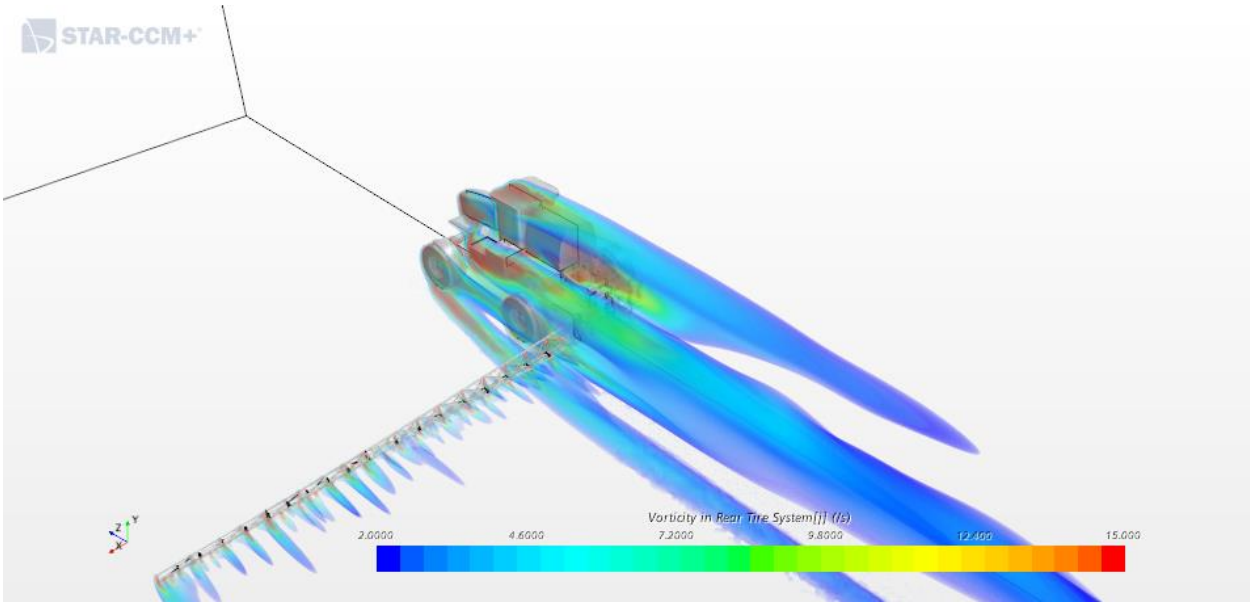

Figure 5.23: 3D visualization of vorticity in the vertical (y) direction, counterclockwise is positive.

5.6.2 Contour Plots

The large-scale structure of the flow has been discussed. In this section, two-dimensional contour and vector plots will be used made to investigate the airflow patterns around the agricultural sprayer.

Two dimensional contour plots are now used to examine the size and magnitude of the wake behind the agricultural sprayer. Figure 5.24 shows a series of contour plots of the streamwise velocity magnitude behind the agricultural sprayer. The series of contour plots begins at the vehicle centerline: a highly disturbed region of flow is shown, with recirculation occurring on the roof of the cab, behind the tank and boom, and in some areas underneath the sprayer (Figure 5.24a). The next location considered is a vertical plane tangent to the sprayer tank and parallel to the side of the cab. Flow accelerates around the cab structure, while recirculation extends slightly above the boom (Figure 5.24b). In the vertical plane through the wheels (Figure 5.24c) the flow velocity is significantly decreased under the boom where the spray is injected.

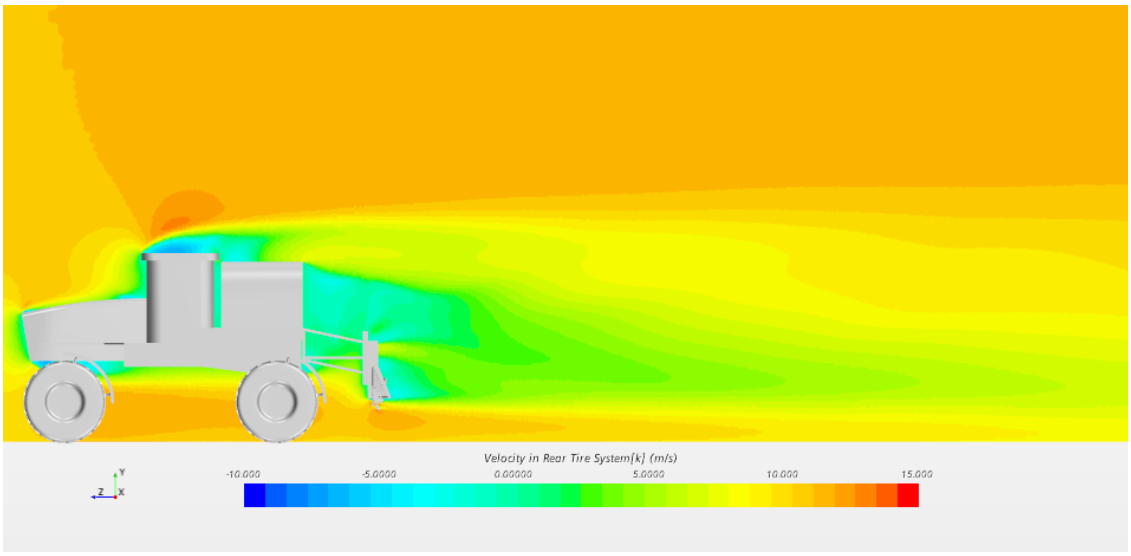
Velocity in Rear Tire System[k] (m/s)
-10.0000
-5.0000
0.00000
5.0000
10.000
15.000
Y
Z
X

a

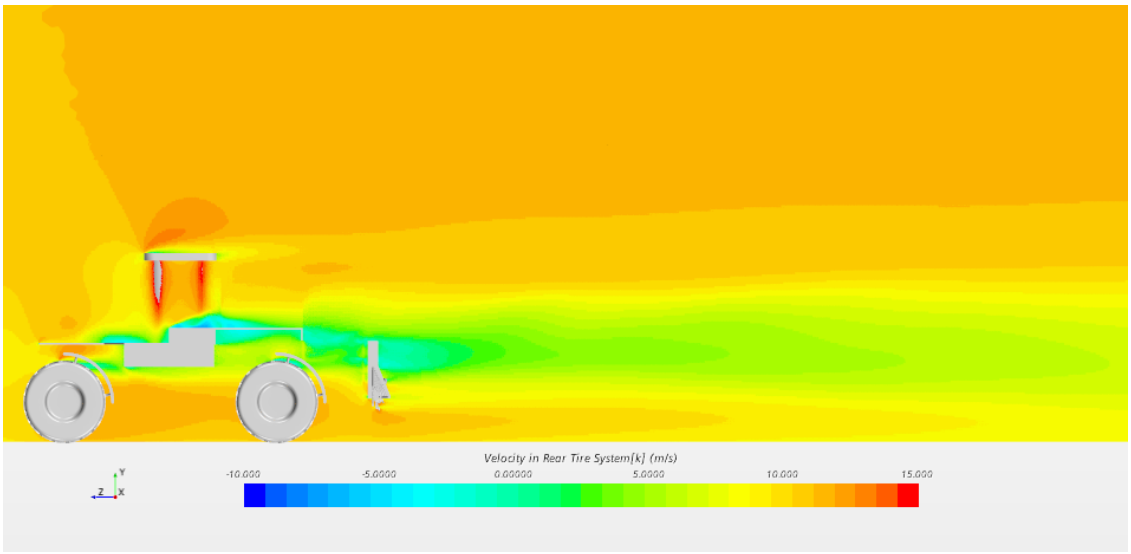
Velocity in Rear Tire System[k] (m/s)
-10.0000
-5.0000
0.00000
5.0000
10.000
15.000
Y
Z
X

b

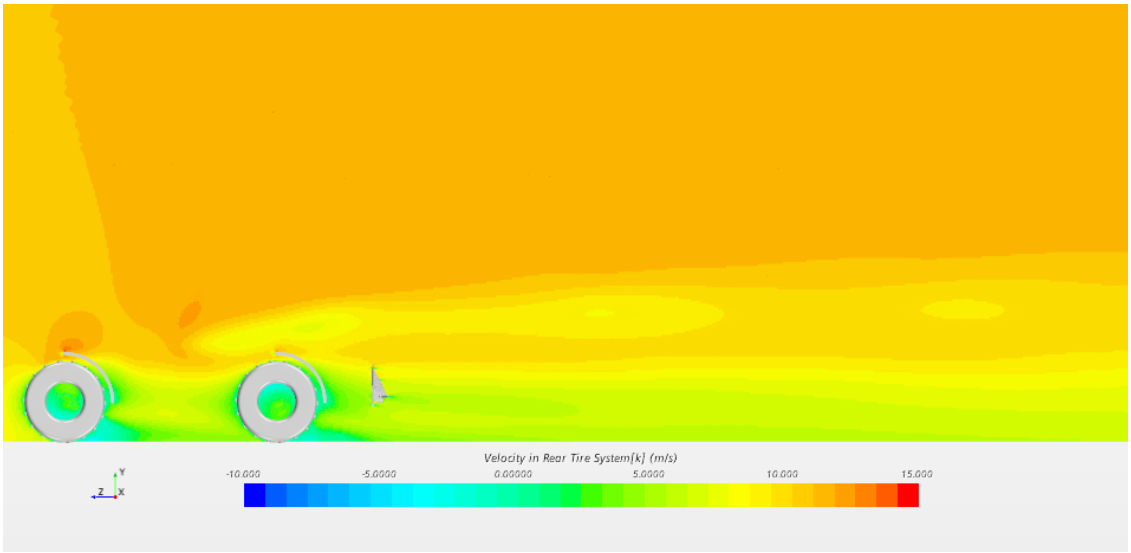
Velocity in Rear Tire System[k] (m/s)
-10.0000
-5.0000
0.00000
5.0000
10.000
15.000
Y
Z
X

c

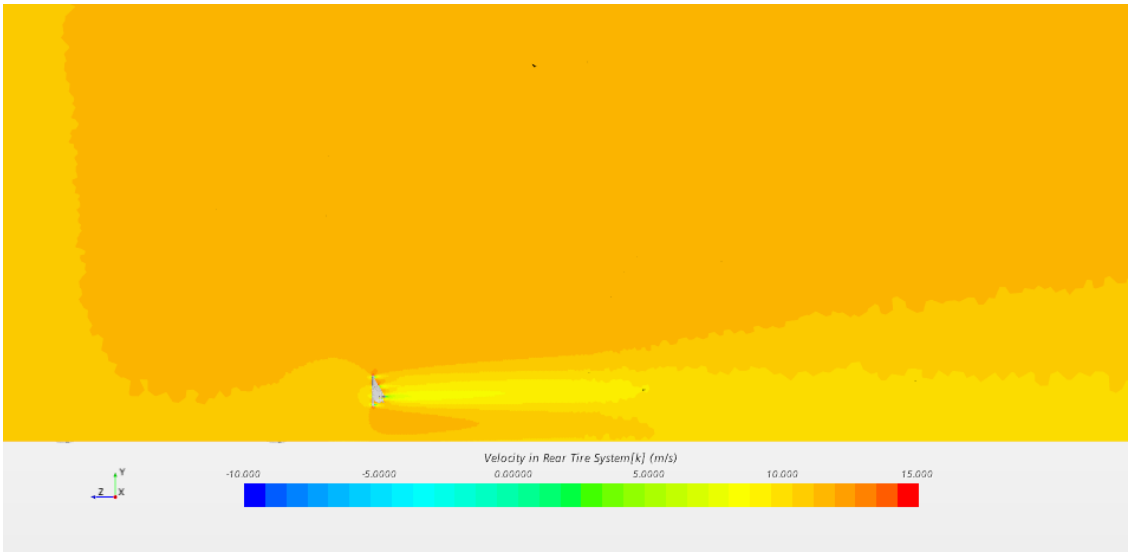

d

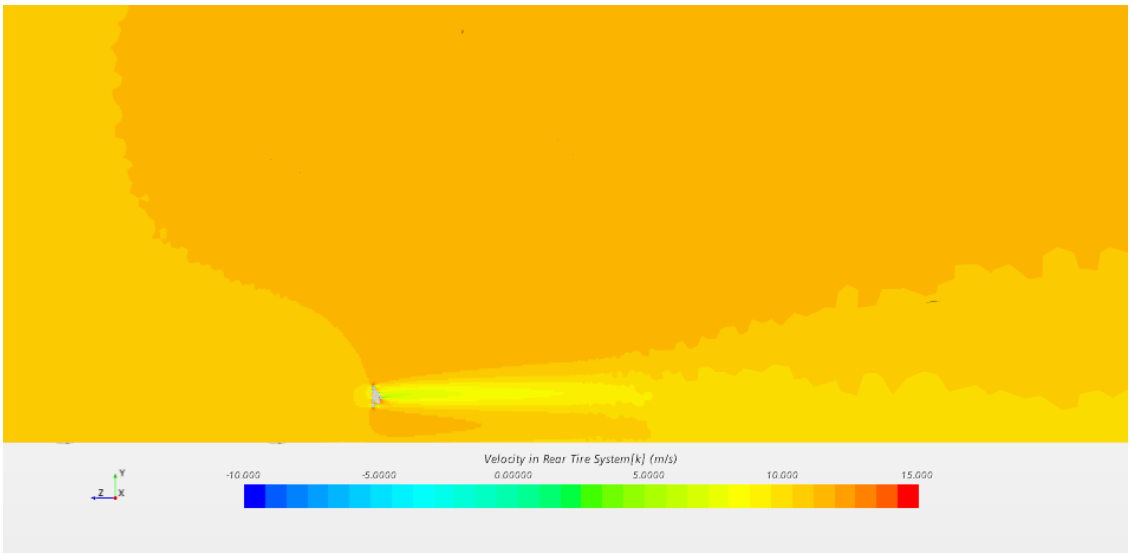

e

Figure 5.24: Lateral development of the wake visualized by streamwise velocity contour plots at the centerline (a), a plane next to the tank edge (b), a plane through the tires (c), down boom locations of 3.45 m (d), and 6.78 m (e),

The two plots along the boom show similar behaviour. The structure of the boom decreases in height moving towards the boom tip, reducing the open area of the boom, and this increases the blockage of the flow. The height of the boom structure decreases and the blockage increases, the wake decreases in height and increases in length. Comparing the vertical planes taken at 3.45 m (Figure 5.24d) and 6.78 m (Figure 5.24e) shows the largest change of the wake profile in the boom zone. All the contours except for the vertical plane at the wheels (Figure 5.24c) show that flow accelerates under the boom. This means that the spray is injected into a region of flow with a velocity higher than the freestream velocity.

5.6.3 Velocity Vector Plots

Vector plots of velocity can be used to identify flow direction and strength. These plots can be used to obtain additional information about the structures of the flow compared to the contour plots. Vector plots are used in this study to visualize the secondary flow field in the wake of the sprayer from the perspective of an observer standing behind the sprayer. Three vertical transverse planes are shown to visualize the secondary flow field, one at the location of the nozzles, one 0.9 m behind the sprayer, and another 5 m behind the sprayer. The plots are shown in Figure 5.25, Figure 5.26, and Figure 5.27, respectively.

In the plane through the nozzles (Figure 5.25) the flow direction under the boom is generally downward oriented. This should drive the spray downwards, which would reduce drift. Around the first knuckle there is a strong upward vector; this is also a feature that was noticed by Teske et al. (2015) in their wind tunnel study of an agricultural sprayer. The strong upward vector also acts as a dividing point in flow direction under the boom. Nearer the boom tip the flow tends to move towards the boom tip, whereas closer to the sprayer the flow tends to move towards the sprayer.

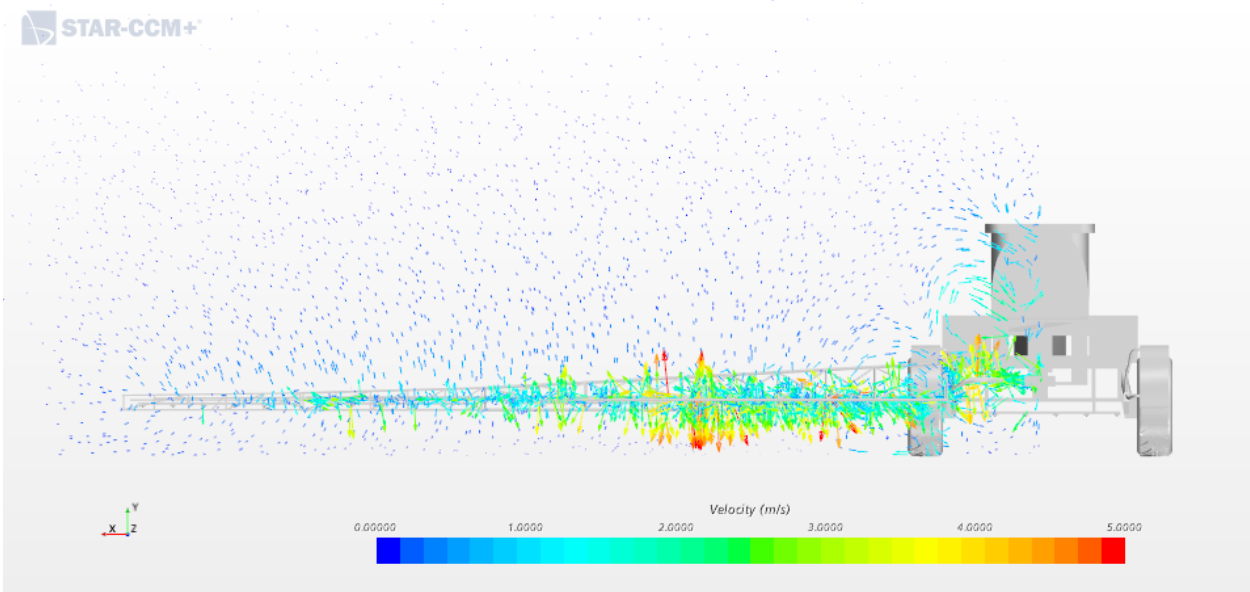

Figure 5.25: Velocity vectors showing the secondary flow field through the nozzles of the agricultural sprayer.

In Figure 5.26 for the plane 0.9 m downstream, the strong vertical vector has washed out, but the flow just above the boom moves upwards at a velocity of about 10% of the freestream. Below the boom the flow is directed downwards and towards the boom tip or towards the sprayer depending on what side of the first knuckle the flow is on. Swirling motion in the wake is more apparent at this location. Close to the ground just outside of the rear wheel the vector field shows a clockwise rotation of the mean velocity. A second recirculation zone occurs next to the tank, likely associated with the flow being entrained into the wake behind the sprayer.

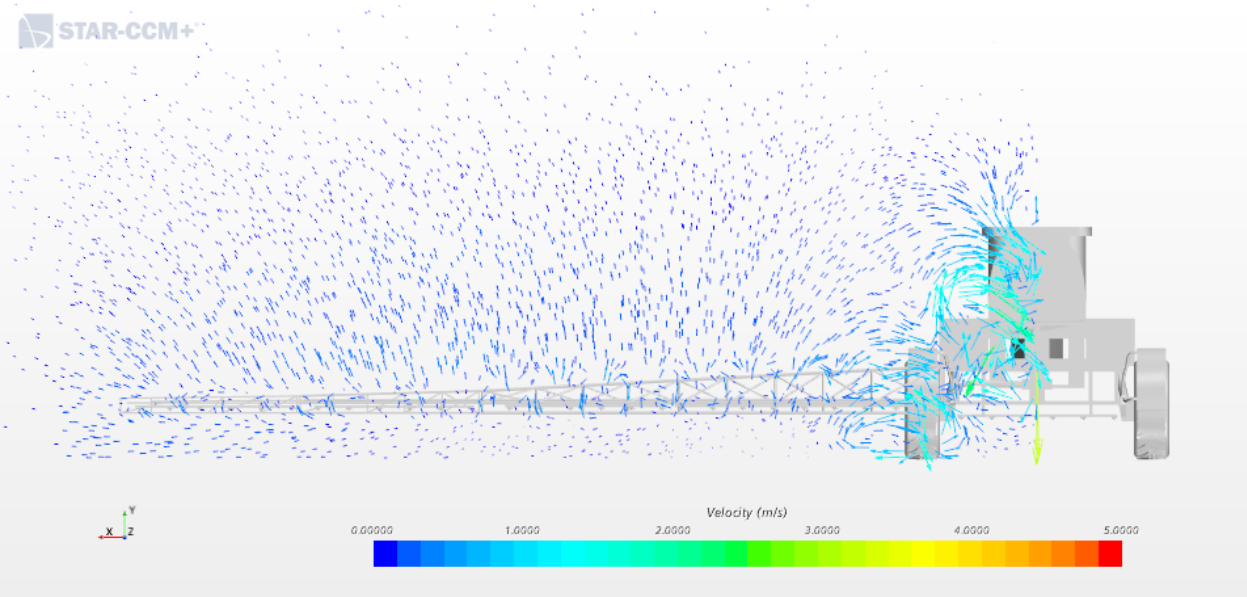

Figure 5.26: Velocity vectors showing the secondary flow field in a vertical transverse plane 0.9 m behind the boom of the agricultural sprayer.

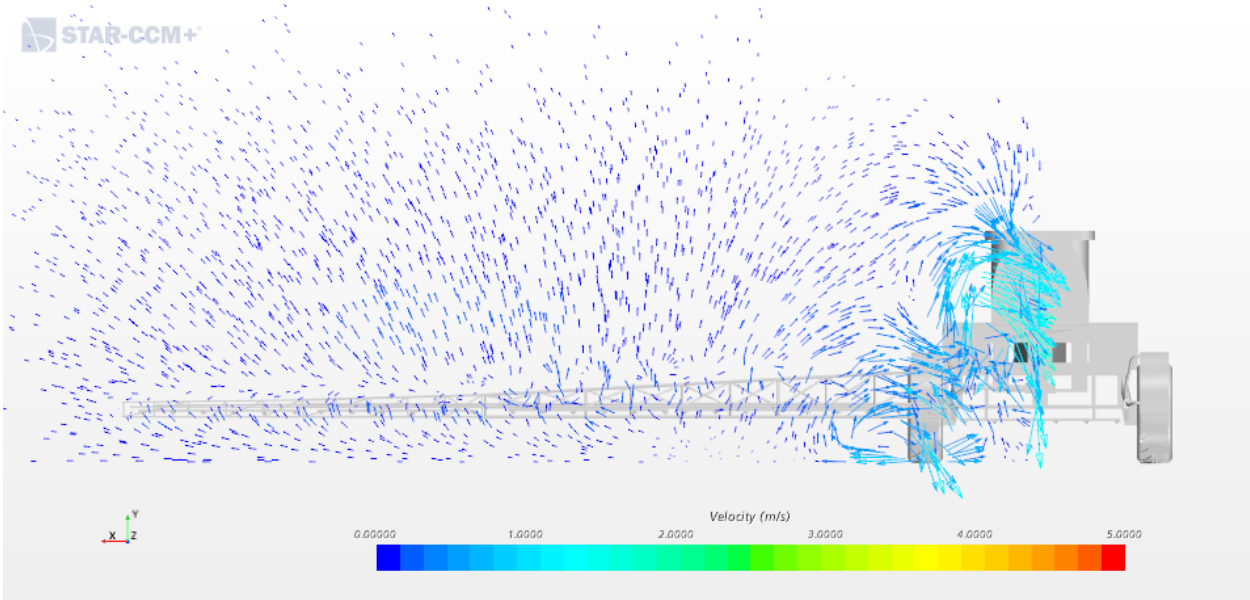

Figure 5.27: Velocity vectors showing the secondary flow field in a vertical transverse plane 5 m behind the boom of the agricultural sprayer.

Figure 5.27 shows similar structures to Figure 5.26, but by 5 m downstream the upwards velocity has been reduced from 10% to 2% of the freestream. At this far downstream location, the velocity is also directed upwards below the boom, but since this location is far downstream it is unlikely to contribute to drift significantly. Both areas where swirling flow was identified have grown larger in size, but the intensity has reduced, indicating that the flow features are tending to recover to the upstream conditions.

5.7 Wake Comparison for Different Operating Conditions

Three operating conditions were tested to determine if changes to the operating conditions affect the structure of the wake. The two other cases tested were the low boom height and slow travel speed (Case 2), where the boom height was 0.64 m and the sprayer speed was 4 m/s, and the high boom height and fast travel speed (Case 3), with a boom height of 1.14 m and a sprayer speed of 11 m/s. These two operating conditions indicate how the wake responds to changes in velocity and boom height. The literature suggests that increasing either of these operating conditions will increase the likelihood of drift occurring (Nuyttens et al. 2007).

5.7.1 Case 2: Low Boom Height and Slow Travel Speed

The low boom height and slow travel speed case (Case 2) should minimise spray drift. Comparing Case 2 and Case 1 helps to determine what flow structures could increase the possibility of spray drift in the high-speed scenario (Case 1).

Using the same criteria as before, the wake is shown in Figure 5.28, as the region where velocity is 87.5% of the freestream or less. The result is like Case 1 (Figure 5.21). The wake has the largest deficit behind the cab and tank of the sprayer, there is a region of slower moving fluid extending downstream above the rear tire, and along the boom the wake is larger towards the tip than for regions near the sprayer (outside of the vehicle affected zone). The streamlines also show a similar flow pattern as seen in Figure 5.29. Above the rear tire the slow-moving air seems to be swirling due to an interaction with the cab, and the flow is attached to the mudguards and directed downwards.

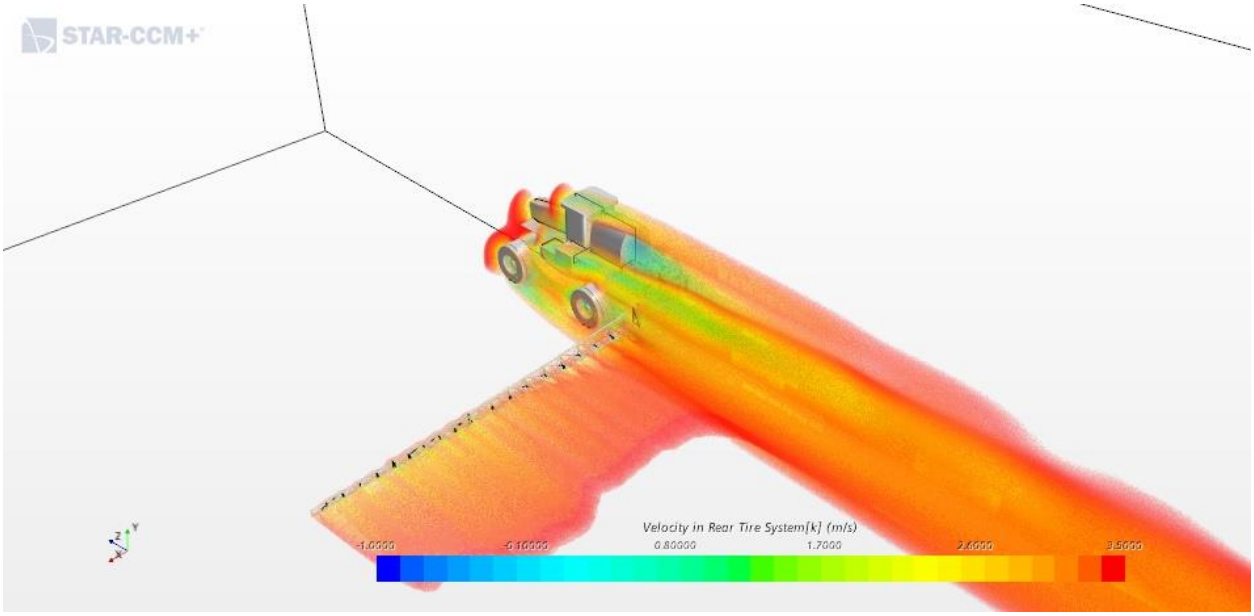

Figure 5.28: Wake region where the fluid velocity is less than 87.5% of the freestream for the low boom height and slow travel speed (Case 2). The freestream velocity in this simulation is 4 m/s.

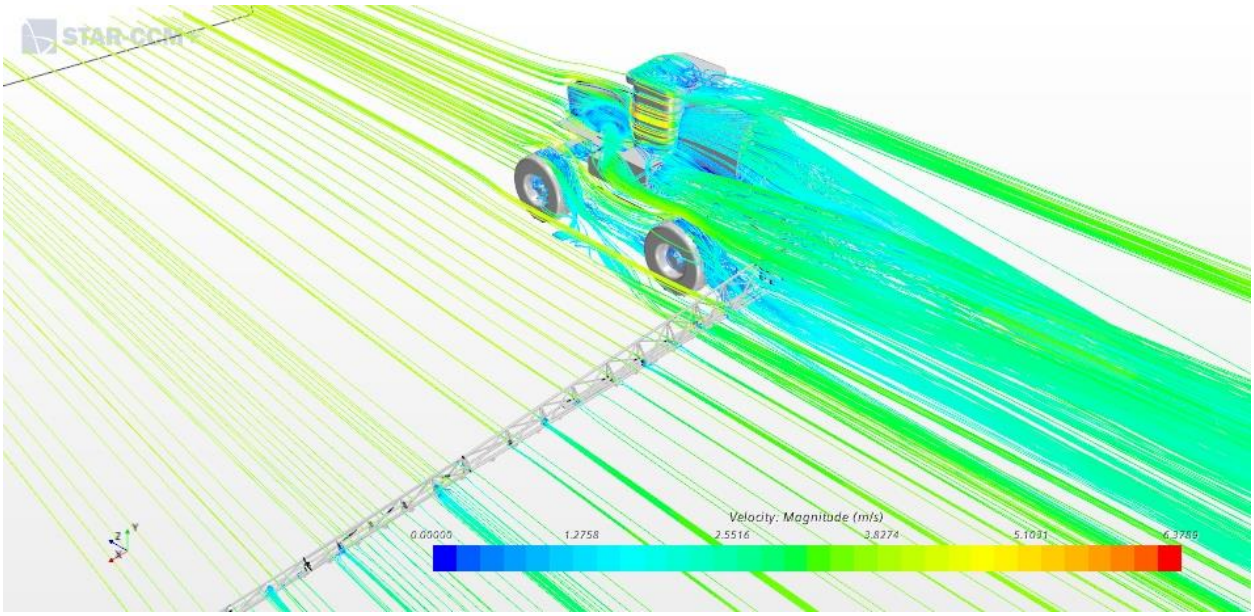

Figure 5.29: Streamlines for the low boom height and slow travel speed (Case 2).

The velocity field appears to be very similar for Case 1 and Case 2. However, the turbulence fields that show some differences. Showing the TKE in the same fashion as Landry and Wolf (2019) yields Figure 5.30, which shows almost no turbulence in the wake of the sprayer except for small patches behind the tank and over the cab. A conclusion in this case is that since the turbulence level is so much smaller for Case 2, the potential to cause spray drift is also reduced.

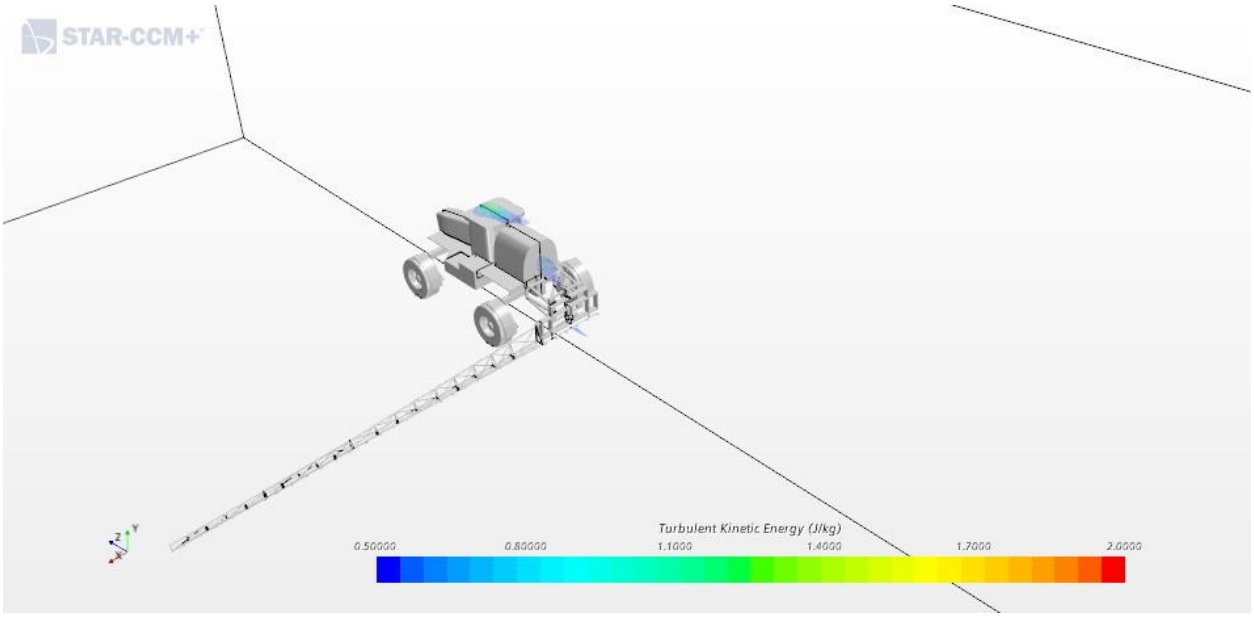

Figure 5.30: TKE for the low boom height and slow travel speed (Case 2).

By changing the contour map to focus only on lower values of TKE, in Figure 5.31, it can now be seen that the locations of highest turbulence for Case 2 correspond to those for Case 1 (low boom height and fast travel speed). These locations are above the cab, behind the tanks, above the wheels stretching downstream, and off the front of the rear tire. Figure 5.31 also shows the boom generating some turbulence in the flow, but when normalized by the square of the freestream velocity the value is approximately 0.625%, which is much less than the wake of the cab.

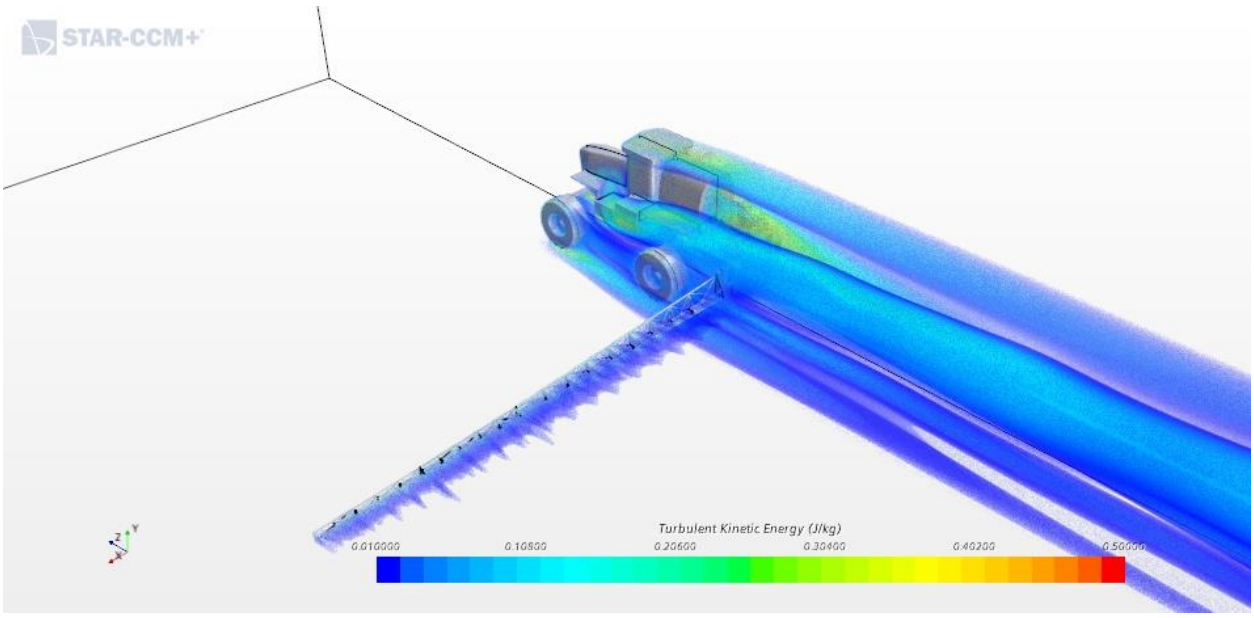

Figure 5.31: TKE for the low boom height and slow travel speed (Case 2) plotted for low turbulence values.

5.7.1.1 Comparison of Downstream Wake Profiles

To further examine the similarity between Case 2 (low and slow) and the Case 1 (high and fast) plots of dimensionless streamwise velocity at three downstream distances, 0.43 m, 0.79 m, and 1.40 m, and at seven lateral locations along the boom are presented. The local streamwise velocity is normalized by the freestream velocity to illustrate how the wake changes at the different downstream locations. In order to create plots that follow the convention of the available literature (Teske et al. 2015; Teske, Thistle, Petersen, et al. 2016b) the streamwise velocity is reported as u instead of w. Considerations of Figure 5.32 indicates that the velocity field at the selected locations is similar between the two studies. There is a small deviation between the profiles near the ground plane for the locations inside the tires (Figure 5.32c), which

suggests that the flow underneath the cab of the sprayer is slightly different between the two studies.

The wake velocity profiles show the relative size of the wake in each region of the sprayer and the rate of recovery. The wake is largest near the centerline of the vehicle and decreases towards the boom tip. In the plane next to the tank (Figure 5.32b) the wake is smaller than on the centerline (Figure 5.32a), and has the largest deficit associated with the hydraulic equipment used to raise and lower the boom height. The wheels (Figure 5.32c) create a different flow pattern compared to other locations: where the profiles do not show a wake structure that could be associated with only the boom, implying the effect of the tires is significant. At 2.08 m along the boom from the tire (Figure 5.32d) the wake shows the individual members of the boom geometry, with the top and bottom structures appearing in the wake. For the remaining boom locations, the wake appears to be a that of a single large structure instead of individual elements. The wake plots in Figure 5.32 show that the normalized velocity profiles are similar, especially for the boom outside of the track width of the sprayer (Figure 5.32d, e, f, g).

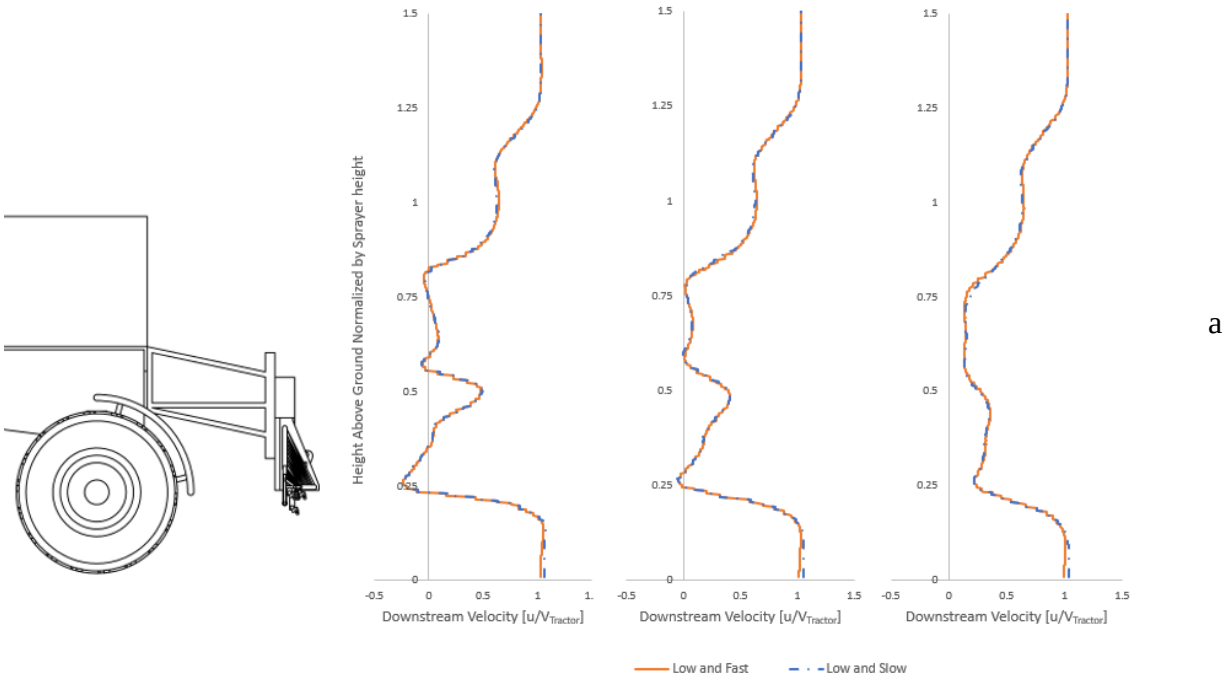

a

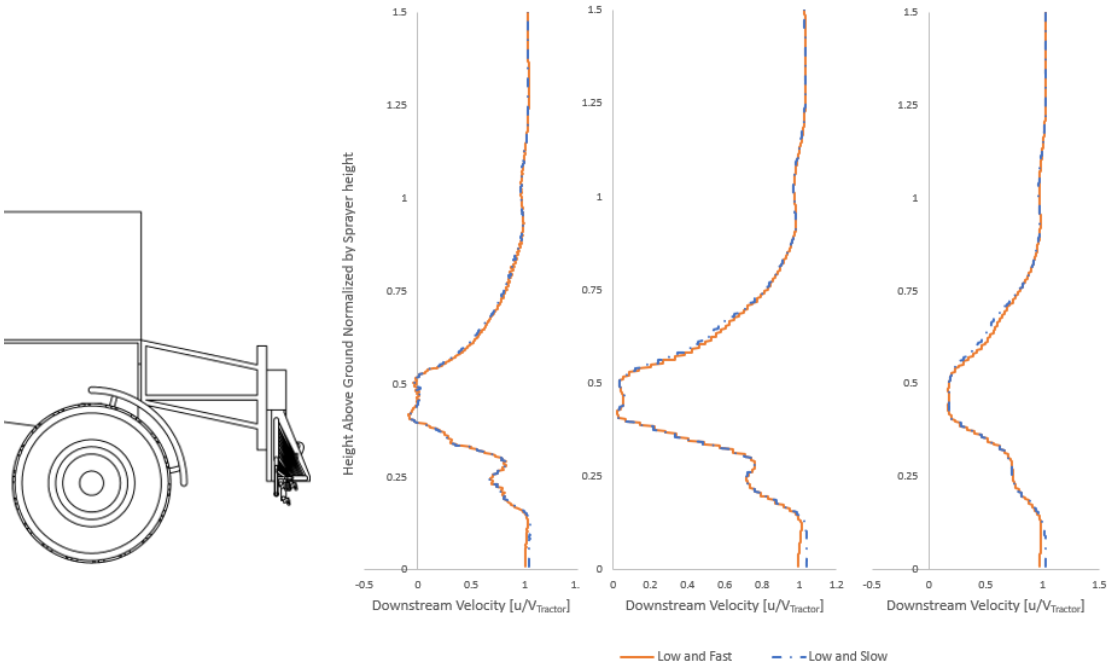
Height Above Ground Normalized by Sprayer height
Downstream Velocity [u/V$_{Tractor}$]
Low and Fast
Low and Slow

b

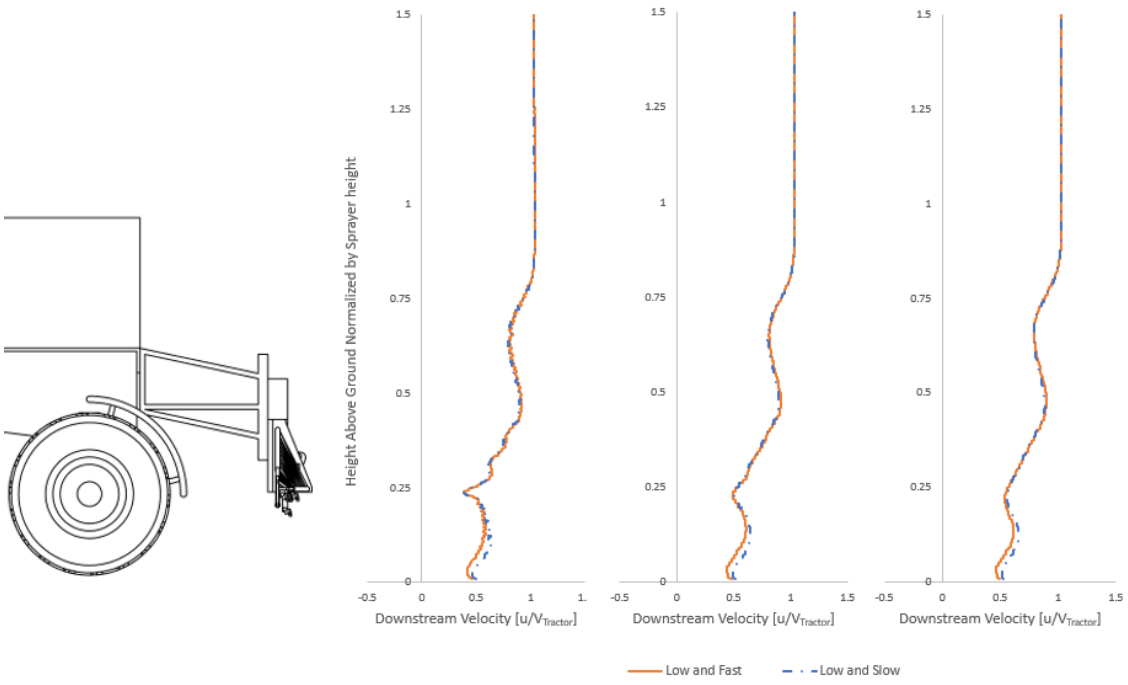
Height Above Ground Normalized by Sprayer height
Downstream Velocity [u/V$_{Tractor}$]
Low and Fast
Low and Slow

c

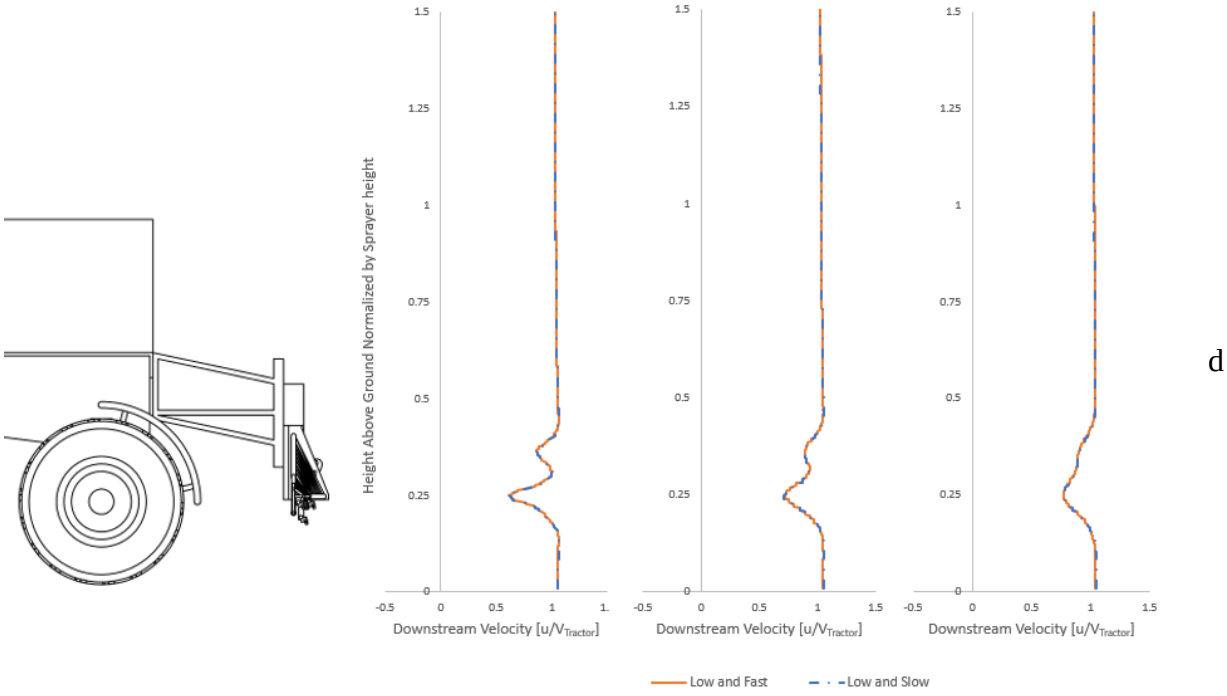
Height Above Ground Normalized by Sprayer height
Downstream Velocity [u/V_Tractor]
Low and Fast
Low and Slow

d

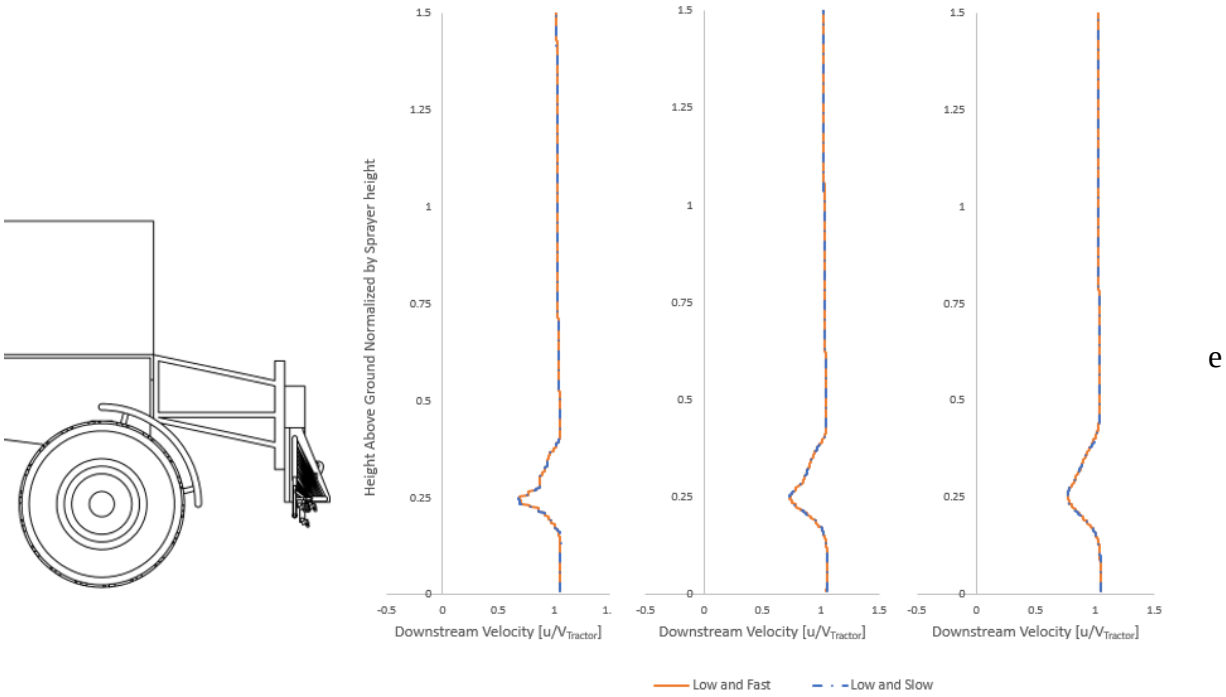
Height Above Ground Normalized by Sprayer height
Downstream Velocity [u/V_Tractor]
Low and Fast
Low and Slow

e

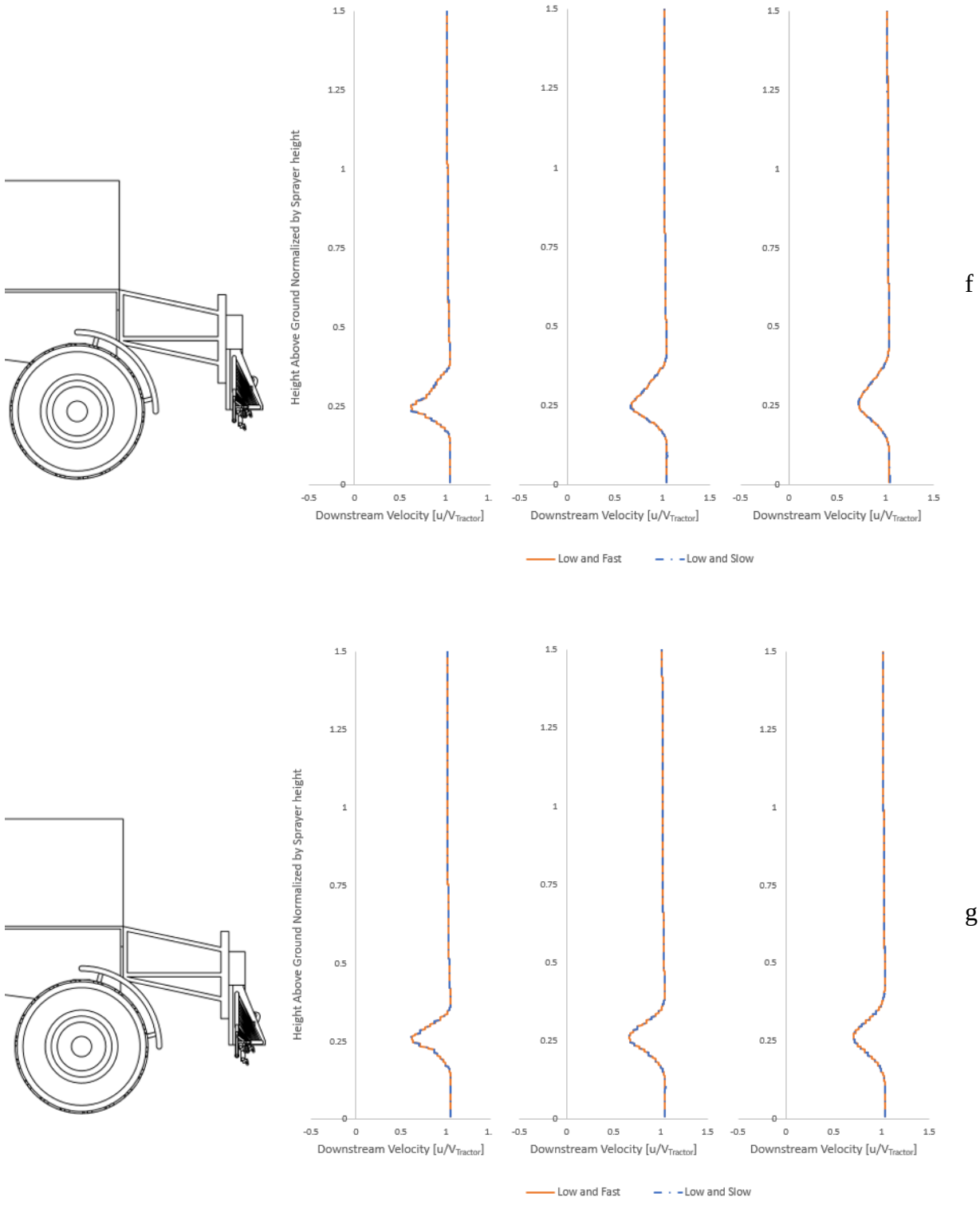

Figure 5.32: Normalized streamwise velocity for Case 1 and Case 2 at three locations downstream of the boom, 0.43 m, 0.79 m, and 1.40 m. The plots are located at the centerline (a), next to the tank (b), through the wheels (c), and at distances down boom from the tire of 2.08 m (d), 3.45 m (e),5.11 m (f) and 6.78 m (g).

The physical size of the wake is longer when the travel speed is increased from slow to fast and plotting the TKE shows a similar pattern. Figure 5.33 shows the TKE at the centerline 0.43 m behind the sprayer. Figure 5.33a compares the TKE normalized by the square of velocity for Case 1 and 2, Figure 5.33b shows the non-normalized TKE. Landry and Wolf (2019) suggested that increases to the level of TKE will increase the possibility of spray drift, the non-normalized TKE level shows that the level of turbulence is significantly higher for Case 1 compared to Case 2, which is expected to minimize spray drift. This increase to turbulent kinetic energy is related to the increase in sprayer speed.

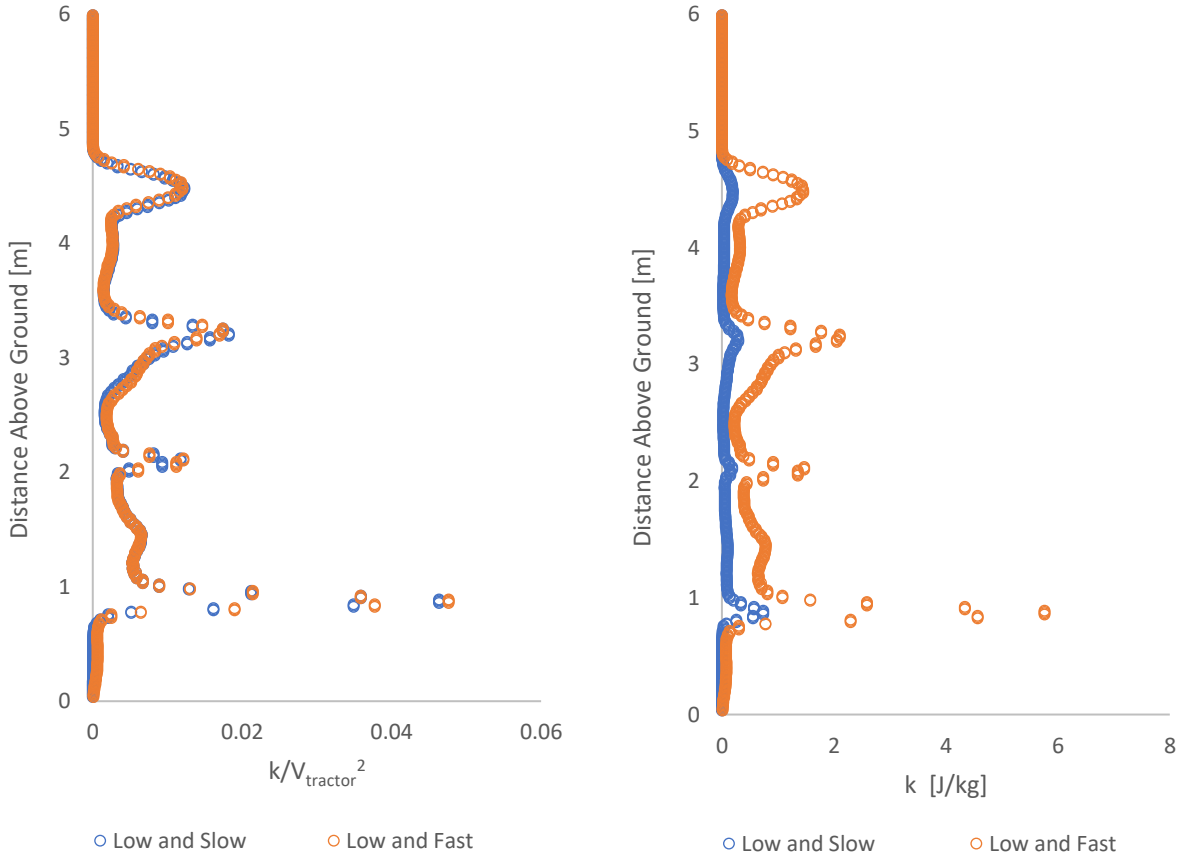

(a) (b)

Figure 5.33:Comparing normalized turbulent kinetic energy (a) to turbulent kinetic energy (b) for the profile at the centerline 0.43 m behind the sprayer.

5.7.2 Case 3: High Boom Height and Fast Travel Speed

The high boom height and fast travel speed simulation (Case 3) was performed to examine a scenario with an enhanced potential for spray drift. It is known that increasing either boom height or sprayer travel speed will increase spray drift (D. Nuyttens et al. 2007). Case 3 will illustrate the wake features for a high drift scenario and the wake prediction will be compared to Case 1.

Figure 5.34 shows the wake for Case 3 as the region where the local velocity is less than 87.5% of the freestream. Comparing these results to Case 1 (Figure 5.21) indicates that the general structure of the wake is similar: velocity deficits occur behind the sprayer tank, along the boom growing towards the tip, and behind the tires. A difference is noticed in the section of the boom closest to the sprayer where the wake is not surrounding the whole boom structure, and instead the wake is aligned with the vertical members of the boom structure. This shows that there is faster moving air inside the boom, and in the area close to the boom structure. Additionally, the strong deficit that exists above the tires passes through the boom structure which increases the strength of the deficit in this location.

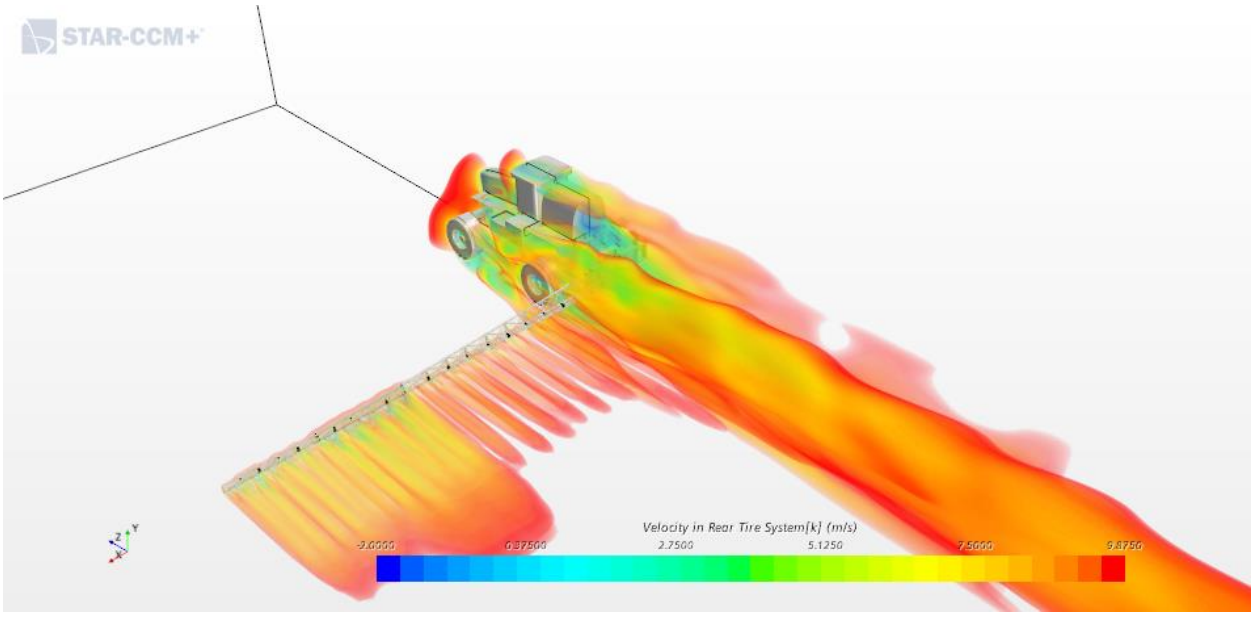

Figure 5.34: Wake of the sprayer displayed as the region where the velocity is less than 87.5% of the freestream for the high boom height and fast travel speed (Case 3) simulation.

Figure 5.35 shows streamlines close to the surface of the agricultural sprayer. The flow in this case shows stronger mean recirculation zones than in Case 1 (Figure 5.22), especially behind the

sprayer tank. This is attributed to the high boom height interfering with the flow behind the agricultural sprayer.

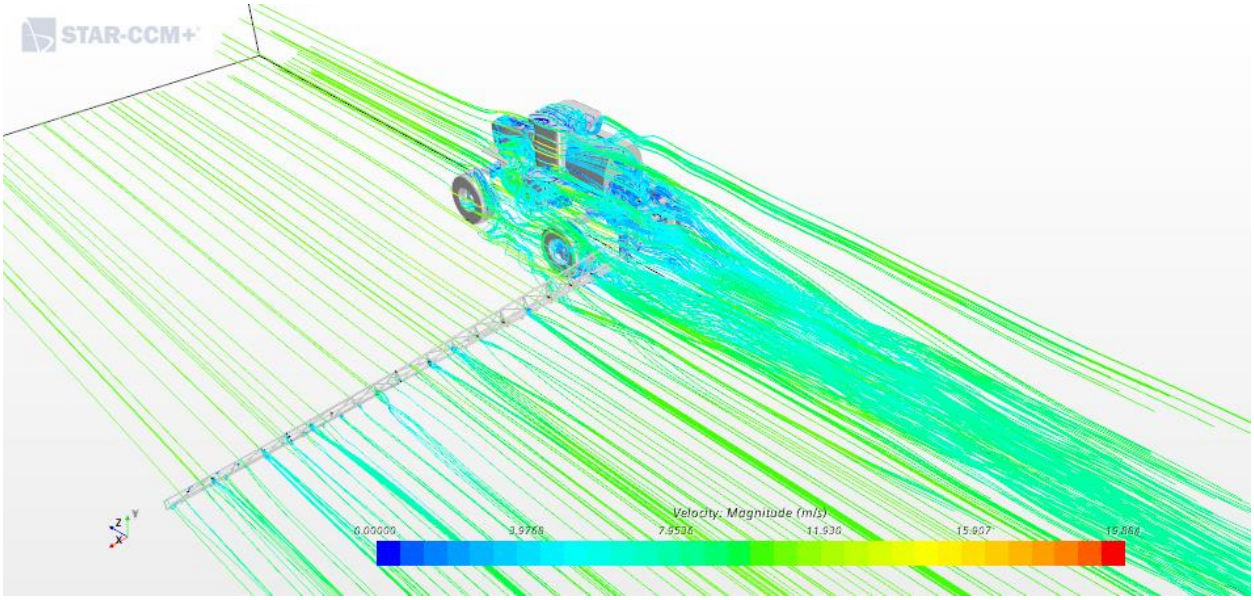

Figure 5.35: Streamlines for the high boom height and fast travel speed (Case 3) simulation.

The TKE in the wake of the sprayer is shown in Figure 5.36. As with Case 1 (Figure 5.20) there are strong flow structures in the wake of the sprayer behind the tank, off the front tire, and above the wheels passing through the boom in the raised position. The strongest turbulence is in the region directly behind the sprayer body, with minimal turbulence associated with the boom wake except for the region beyond the first knuckle where the size of the velocity deficit increases (as discussed in Section 5.6.3).

The vertical axis (y) vorticity shown in Figure 5.37 shows that the vorticity around the sprayer for Case 3 is higher than for Case 1. In the boom there are appreciable levels of vorticity which were not shown in Case 1 (Figure 5.23). This pattern continues along the boom where the size of the wake increases down boom towards the tip. For the core of vorticity that exists above the tires, the pattern has changed slightly since the flow now passes through the boom. This slightly increases the level of vorticity in this region and leads to a different flow structure downstream.

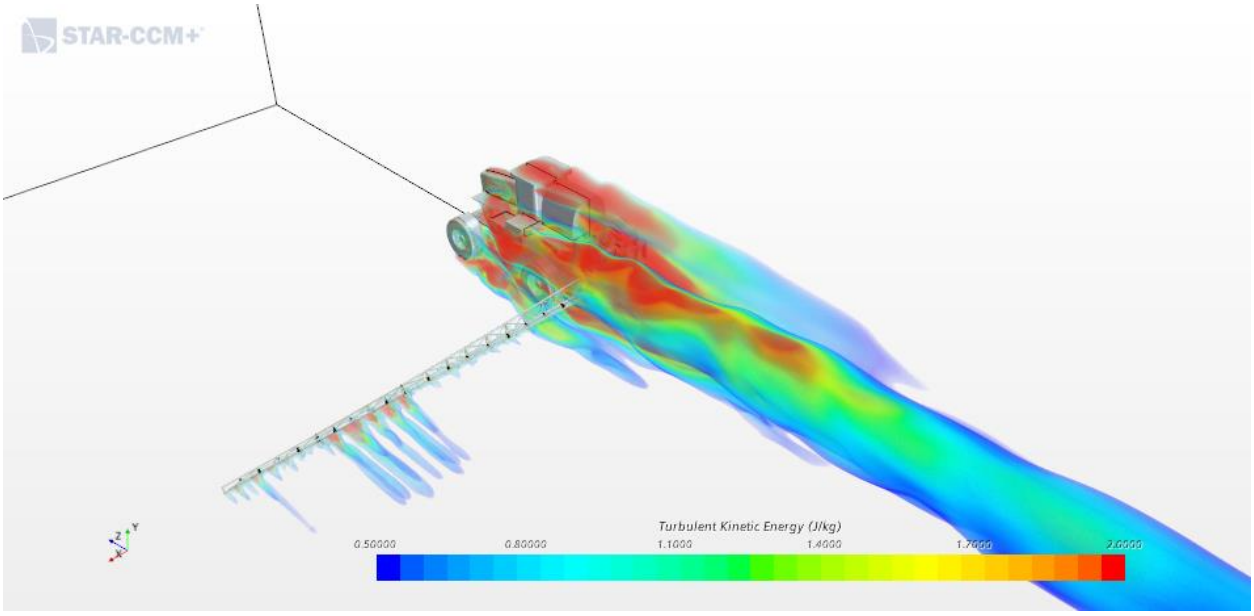

Figure 5.36: TKE for the high boom height and fast travel speed simulation.

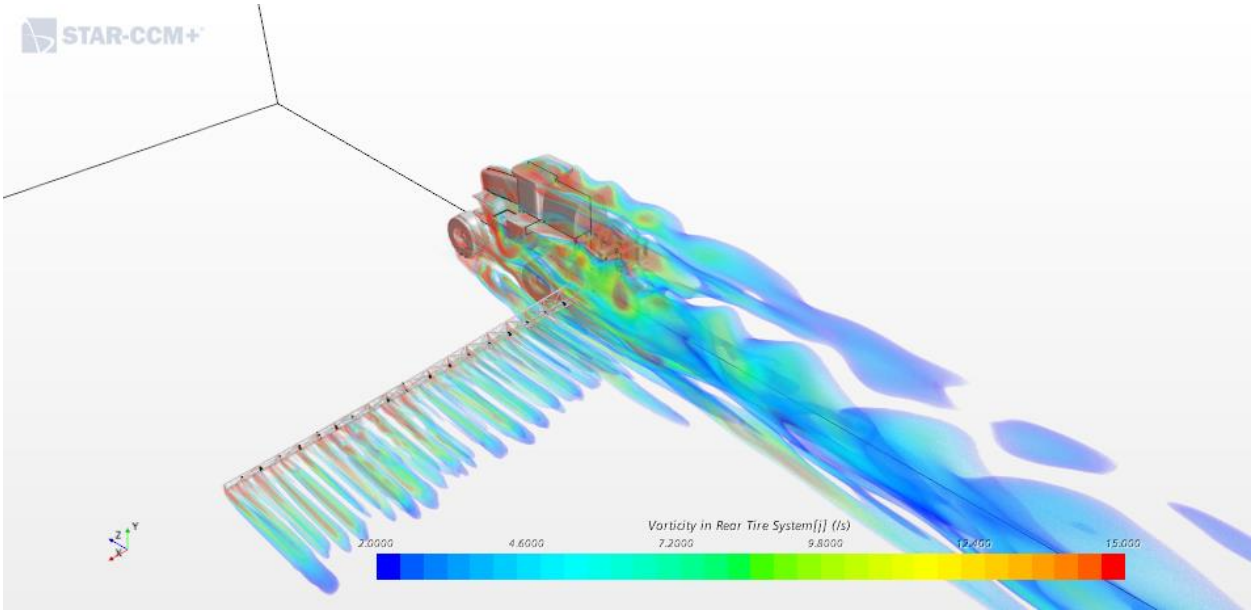

Figure 5.37: Wake of the agricultural sprayer visualized with vertical (y) vorticity for the high boom height and fast travel speed simulation (Case 3).

5.7.2.1 Wake Contour Plots of Streamwise Velocity

Two-dimensional contour plots of streamwise velocity at known locations are used in Figure 5.38 to visually characterize the wake. The largest deficit exists at the centerline (Figure 5.38a) due to the obstruction of the vehicle body. For the high boom height and fast travel speed (Case 3) simulation, the boom is more influenced by the flow behind the sprayer body; together the

boom and sprayer body create a combined wake instead of two independent wakes that merge downstream. Below the sprayer body the flow is accelerated and there is a larger zone of accelerated air that the spray must travel through to reach the ground.

In the section aligned with the tank (Figure 5.38b) the wheel effect is clearly shown. The boom affects the deficit that is observed above the tires. The length of this deficit is increased for both the section aligned with the tank and the section through the tires. For the sections along the boom (Figure 5.38d, and e) similar behavior as before is noted with the wake being smaller closer to the sprayer body than further down boom where there is increased blockage. Below the boom there is a larger area of increased flow, with the accelerated flow penetrating further downstream compared to the low boom case.

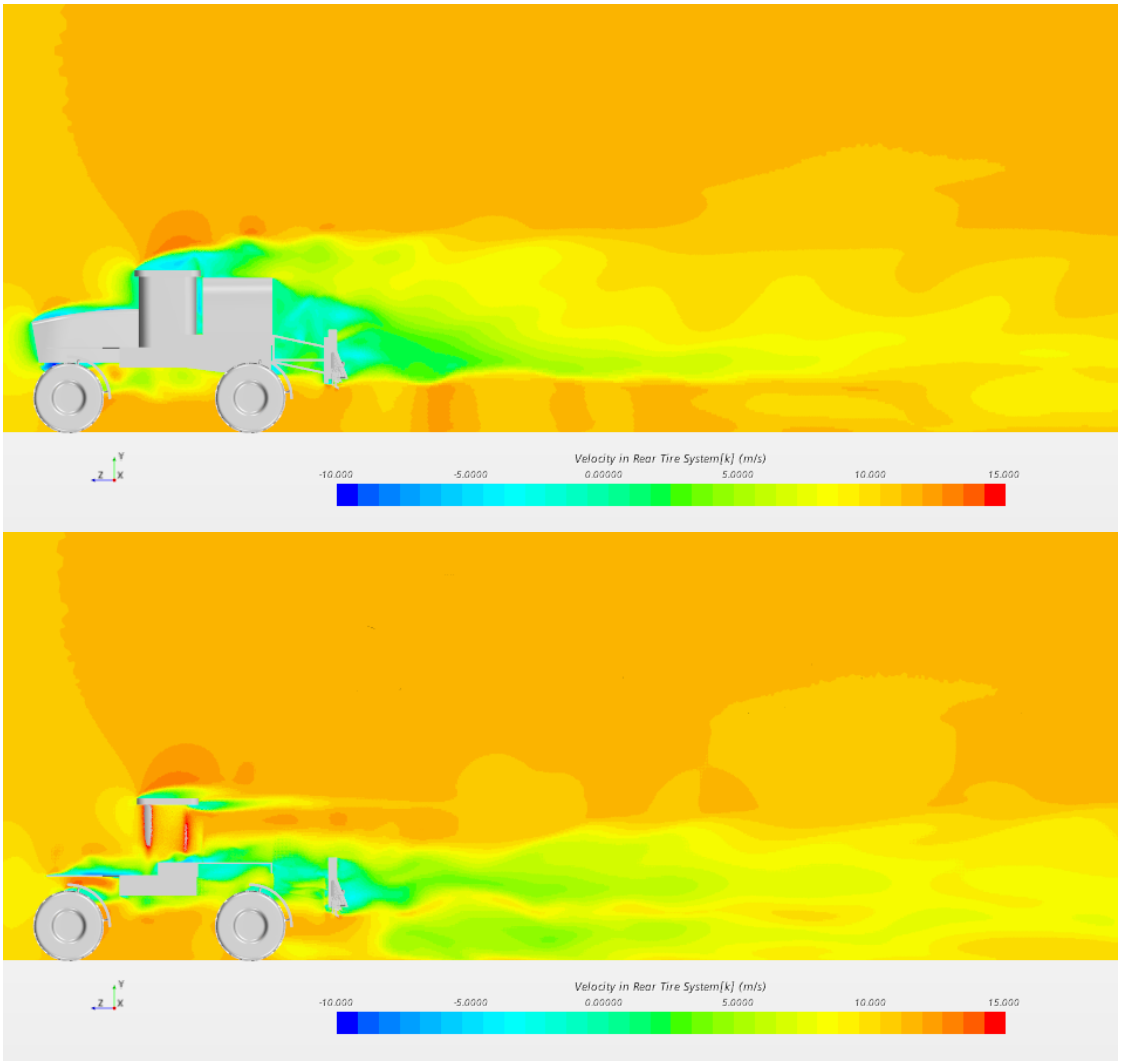

a

b

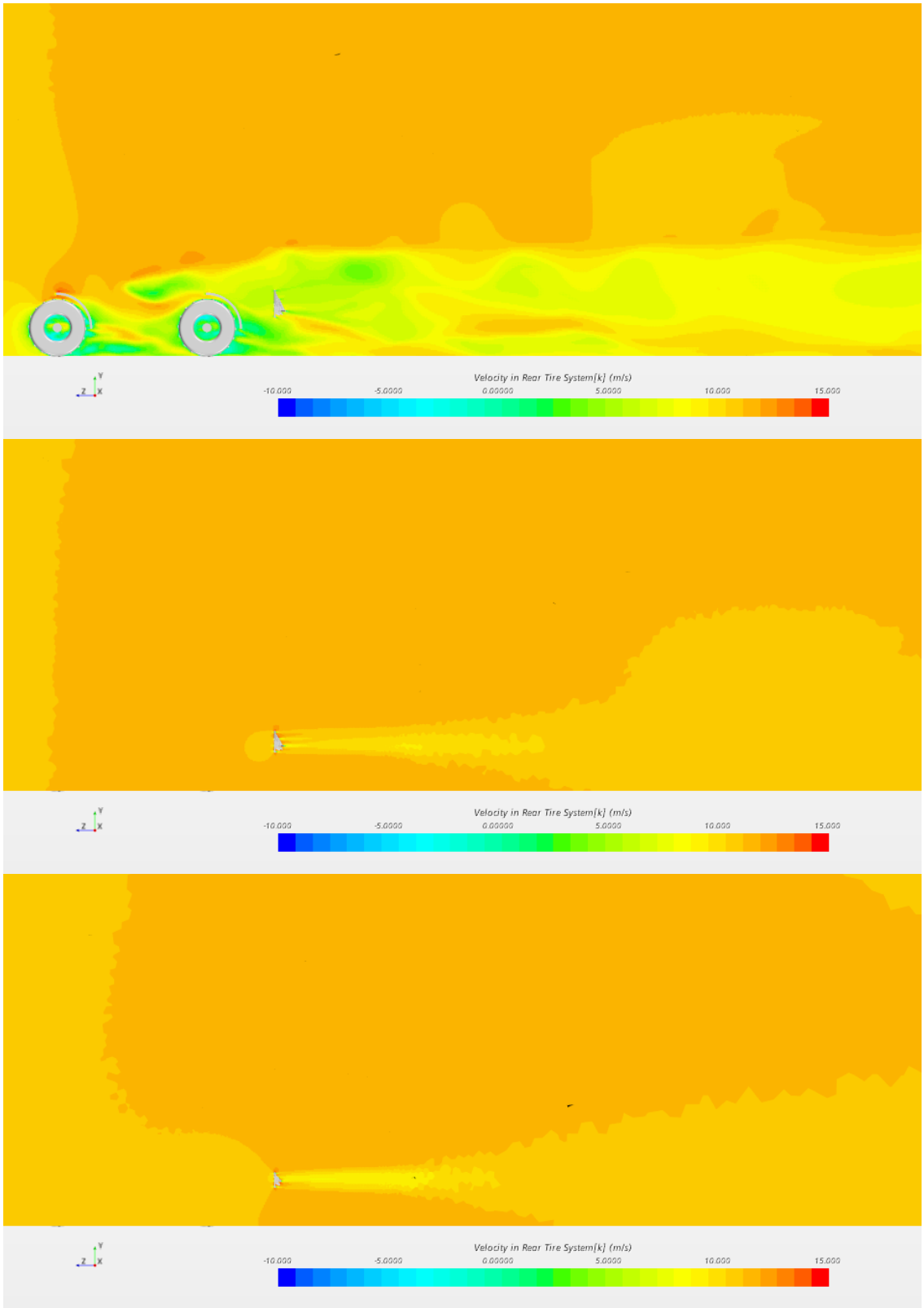

c

d

e

Figure 5.38: Progression of the wake visualized as streamwise velocity at the centerline (a), a plane next to the tank edge (b), a plane through the tires (c), down boom locations 3.45 m (d), and 6.78 m (e).

5.7.2.2 Profiles of Streamwise Velocity

When the profiles of streamwise velocity for Case 2 and Case 1 were compared, they showed strong similarity, i.e., the normalized velocity and TKE were virtually the same for both cases. There is no similar expectation for Case 3 since the geometry of the sprayer has changed with a higher boom height. It is important to characterize which elements of the flow change with the raised boom to determine if the new flow conditions could increase spray drift. Figure 5.39 compares normalized velocity for the low boom height and fast travel speed (Case 1) to the high boom height and fast travel speed (Case 3). In Figure 5.39 comparing Case 1 and Case 3 the overall size of the wake is unchanged, instead the boom wake is shifted upwards. This upward shift of the wake is most prominently featured in the locations down boom from the sprayer (Figure 5.39d, e, f and g). Two observations are made from these figures. First, increasing the boom height creates a vertically extended region of flow underneath the boom, which spray must travel through to reach the ground. This elevation of the boom and nozzles could enhance spray drift. Second, with the boom further from the ground, the elements of the boom act more as individual members in the flow, which causes the overall deficit of the wake to be smaller.

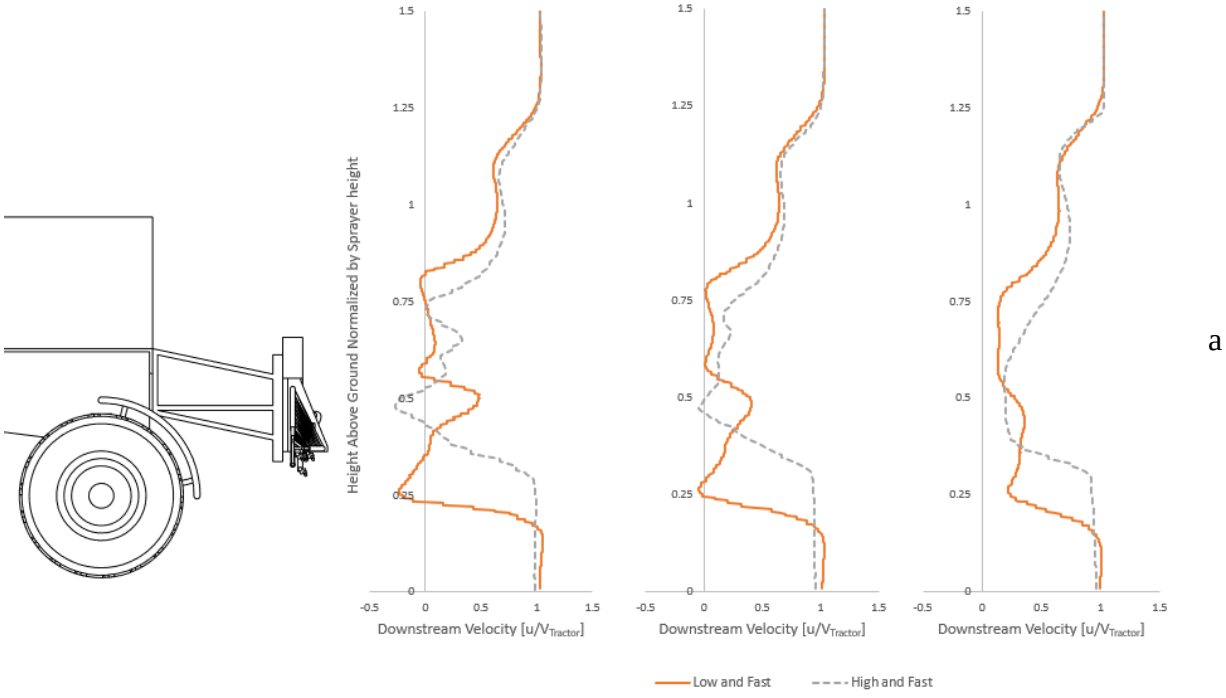

a

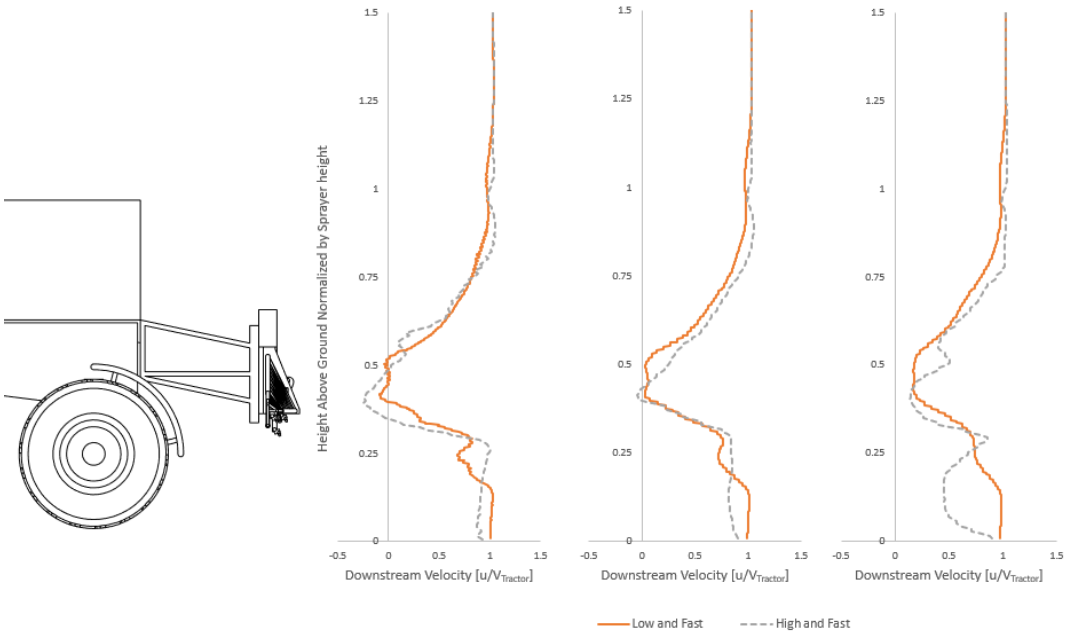
Height Above Ground Normalized by Sprayer height
Downstream Velocity [u/V_Tractor]
Low and Fast
High and Fast

b

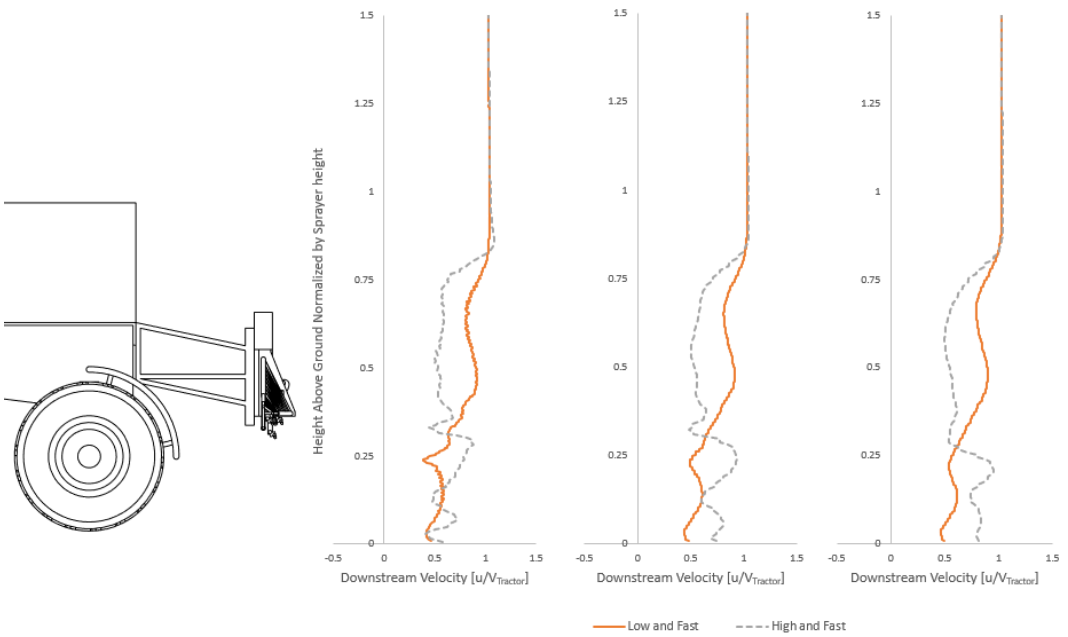
Height Above Ground Normalized by Sprayer height
Downstream Velocity [u/V_Tractor]
Low and Fast
High and Fast

c

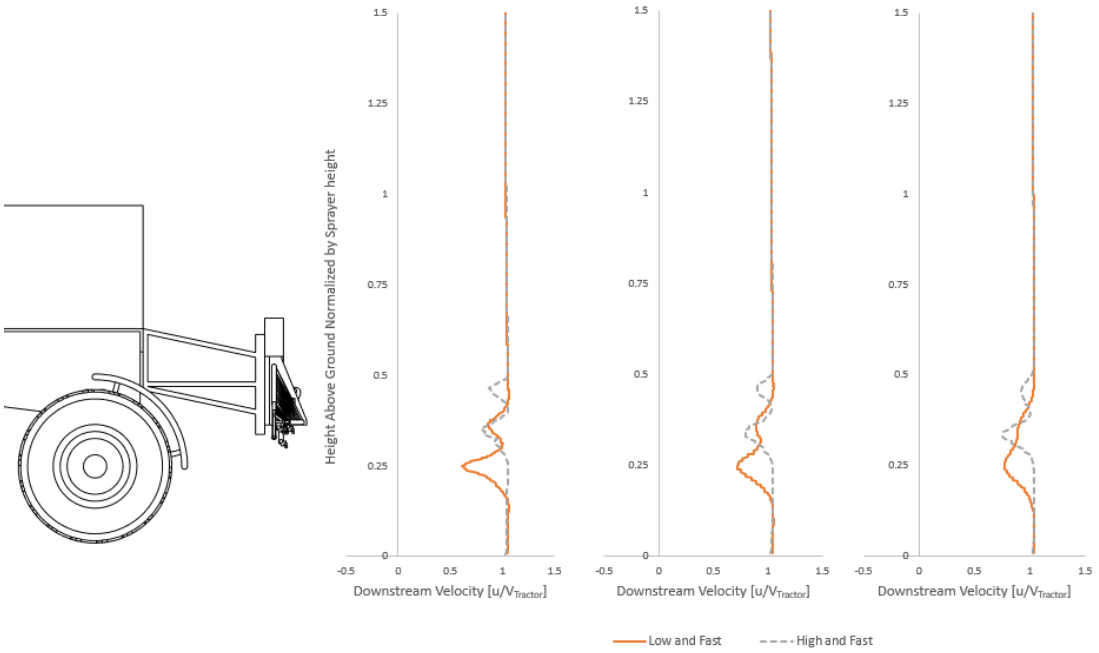
Height Above Ground Normalized by Sprayer height
Downstream Velocity [u/V_Tractor]
Low and Fast
High and Fast

d

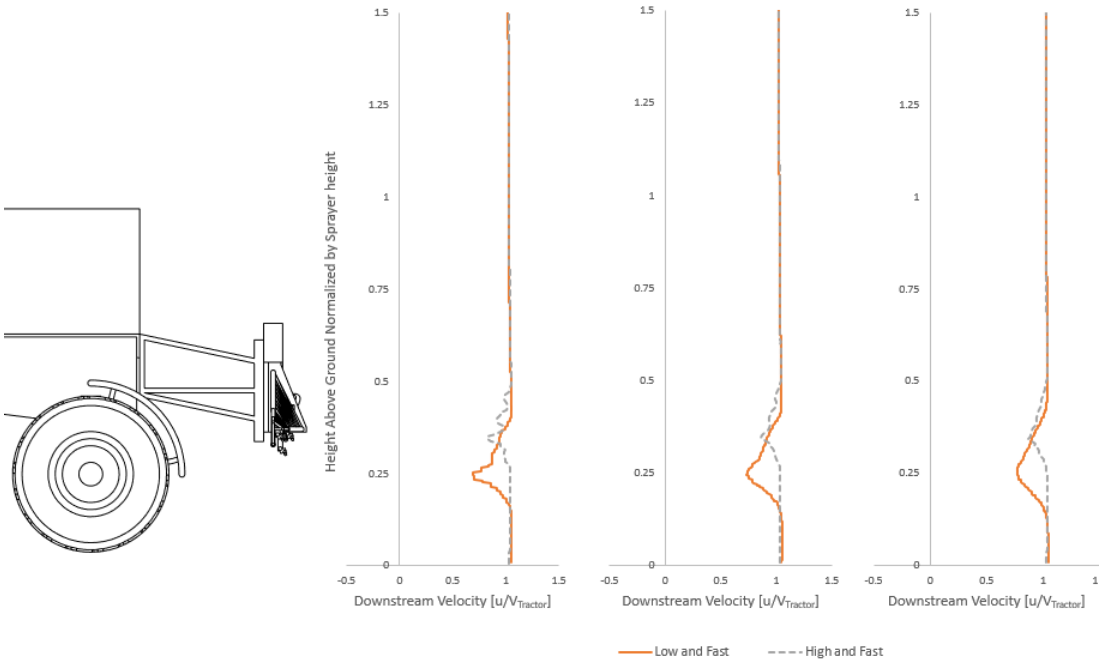
Height Above Ground Normalized by Sprayer height
Downstream Velocity [u/V_Tractor]
Low and Fast
High and Fast

e

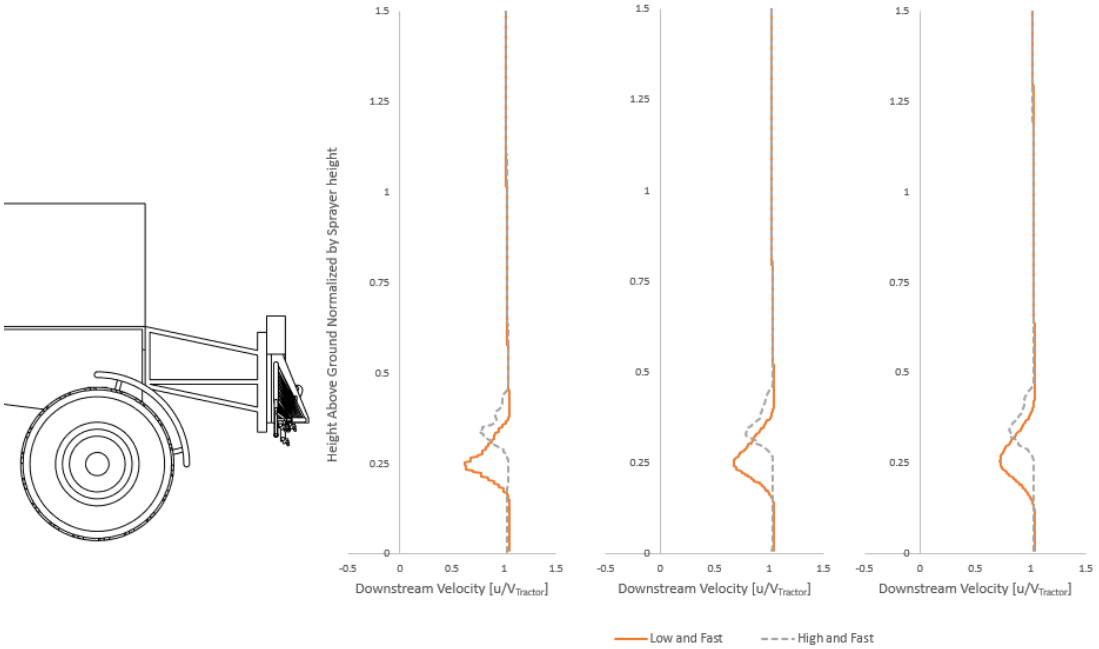

f

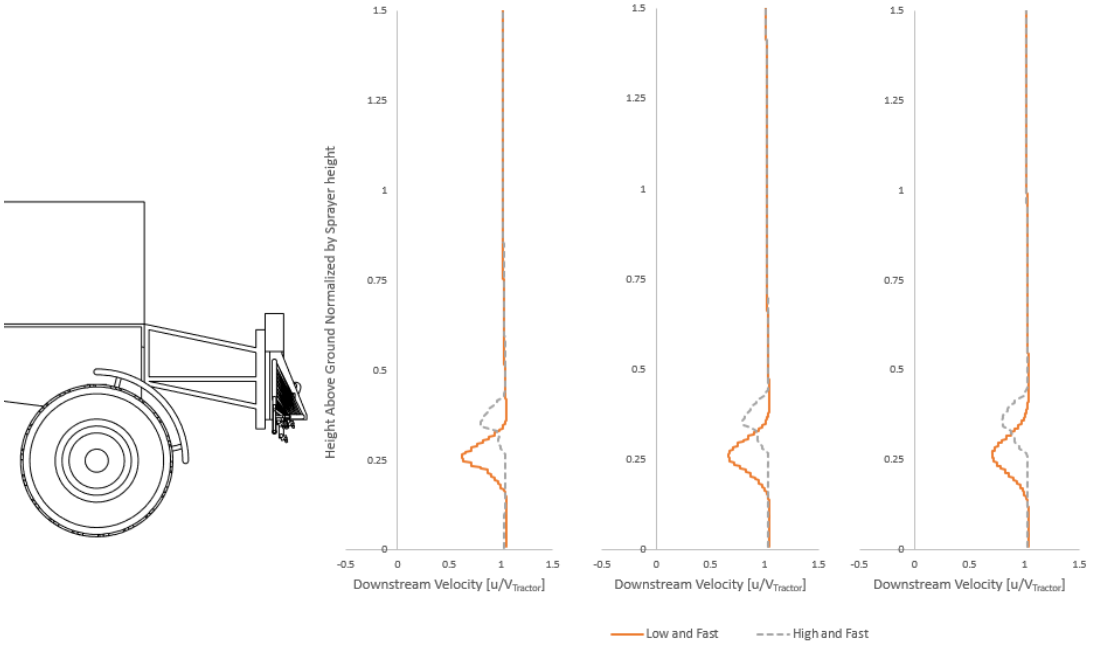

g

Figure 5.39: Plots showing normalized streamwise velocity to compare the low boom height and fast travel speed (Case 1) simulation to the high boom height and fast travel speed (Case 3) at three downstream locations, 0.43 m, 0.79 m, and 1.40 m, to visualize downstream recovery of the wake. The plots are made at the centerline (a), next to the tank (b), through the wheels (c), and at distances down

boom from the tire of 2.08 m (d), 3.45 m (e), 5.11 m (f) and 6.78 m (g). Note that the sprayer boom is in the high position.

5.7.2.3 Vector Plots

The wake behind the sprayer in the high boom case is shown to be more turbulent, especially behind the vehicle body. To further describe the wake of the high boom height and fast travel speed (Case 3) simulation, it is helpful to examine the secondary flow field using vector plots. Figure 5.40, Figure 5.41, and Figure 5.42 show the secondary flow field at the nozzles, 0.9 m behind the sprayer and 5 m behind the sprayer, respectively.

In the plane at the nozzles (Figure 5.40), there are locations of strong downward flow at or just under the nozzles, especially at the location of the first knuckle of the boom below which the boom air is directed downwards and above the boom air is directed upwards. This is caused by the mostly solid geometry that exists at this point, whereas the rest of the boom the geometry is more open. For all the locations (Figure 5.40, Figure 5.41, and Figure 5.42) similar flow patterns to the other simulations exist: flow is directed away from the sprayer down boom of the first knuckle and towards the sprayer inside the knuckle; formation of a vortex beside the tank and above the wheels of the sprayer; and generally upwards directed flow above the boom except for the regions impacted by the tank recirculation zone. The recirculation zone near the wheel and below the sprayer, which in previous cases was rather small, has increased in size and strength.

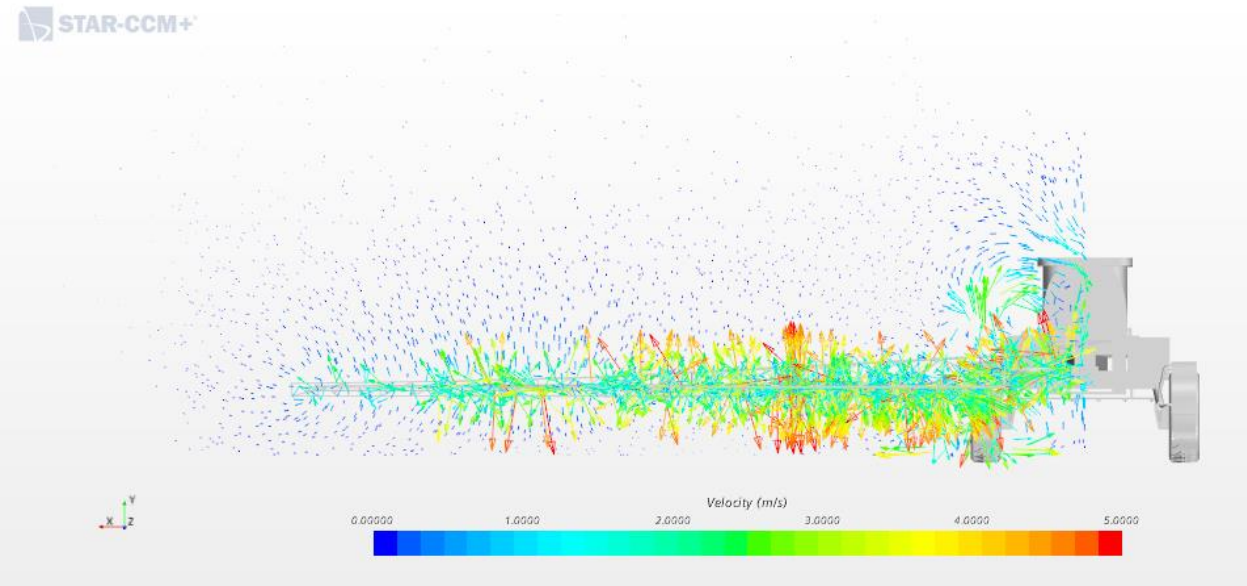

Figure 5.40: Velocity vectors in a cross-sectional plane aligned with the nozzles of the sprayer for the high boom height and fast travel speed (Case 3) simulation.

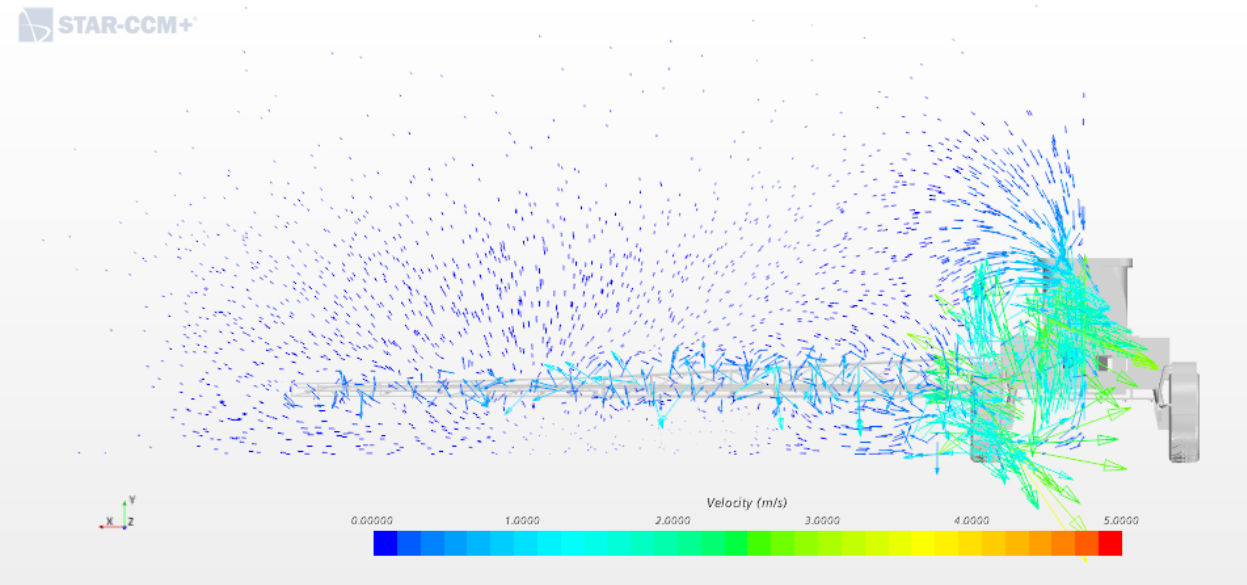

Figure 5.41: Velocity vectors in a cross-sectional plane 0.9 m behind the sprayer boom for the high boom height and fast travel speed (Case 3) simulation.

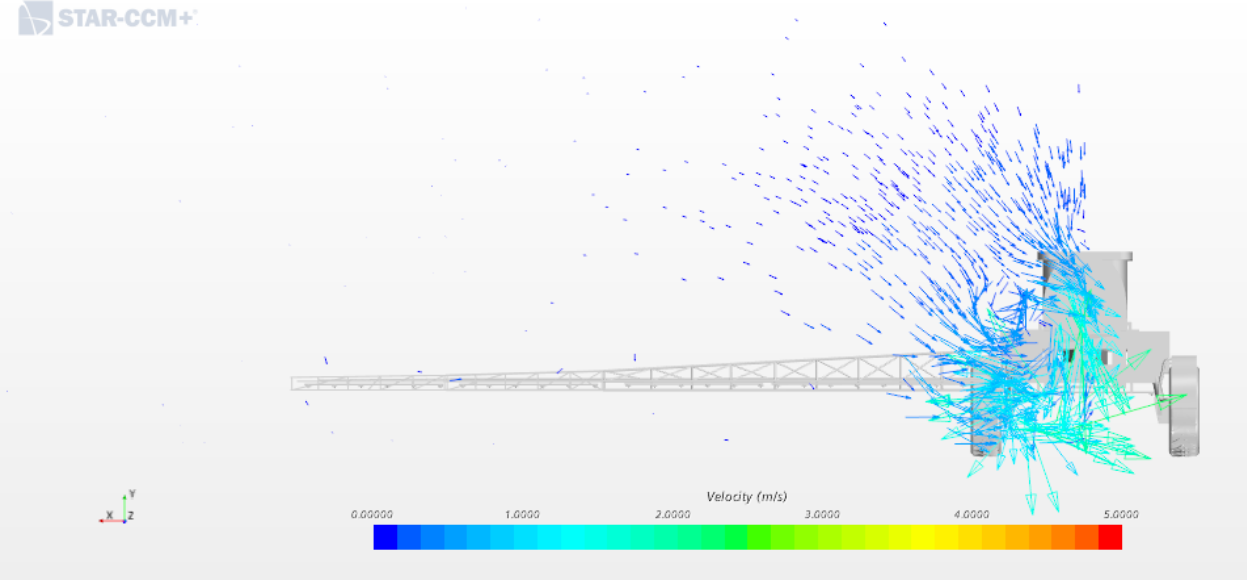

Figure 5.42: Velocity vectors in a cross-sectional plane 5 m behind the sprayer boom for the high boom height and fast travel speed (Case 3) simulation.

5.8 Discussion of Results for all Three Cases

The literature review identified two key operating conditions which will affect spray drift: travel speed and boom height. Considering travel speed, the non-dimensional velocity profiles between the low speed and high-speed cases were very similar. This would suggest that the increased likelihood for spray drift is less influenced by the velocity field, and instead is more influenced by the turbulent kinetic energy field. The magnitude of the TKE is much higher for the cases at a higher speed. For boom height, it is concluded that the increased likelihood for spray drift is caused by two factors. First, the increase in height above the ground requires any spray particles to travel further before deposition. Second the TKE around the boom is higher for the raised boom case versus the same boom at a lower height. The increased boom height also allows for local flow features to affect the region where the spray is injected, namely the formation of a large recirculation zone under the sprayer vehicle caused by flow around the tires.

5.8.1 Turbulence Kinetic Energy

Regions with increased turbulence have the potential for increased spray drift. Identifying these regions and the source of the turbulence allow manufacturers to design for reduced turbulence. Figure 5.43 illustrates the downstream decay of TKE and the down boom profiles of TKE.

At the centerline (Figure 5.43a), the TKE is higher overall for the high boom height and fast travel speed (Case 3); the effect of the boom, however, is greater for the low boom height and fast travel speed (Case 1) such that at the boom height the TKE is higher. Case 3 also shows more turbulence in the vehicle wake behind the tank (Figure 5.43b), which is likely due to the boom interacting with the recirculating zone behind the tank. In the plane next to the tank the TKE is much higher for Case 3. The boom, in combination with the recirculation zone formed beside the tank and above the wheels, causes a large increase in TKE in this region. In addition, near the ground where the spray is concentrated there is increased TKE. In the plane next to the tank there is an increase in TKE further downstream from the wheels. This wheel effect was shown to cause recirculation between the ground plane and the boom, which increases the turbulence significantly in the spray region. At the wheels (Figure 5.43c), the TKE is shown to be significantly higher for Case 3, which again suggests that there is a higher potential for drift with a higher boom height.

For the sections which are considered in the boom of the sprayer (Figure 5.43d, e, f, g) the maximum levels of TKE seen are approximately one order of magnitude less than in the regions influenced by the sprayer body. In the boom all four of the locations considered show similar behavior. Because the boom is higher in this region the TKE maximum exists higher above the ground at 1.30 m, where for the low boom heights the TKE maximum was at 0.94 m above the ground. These maximum TKE values are caused by the lowest structural members of the boom, from which the nozzles protrude. The TKE begins to increase at 1.02 m above the ground for the high boom height and 0.64 m off the ground for the low boom height. In both cases this TKE increase within 0.13 m of the nozzle, which means the spray is injected into a region of elevated TKE, which might influence spray drift, although less than regions behind the sprayer body.

For the boom sections (Figure 5.43d, e, f, g) it is also shown that the normalized TKE values are higher for the low boom height and fast travel speed (Case 1) simulation versus the low boom height and slow travel speed (Case 2) simulation. This is interesting because behind the sprayer body the two simulations showed very good agreement when normalized. This shows that there is more turbulence than otherwise would be predicted by assuming TKE increases with the square of velocity. Another feature in the TKE field that is shown is that, unlike the velocity field, where there was a larger deficit down boom, there is not as drastic of an increase to TKE in

the far down boom locations. TKE in the boom section was highest for the 2.08 m section, and decreased for the 3.45 m, and 5.11 m sections, before slightly increasing at the 6.78 m section.

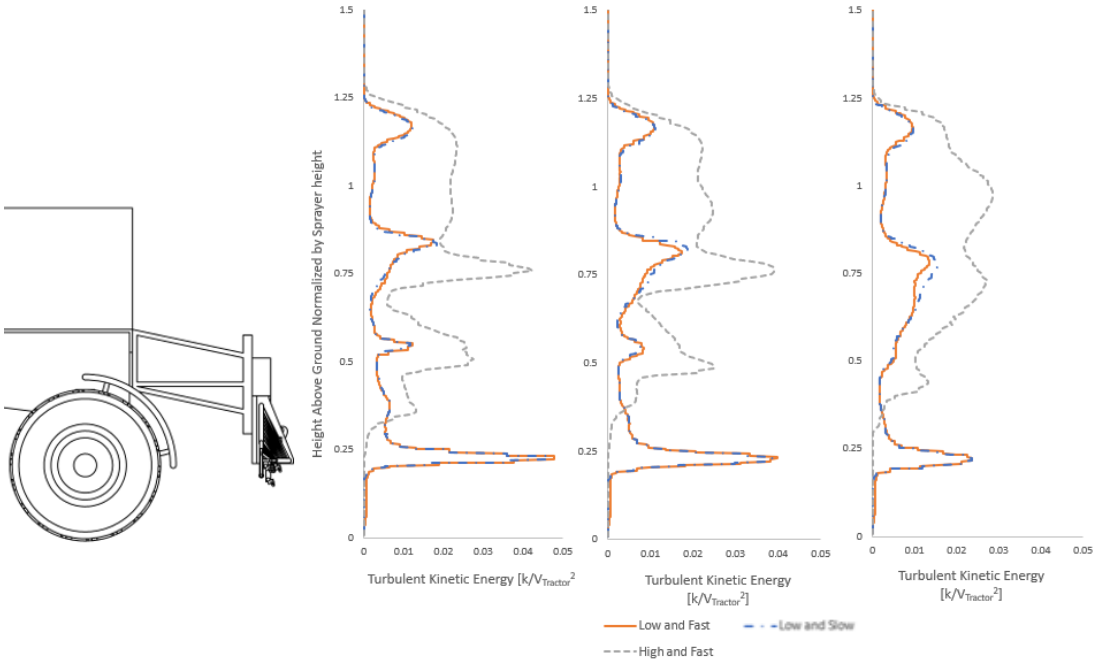

a

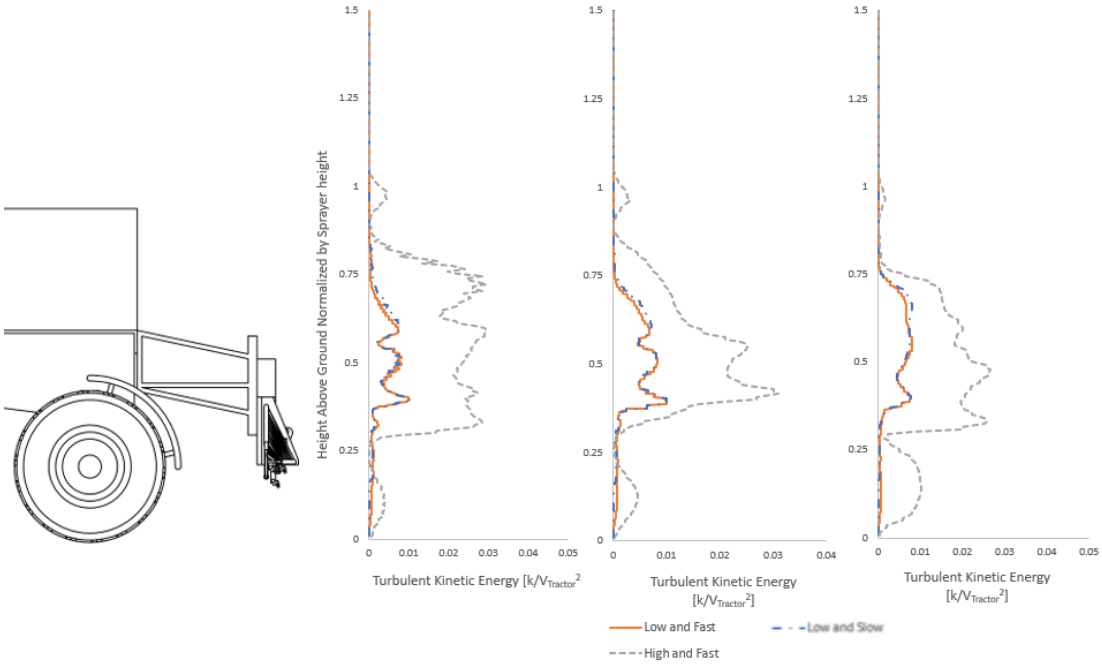

b

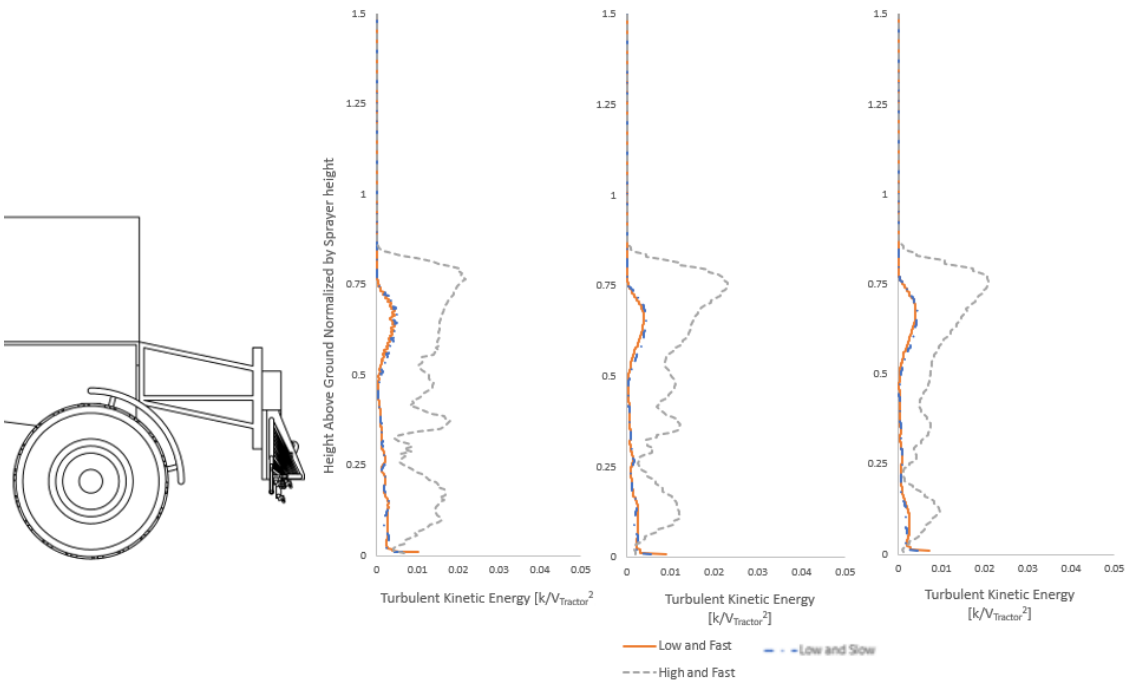
Height Above Ground Normalized by Sprayer height
Turbulent Kinetic Energy [k/V_Tractor^2]
Turbulent Kinetic Energy [k/V_Tractor^2]
Turbulent Kinetic Energy [k/V_Tractor^2]
Low and Fast
Low and Slow
High and Fast

c

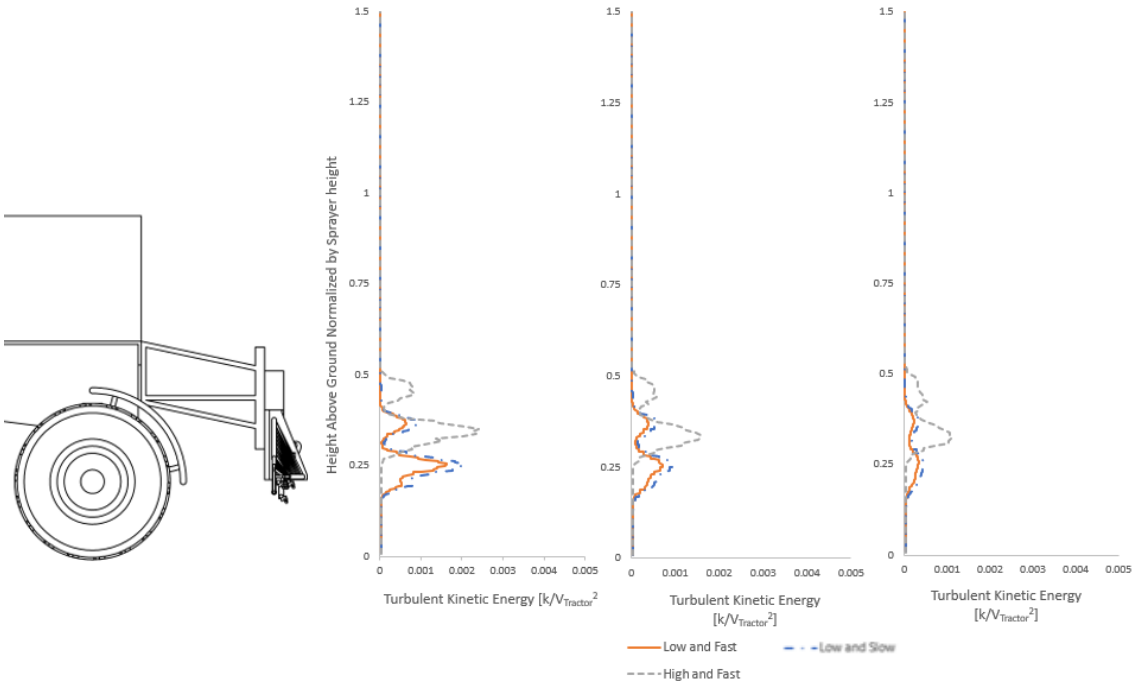
Height Above Ground Normalized by Sprayer height
Turbulent Kinetic Energy [k/V_Tractor^2]
Turbulent Kinetic Energy [k/V_Tractor^2]
Turbulent Kinetic Energy [k/V_Tractor^2]
Low and Fast
Low and Slow
High and Fast

d

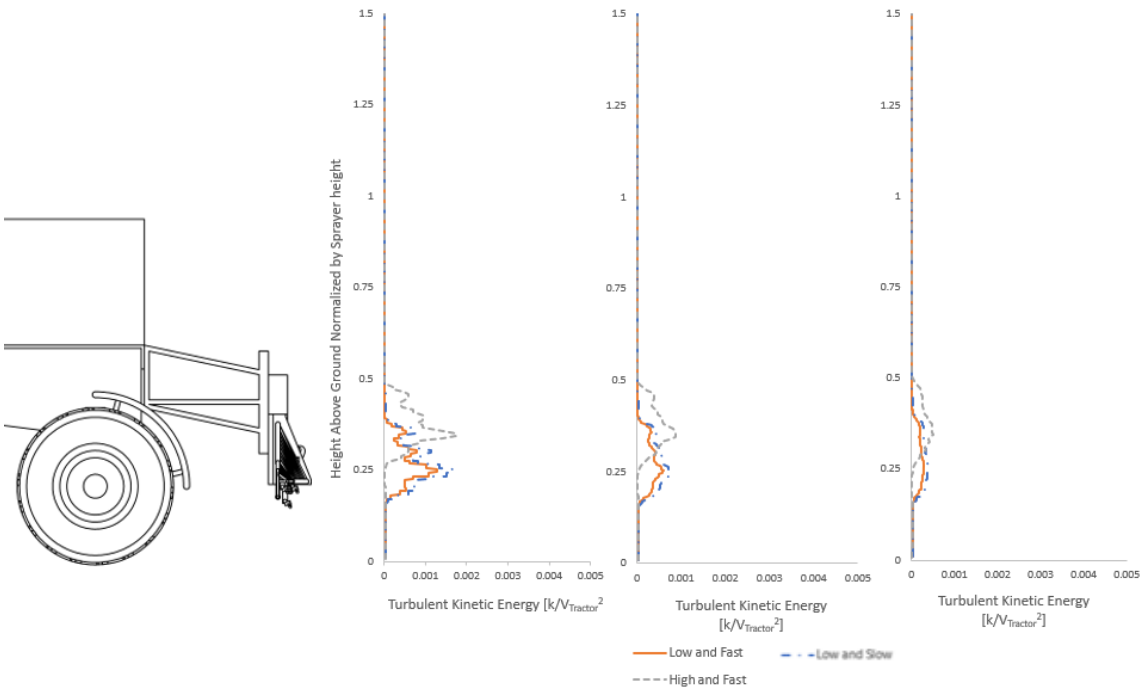
Height Above Ground Normalized by Sprayer height
Turbulent Kinetic Energy [k/V_Tractor^2]
Turbulent Kinetic Energy [k/V_Tractor^2]
Turbulent Kinetic Energy [k/V_Tractor^2]
Low and Fast
Low and Slow
High and Fast

e

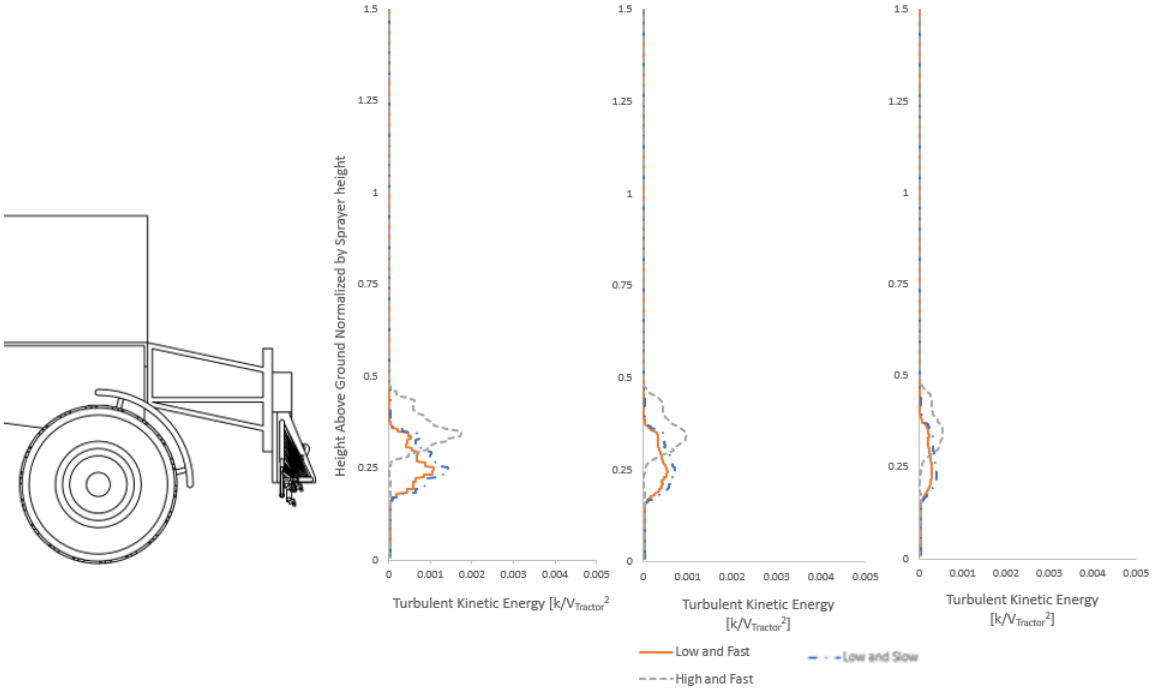
Height Above Ground Normalized by Sprayer height
Turbulent Kinetic Energy [k/V_Tractor^2]
Turbulent Kinetic Energy [k/V_Tractor^2]
Turbulent Kinetic Energy [k/V_Tractor^2]
Low and Fast
Low and Slow
High and Fast

f

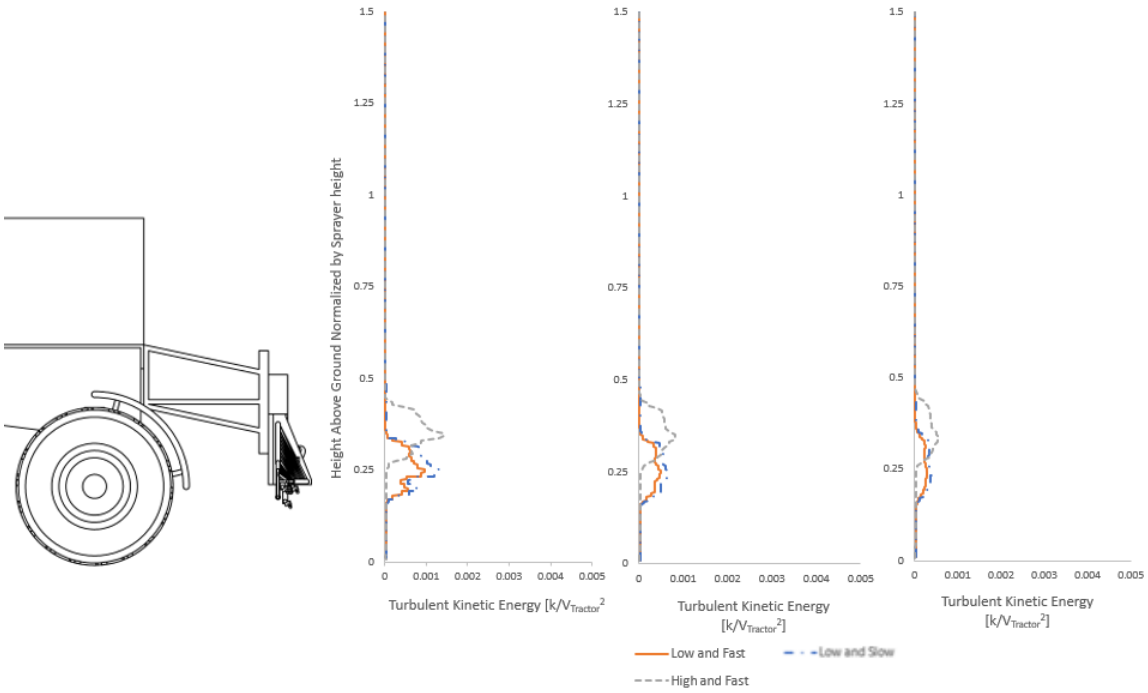

g

Figure 5.43: Progression of the wake visualized using profiles of turbulent kinetic energy at the centerline (a), a plane next to the tank edge (b), a plane through the tires (c), down boom locations of 2.08 m (d), 3.45 m (e), 5.11 m (f), and 6.78 m (g).

5.8.2 Assessing the Wake Near the Nozzles

In terms of assessing spray drift, an important location to consider would be the flow in the region very close to the nozzles. The spray is injected into this region, and any significant changes to the airflow in this region will be likely to cause drift. Figure 5.44 shows the streamwise velocity along a line 10 cm below and 10 cm behind the sprayer boom. Since the boom height is changed between the two cases considered in this figure, different parts of the sprayer affect the wake. For instance, in the low boom height and fast travel speed (Case 1) the wheel has a larger wake deficit than the far boom. For the high boom height and fast travel speed (Case 3) the far boom wake is about the same size compared to the wake behind the wheel.

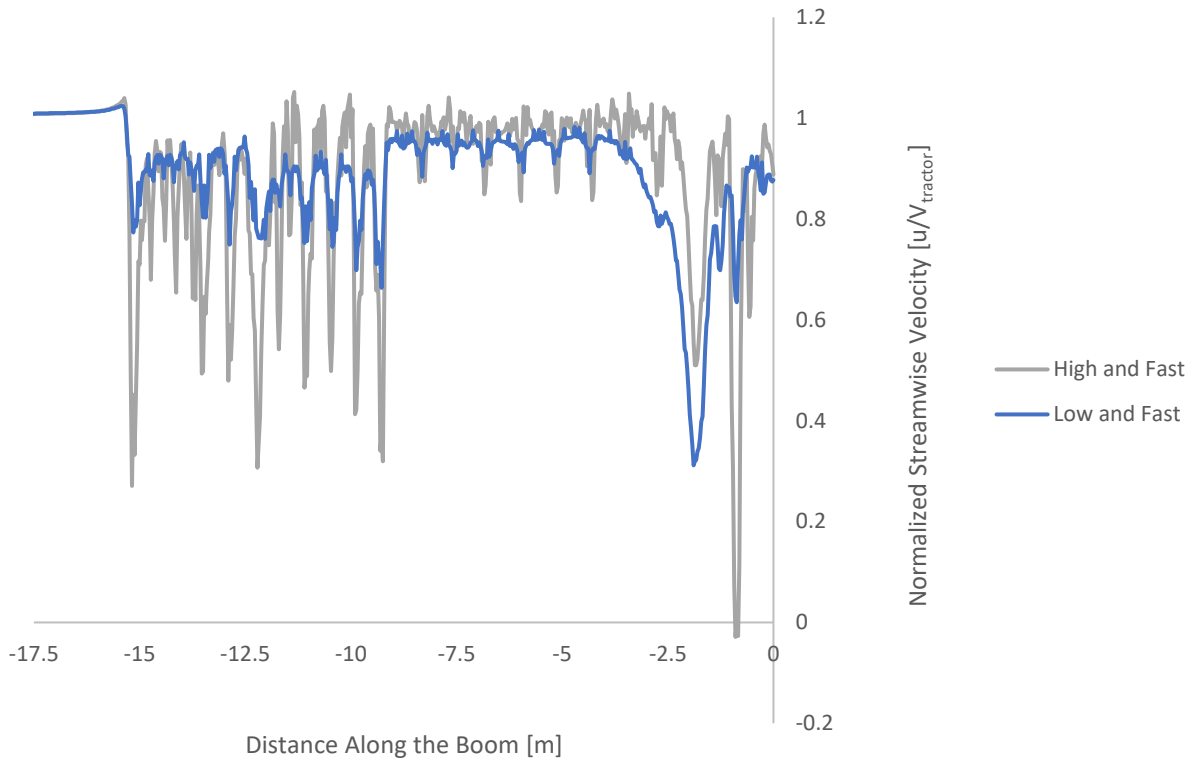

Figure 5.44: Streamwise velocity along a line close to the nozzles where spray initially interacts with the flow.

The normalized TKE is shown in Figure 5.45. The wake close to the nozzles when the boom is in the high position is significantly larger than when the boom is in the low position. This is the same pattern that was observed for the velocity deficit. Higher levels of TKE near the nozzles would suggest that there is an increased potential for spray drift to occur for a high boom height.

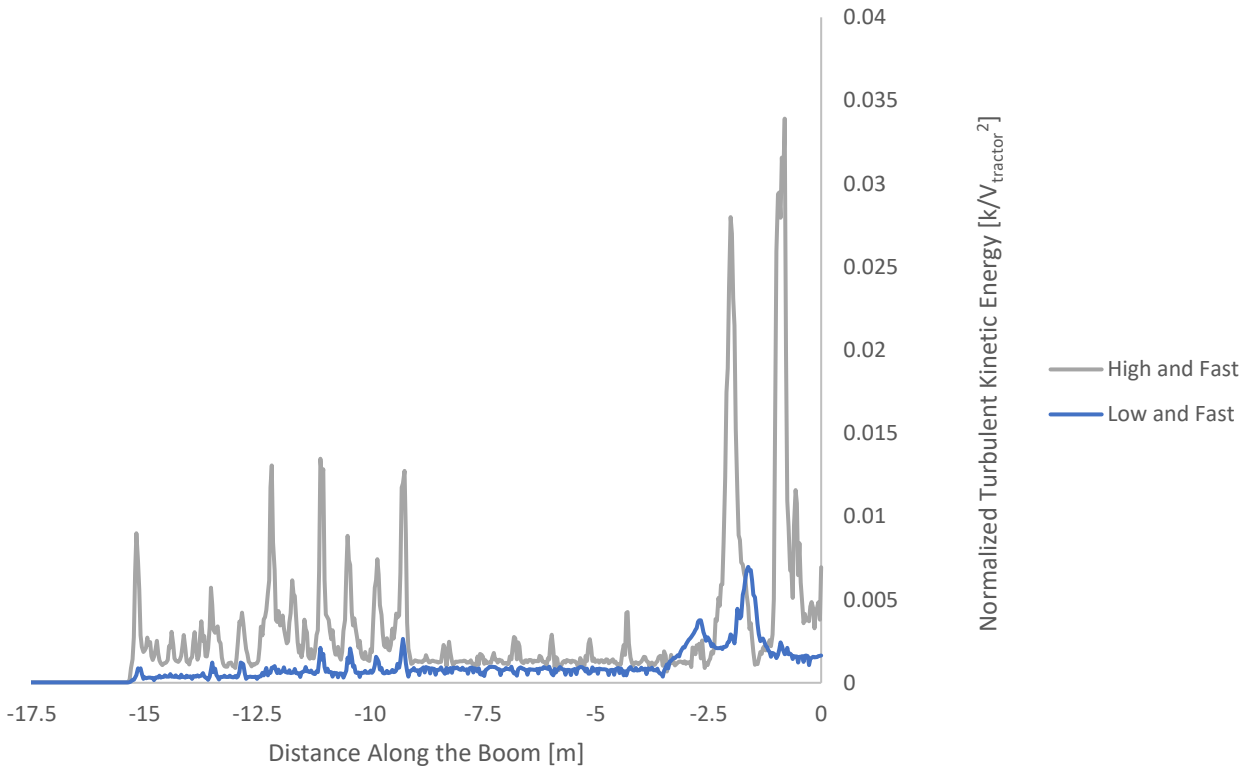

Figure 5.45: Turbulent kinetic energy along a line close to the nozzles.

5.8.3 Comparison to 2019 Field Data

The field data provided in Appendix A came from testing in the fall of 2019 utilizing a John Deere 4830 agricultural sprayer. The data were collected using ultrasonic anemometers. The results of these field tests can be used to determine if similar patterns are evident between the field tests and the computer simulations. Figure 5.46 shows the simulation results compared to measurements of the streamwise velocity. Overall, the field data and simulation data show good agreement. For the results in line with the tires the velocity deficit is greatest for both the simulation and field data.

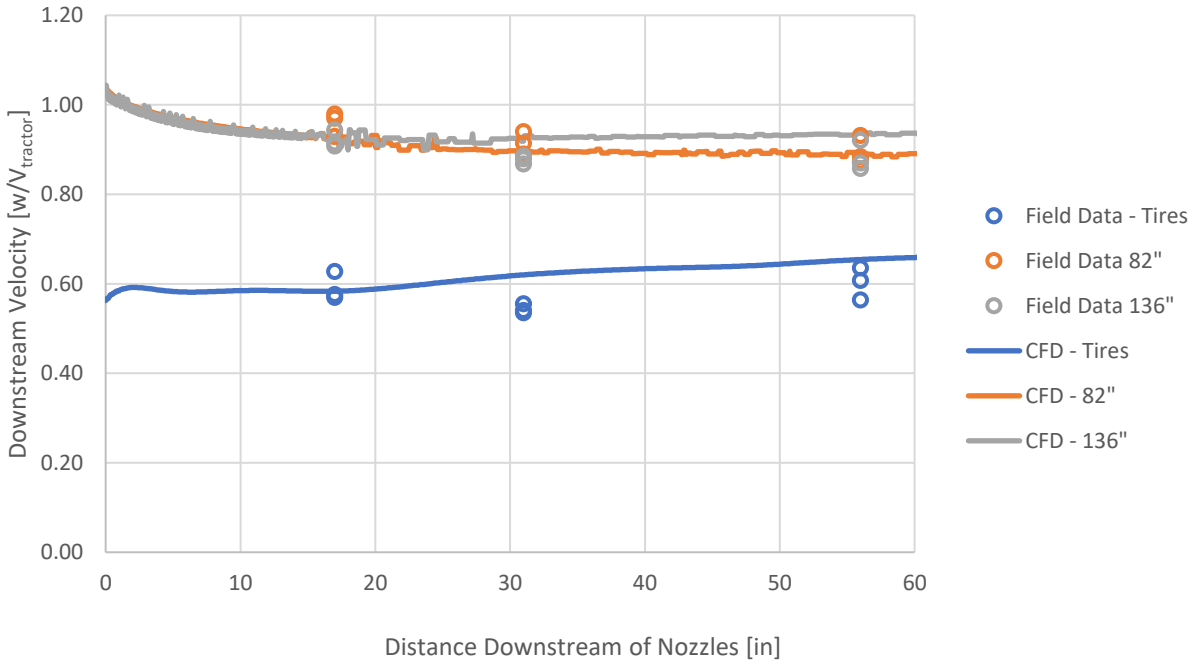

Figure 5.46: Comparison between 2019 field data for sprayer with a low boom height and the low boom height and fast travel speed (Case 1) simulation.

5.8.4 A Generalized Description for the Wake of an Agricultural Sprayer

Based on the CFD study, the wake of the agricultural sprayer can be divided into four regions. The four zones of the wake of an agricultural sprayer are shown in Figure 5.47.

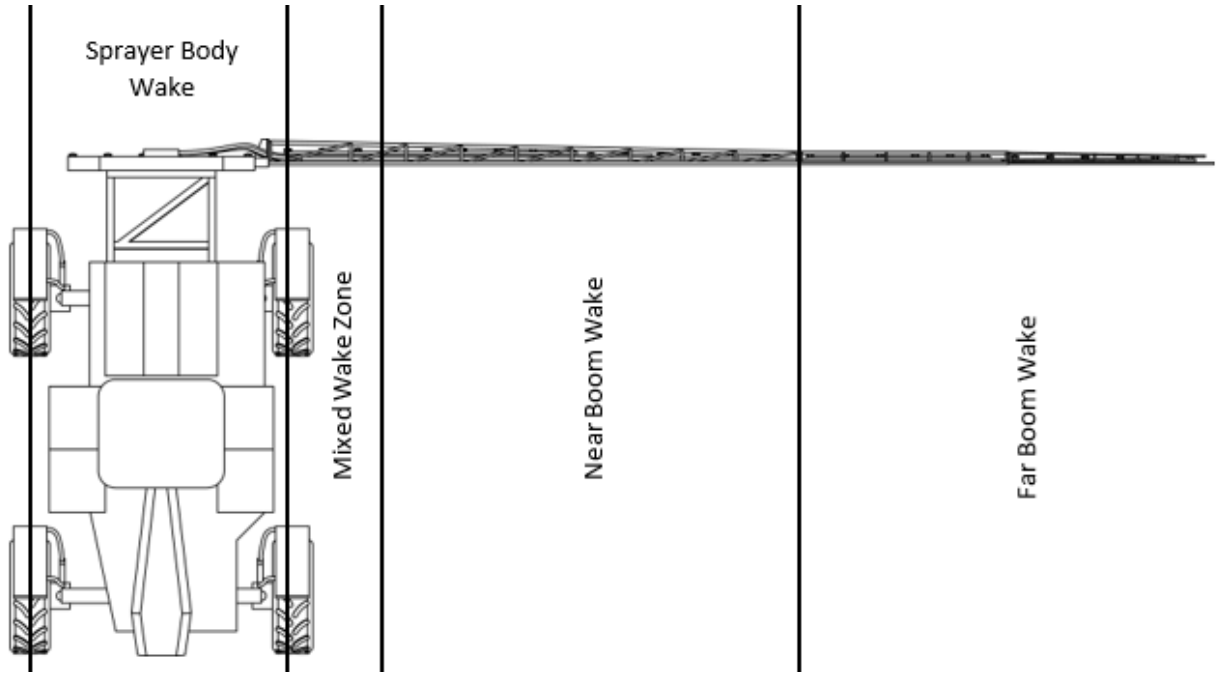

Figure 5.47: Top view showing the four wake zones behind the agricultural sprayer.

5.8.4.1 Sprayer Body Wake

The sprayer body wake is the region confined to the trackwidth of the sprayer. Within the sprayer body wake zone, the velocity deficit is highest, with significant reversed flow in the region behind the tank of the sprayer. The TKE is also the highest in this region. While the sprayer body has the most significant effect on the airflow in this region there is also significant influence from the wheels of the sprayer, and from the boom. With the boom in a lower position the two wakes appear independent albeit, merging downstream, whereas with higher boom heights the two wakes are combined into a single wake immediately behind the sprayer.

5.8.4.2 Mixed Wake Zone

The mixed wake zone extends approximately from the center of the outside tire to about two and a half tire widths down boom. This zone is the second highest region of TKE and has the second highest velocity deficit. Below the boom there are wake effects from the tires of the sprayer and above the boom there are some effects from the recirculation zone that develops on the side of

the cab and above the sprayer. The wheel wake in this region is likely to have the largest influence on spray drift due to the increased TKE under the boom and very close to the ground.

5.8.4.3 Near Boom Wake

The near boom wake is the region that extends from the end of the mixed wake zone to the approximate midpoint of the boom. At the midpoint there is a knuckle where the boom folds in half for transport. This region shows the smallest velocity deficit since the geometry provides less blockage to the incoming flow when compared with the far boom section. This region has the lowest turbulent kinetic energy near the nozzles and is expected to be the region with the lowest chance of spray drift occurring.

5.8.4.4 Far Boom Wake

The far boom wake extends from the midpoint boom knuckle to the boom tip. This region shows higher levels of TKE compared to the near boom wake and shows a higher velocity deficit. The increased velocity deficit is due to the increased blockage from the boom structure. In this region turbulence is slightly higher, thereby increasing the potential of drift occurring.

Chapter 6: Conclusions

The air flow around an agricultural sprayer in three different operating conditions was simulated using commercial computational fluid dynamics software. The objective was to determine major flow structures within the wake of the sprayer and identify which aspects of the wake might influence spray drift. Determining which operating conditions give lower chances for drift to occur will help farmers to use less pesticides while spraying their fields.

Prior to studying the wake of an agricultural sprayer, it was necessary to start with small simulations to determine how different meshing techniques would affect the wake of a cylinder, the main structural component in the boom of an agricultural sprayer. This was explained in Chapter 3. Three types of meshing elements were considered: tetrahedral, hexahedral, and polyhedral; and three sizes of elements on the surface of the cylinder were used: 4 mm, 2 mm, and 1 mm. It was determined that polyhedral elements gave the best results. Testing the different surface sizes showed that larger elements gave more realistic results in producing a mean velocity field. The smaller elements showed vortex shedding. In a transient simulation this behavior would be realistic, but it is an undesirable characteristic in an averaged flow field.

To ensure that the element type and size selected would work for the entire vehicle it was decided to simulate a section of the boom of the agricultural sprayer. This simulation was presented in Chapter 4 and verified that the element type and size selected was appropriate for use on simulations of the entire agricultural sprayer. Simulations of a small section of the boom showed that the wake appears to be more influenced by vertical members than horizontal members. The largest deficits in the wake are observed to be behind the vertical members and the wake effects of these members are limited to the region directly behind the member with minimal spread into the other regions of the boom.

Three operating conditions were then simulated for the agricultural sprayer with the results given in Chapter 5. These three operating conditions represented a base scenario, a minimum drift potential, and a maximum drift potential. A literature review showed that increasing either the boom height or sprayer travel speed would increase the likelihood of drift occurring. Using TKE as a method to measure potential for drift, it was seen that the turbulence in the wake increased with both sprayer travel speed and boom height. Suggesting potential for spray drift increased

with increased boom height and sprayer speed. The simulations further showed that increasing the boom height gave a larger turbulence increase than increasing the velocity.

The air flow field around the agricultural sprayer was studied to further examine the secondary flow. Recirculation zones were discovered in the wake behind the sprayer tank, and, in the case of the high boom treatment, below the boom inside the rear tires. The recirculation under the boom could contribute to spray drift behind the sprayer. Spraying with a low boom will prevent the development of this vortex and hence reduce spray drift in this region.

The simulations showed that the wake of an agricultural sprayer is complex, but it can be broken down into four regions. The vehicle body wake is by far the most powerful part of the wake, located behind the sprayer body this region is dominated by the vehicle effects. With the boom in the low position the wake is independent of the vehicle wake, and the two wakes merge together downstream. With the boom in the high position the vehicle wake and boom wake show combined effects immediately behind the boom. The potential for drift is high in the vehicle wake zone, since this region has the highest levels of turbulent kinetic energy, strongest velocity deficit, and strong vorticity.

The wake created by the sprayer body generally aligns with the vehicle itself, but the flow must accelerate around the vehicle body. This accelerated flow causes the wake effects to stretch beyond the vehicle body, creating a mixed wake zone. In this region, a large velocity deficit exists, and turbulent kinetic energy is relatively high. Flow around the front tire is observed to be the largest contributor to the mixed wake zone. Within the mixed wake zone the boom wake is the primary wake observed. Below the boom, where the spray will be injected, there is significant secondary flow and increased turbulence which could contribute to spray drift.

The boom wake has two independent zones. From the mixed wake zone to the knuckle (where the boom folds in half for transit) is the near wake zone. This zone has the lowest observed turbulence and velocity deficit. This would be the region where drift is least likely to occur. From the knuckle to the tip is the far wake region, and in this zone the turbulence and velocity deficit is higher than in the near wake zone. The increased size and intensity of the wake is attributed to the increased blockage within the structure of the boom.

The results of these simulations allow for recommendations to be made to farmers who use agricultural sprayers and to manufacturers who design these sprayers. For farmers who want to reduce potential for spray drift it is recommended to:

1. Spray with as low a boom height as possible, and
2. Reduce the travel speed of the spraying vehicle.

For the manufacturers of agricultural sprayers, the following features of the wake should be investigated to reduce spray drift potential in the wake of the sprayer:

1. Prevent the development of intense vortices near the ground produced by air accelerating around the front wheels,
2. Include aerodynamic considerations to the design of elements of the structure of the vehicle such as the cab and tank design,
3. Reduce the blockage effect of the boom in the far wake zone where there is a substantial increase to turbulence,
4. Make aerodynamic improvements to the knuckles of the boom where significant turbulence and secondary flow features exist, and
5. Reduce the maximum allowable boom height to prevent increased spray drift associated with high spraying.

This research was intentionally limited to be a no-wind scenario with half the vehicle simulated to reduce the computational size. Future studies could be made which include a full vehicle and different wind conditions could be investigated such as done by Teske, Thistle, Petersen, et al. (2016b). The present work was done using a steady SST turbulence model; but a transient simulation using a DES or LES model would improve the accuracy of the simulation, albeit at significant computational cost. Furthermore, adding droplets to the simulation will allow a prediction of spray drift. A more detailed simulation of the sprayer would also simulate vibrations within the boom to determine that effect of spray drift.

The objective of this research was to create a realistic model of the wake of an agricultural sprayer using computational fluid dynamics. This was achieved, and three operating conditions (cases) of a specific model of agricultural sprayer were simulated using STAR-CCM+. The simulations showed good similarity to field results at three locations. The results of the simulations were discussed in terms of the major structures found in the wake of an agricultural sprayer, and the effect that these structures would have on spray drift.

References

Alves Portela, F., G. Papadakis, and J. C. Vassilicos. 2017. “The Turbulence Cascade in the near Wake of a Square Prism.” *Journal of Fluid Mechanics* 825 (August): 315–52. https://doi.org/10.1017/jfm.2017.390.

Baetens, K., D. Nuyttens, P. Verboven, M. De Schampheleire, B. Nicolaï, and H. Ramon. 2007. “Predicting Drift from Field Spraying by Means of a 3D Computational Fluid Dynamics Model.” *Computers and Electronics in Agriculture* 56 (2): 161–73. https://doi.org/10.1016/j.compag.2007.01.009.

Butler Ellis, M.C., R. Alanis, A.G. Lane, C.R. Tuck, D. Nuyttens, and J.C. van de Zande. 2017. “Wind Tunnel Measurements and Model Predictions for Estimating Spray Drift Reduction under Field Conditions.” *Biosystems Engineering* 154 (February): 25–34. https://doi.org/10.1016/j.biosystemseng.2016.08.013.

Casadei, L., L. Könözsy, and N. J. Lawson. 2019. “Unsteady Detached-Eddy Simulation (DES) of the Jetstream 31 Aircraft in One Engine Inoperative (OEI) Condition with Propeller Modelling.” *Aerospace Science and Technology* 91 (August): 287–300. https://doi.org/10.1016/j.ast.2019.05.034.

Catalano, P., M. Wang, G. Iaccarino, and P. Moin. 2003. “Numerical Simulation of the Flow around a Circular Cylinder at High Reynolds Numbers,” *International Journal of Heat and Fluid Flow* 24 (4): 463-469

Delele, M.A., A. De Moor, B. Sonck, H. Ramon, B.M. Nicolaï, and P. Verboven. 2005. “Modelling and Validation of the Air Flow Generated by a Cross Flow Air Sprayer as Affected by Travel Speed and Fan Speed.” *Biosystems Engineering* 92 (2): 165–74. https://doi.org/10.1016/j.biosystemseng.2005.05.018.

Elmiligui, A. A., K. S. Abdol-Hamid, and E. Parlette. 2015. “Detached Eddy Simulation for the F-16XL Aircraft Configuration.” In *53rd AIAA Aerospace Sciences Meeting*. Kissimmee, Florida: American Institute of Aeronautics and Astronautics. https://doi.org/10.2514/6.2015-1496.

Endalew, A. Melese, M. Hertog, M.A. Delele, K. Baetens, T. Persoons, M. Baelmans, H. Ramon, B.M. Nicolaï, and P. Verboven. 2009. “CFD Modelling and Wind Tunnel Validation of Airflow through Plant Canopies Using 3D Canopy Architecture.” *International Journal of Heat and Fluid Flow* 30 (2): 356–68. https://doi.org/10.1016/j.ijheatfluidflow.2008.12.007.

Forrest, J. S., and I. Owen. 2010. “An Investigation of Ship Airwakes Using Detached-Eddy Simulation.” *Computers & Fluids* 39 (4): 656–73. https://doi.org/10.1016/j.compfluid.2009.11.002.

Gil, E., M. Gallart, P. Balsari, P. Marucco, M. P. Almajano, and J. Llop. 2015. “Influence of Wind Velocity and Wind Direction on Measurements of Spray Drift Potential of Boom Sprayers Using Drift Test Bench.” *Agricultural and Forest Meteorology* 202 (March): 94–101. https://doi.org/10.1016/j.agrformet.2014.12.002.

Gil, Y., and C. Sinfort. 2005. “Emission of Pesticides to the Air during Sprayer Application: A Bibliographic Review.” *Atmospheric Environment* 39 (28): 5183–93. https://doi.org/10.1016/j.atmosenv.2005.05.019.

Holterman, H. J., J. C. van de Zande, H. A. J. Porskamp, and J. F. M. Huijsmans. 1997. “Modelling Spray Drift from Boom Sprayers.” *Computers and Electronics in Agriculture* 19 (1): 1–22. https://doi.org/10.1016/S0168-1699(97)00018-5.

Hsu, F. H., and R. L. Davis. 2010. “Drag Reduction of Tractor-Trailers Using Optimized Add-On Devices.” *Journal of Fluids Engineering* 132 (8): 084504. https://doi.org/10.1115/1.4001587.

Landry, H., and T. Wolf. 2019. “An Investigation of Airflow Patterns Created by High-Clearance Sprayers during Field Operations.” *Canadian Biosystems Engineering* 61 (1): 2.01-2.12. https://doi.org/10.7451/CBE.2019.61.2.01.

Maryami, R. 2020. “Turbulent Flow Interaction with a Circular Cylinder.” *Physics of Fluids* 32 (015105): 19. https://doi.org/10.1063/1.5119967.

Menter, F. R. 1994. “Two-Equation Eddy-Viscosity Turbulence Models for Engineering Applications.” *AIAA Journal* 32 (8): 1598–1605. https://doi.org/10.2514/3.12149.

Murphy, S.D., P.C.H. Miller, and C.S. Parkin. 2000. “The Effect of Boom Section and Nozzle Configuration on the Risk of Spray Drift.” *Journal of Agricultural Engineering Research* 75 (2): 127–37. https://doi.org/10.1006/jaer.1999.0491.

Nasir, R. E. M., Z. Ali, W. Kuntjoro, and W. Wisnoe. 2012. “Investigation on Aerodynamic Characteristics of Baseline-II E-2 Blended Wing-Body Aircraft with Canard via Computational Simulation.” In *AIP Conf. Proc*, 1440:700–706. Melaka, Malaysia. https://doi.org/10.1063/1.4704280.

Norberg, C. 1998. “LDV-Measurements in the near Wake of a Circular Cylinder.” In *Advances in Understanding of Bluff Body Wakes and Vortex-Induced Vibration*, 1–12. Washington DC.

Nuyttens, D., M. De Schampheleire, K. Baetens, and B. Sonck. 2007. “The Influence of Operator-Controlled Variables on Spray Drift from Field Crop Sprayers.” *Transactions of the ASABE* 50 (4): 1129–40. https://doi.org/10.13031/2013.23622.

Ong, M. C., T. Utnes, L. E. Holmedal, D. Myrhaug, and B. Pettersen. 2009. “Numerical Simulation of FLow around a Smooth Circular Cylinder at Very High Reynolds Numbers.” *Marine Structures* 22: 142–53.

Sidahmed, M. M., and R. B. Brown. 2002. “Computer Simulation of Factors Affecting Drift from a Forestry Airblast Sprayer.” *Canadian Biosystems Engineering* 44 (2): 27–35.

Siemens PLM Software. 2019. *Simcenter STAR-CCM+ Documentation*. 2019.3.

Teske, M. E., P. C. H. Miller, H. W. Thistle, and N. B. Birchfield. 2009. “Initial Development and Validation of a Mechanistic Spray Drift Model for Ground Boom Sprayers.” *Transactions of the ASABE* 52 (4): 1089–97. https://doi.org/10.13031/2013.27779.

Teske, M. E., G. W. Thistle, T. C. R. Lawton, R. L. Petersen, and T. G. Funseth. 2015. "Evaluation of the Wake of an Agricultural Ground Sprayer." *Transactions of the ASABE* 58 (3): 621–28. https://doi.org/10.13031/trans.58.10996.

Teske, M. E., H. W. Thistle, T. C. R. Lawton, and R. L. Petersen. 2016a. "Evaluation of the Flow Downwind of an Agricultural Ground Sprayer Boom." *Transactions of the ASABE* 59 (3): 839–46. https://doi.org/10.13031/trans.59.11442.

Teske, M. E., H. W. Thistle, R. L. Petersen, T. C. R. Lawton, S. A. Guerra, and T. G. Funseth. 2016b. "Evaluation of the Wake of an Agricultural Ground Sprayer with the Wind from Any Direction." *Transactions of the ASABE* 59 (5): 1205–19. https://doi.org/10.13031/trans.59.11844.

Thistle, H. W., J. A. S. Bonds, G. J. Kees, and B. K. Fritz. 2017. "Evaluation of Spray Drift from Backpack and UTV Spraying." *Transactions of the ASABE* 60 (1): 41–50. https://doi.org/10.13031/trans.11990.

Tieleman, H. W. 2003. "Roughness Estimation for Wind-Load Simulation Experiments." *Journal of Wind Engineering and Industrial Aerodynamics* 91 (9): 1163–73. https://doi.org/10.1016/S0167-6105(03)00058-8.

Tsay, J., H. E. Ozkan, R. D. Fox, and R. D. Brazee. 2002. "CFD Simulation of Mechanical Spray Shields." *Transactions of the ASAE* 45 (5): 1271–80. https://doi.org/10.13031/2013.11055.

Van Den Berg, F., R. Kubiak, W. G. Benjey, M. S. Majewski, S. R Yates, G. L. Reeves, J. H. Smelt, and A. M. A. Van Der Linden. 1999. "Emission of Pesticides into the Air." *Water, Air, and Soil Pollution* 115: 195–218.

Viola, I. M., S. Bartesaghi, T. Van-Renterghem, and R. Ponzini. 2014. "Detached Eddy Simulation of a Sailing Yacht." *Ocean Engineering* 90 (November): 93–103. https://doi.org/10.1016/j.oceaneng.2014.07.019.

Watson, N.A., M.F. Kelly, I. Owen, S.J. Hodge, and M.D. White. 2019. "Computational and Experimental Modelling Study of the Unsteady Airflow over the Aircraft Carrier HMS Queen Elizabeth." *Ocean Engineering* 172 (January): 562–74. https://doi.org/10.1016/j.oceaneng.2018.12.024.

Weiner, K. L., and C.S. Parkin. 1993. "The Use of Computational Fluid Dynamic Code for Modelling Spray from a Mistblower." *Journal of Agricultural Engineering Research* 55: 313–24.

Wolf, T. M., R. Grover, K. Wallace, S. R. Shewchuk, and J. Maybank. 1993. "Effect of Protective Shields on Drift and Deposition Characteristics of Field Sprayers." *Canadian Journal of Plant Science* 73 (4): 1261–73. https://doi.org/10.4141/cjps93-165.

Yao, S. B., Z. X. Sun, D. L. Guo, D. W. Chen, and G. W. Yang. 2013. "Numerical Study on Wake Characteristics of High-Speed Trains." *Acta Mechanica Sinica* 29 (6): 811–22. https://doi.org/10.1007/s10409-013-0077-3.

Appendix A - 2019 Field Data

Field tests occurred using a John Deere 4830 Agricultural Sprayer with 90ft booms in October of 2019. Velocity measurements were made using four ultrasonic anemometers, three mounted on an adjustable frame behind the boom as shown in Figure A.1, and the fourth mounted off the front of the sprayer to get the “clean” air. A weather station was placed in the same plot that the tests occurred in, but far enough away from the travel section to prevent any effects from the sprayer velocity. The ultrasonic anemometers measure three components of velocity at 50 Hz, and from this turbulence statistics are determined. The three components of velocity and the turbulent kinetic energy are the variables considered in this data set. The locations of the anemometers on the sprayer are shown in Figure A.2. The frame that the anemometers are fixed to was mounted level to the nozzles, and two boom (nozzle) heights off the ground are considered, 25” and 45”. For one boom height the anemometers were mounted to measure the velocity components above and below the boom at the furthest rear position on the frame. Figure A.3 shows the normalized streamwise velocity measured behind the sprayer at the three locations for a series of runs in the south direction.

Figure A.1: Image of the agricultural sprayer with the anemometer frame attached to the boom.

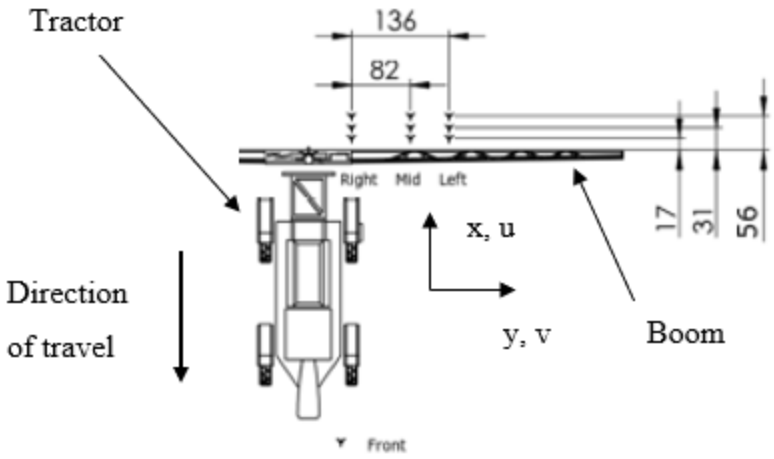

Figure A.2: Locations of anemometers mounted to the agricultural sprayer during field tests. Dimensions are in inches.

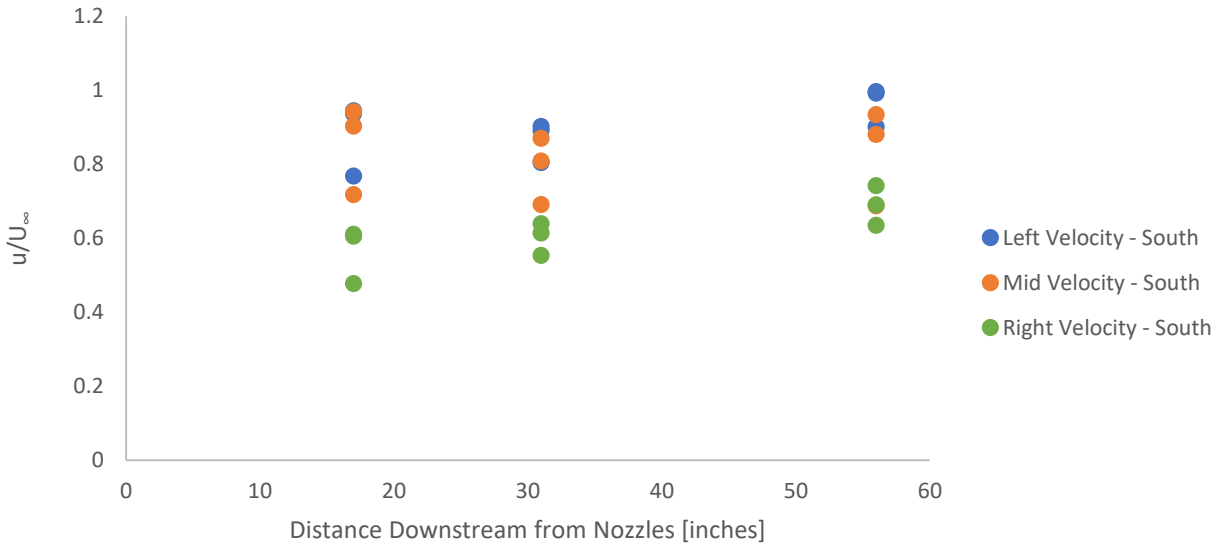

Figure A.3: Field data captured at a boom height of 28 in above the ground. The local mean velocity (u) is normalized with the effective external velocity (U_∞) accounting for wind effects.